FORMULACIÓN Y CARACTERIZACIÓN DE EMULSIONE DE LIMONENO ESTABILIZADAS POR UN TENSIOACTIVO POLIMÉRICO

Luís María Pérez Mosqueda

Universidad de Sevilla

Sevilla, 2014

UNIVERSIDAD DE SEVILLA

FACULTAD DE QUÍMICA

Departamento de Ingeniería Química

Luis Mª Pérez Mosqueda

Tesis Doctoral

FORMULACIÓN Y CARACTERIZACIÓN DE EMULSIONES MODELO DE POTENCIAL USO AGROQUÍMICO BASADAS EN UN DISOLVENTE VERDE: D-LIMONENO

por

Luis Mª Pérez Mosqueda

Directores del trabajo:

Dr. José Muñoz García
Profesor Titular

Dr. Pablo Ramírez del Amo
Profesor Ayudante Doctor

Trabajo presentado para aspirar al título de Doctor por la Universidad de Sevilla

Sevilla, marzo de 2014

Dr. D. Felipe Cordobés Carmona, Director del Departamento de Ingeniería Química de la Universidad de Sevilla:

CERTIFICA:

Que la Tesis Doctoral que presenta D. Luis Mª Pérez Mosqueda ha sido realizada dentro de la línea “Reología aplicada y tenología de fluidos complejos”.

Fdo: Dr. Felipe Cordobés Carmona

AGRADECIMIENTOS

En primer lugar creo que tengo que decir que voy a ser un poco injusto en estos agradecimientos porque seguro que no voy a ser capaz de transmitir el enorme sentimiento de gratitud que tengo hacia tanta gente que me ha ayudado, apoyado, soportado, sufrido, aguantado, etc…durante este tiempo.

En primer lugar me gustaría acordarme de mis directores de tesis, José Muñoz y Pablo Ramírez por su inestimable ayuda en la realización de esta tesis doctoral. Me gustaría agradecer a Pepe la oportunidad que me dio de incorporarme en el grupo de investigación, hace ya algunos años, que al final me ha traído hasta aquí y por su ayuda durante este tiempo. A Pablo debería agradecerle su paciencia durante este tiempo y sobre todo el que sea un gran amigo.

A los compañeros del departamento (Cecilio, Carlos, Cristina, Manolo, Juan Carlos, José Antonio, Nieves, Paco Toscano, Montse, Mª Carmen, Nuria, Lucía etc…) debería agradecerles el hacer el día a día más sencillo y generar ese buen ambiente que hace ir a trabajar con alegría y que negocios como “La bodeguita” y “El Aljibe” sean prósperos. En particular agradecer a Paco sus consejos, el tener la puerta del despacho siempre abierta y principalmente por ser un gran amigo. A mis hermanitos Luis y Jeni por seguir aguantándome día tras día, especialmente últimamente con los agobios de final de tesis

Quisiera agradecer a Julia Maldonado la oportunidad que me dio de realizar una estancia de investigación en el grupo de Física de Fluidos y Biocoloides en la Universidad de Granada y a la gente de “la sala” (Azahara, César, Juan Pablo, Jose, Miguel, Felipe, Carmen Lucía, Germán, Miguel Ángel, Leonor) por hacer que ese experiencia fuera tan reconfortante tanto a nivel personal como profesional. De la

misma manera debo agradecer al doctor Reinhard Miller el concederme la posibilidad de pasar seis meses trabajando en su grupo de investigación en el Max Planck for Collids and Interface en Berlín. También debo acordarme de toda esa gente que me ha facilitado y ha hecho tan llevadero mi tiempo en Berlin (Vamsee, Antonio, Georgi, Nenad, Sabine, Jooyoung Inga, Ali, Jurgen, Narges, Marzy, Altynay, Bota, Samee).

A mi familia y amigos quisiera agradecerle toda la ayuda prestada durante todo este tiempo. Solo deciros que no sé cómo transmitiros el sentimiento de gratitud tan grande que produce el sentirse tan apoyado y acompañado como me he sentido yo en los momentos más feos. Al principio dije que los agradecimientos iban a ser injustos porque era imposible nombraros a todos, pero no os preocupéis porque sabéis que esto lo celebraremos convenientemente.

Y por último, a las personas que más les debo, a mis padres. Gracias por tener siempre tanta paciencia y tantísima confianza en mí. A los dos os tengo que agradecer el haber sido siempre un ejemplo y el tener tantísimo coraje y fuerza de voluntad y sobre todo por enseñarme a vivir la vida como la vivís vosotros, siempre mirando hacia adelante. Gracias.

A mis padres

Summary

This Ph.D. Thesis is part of the research project “Caracterización Reológica y Estabilidad Física de Emulsiones Formuladas con Disolventes Verdes” (CTQ2011-27371) supported by the Spanish Ministerio de Economía y Competitividad (MINECO) and by the European Commission (FEDER Programme). This PhD was possible due to finantial support from University of Seville “Beca IV Plan Propio Universidad de Sevilla”

The role of solvents in the agrochemical industry is becoming increasingly more important. Many organic solvents have been withdrawn or are expected to be banned soon since they pose hazards to the environment due to their toxicity, low biodegradability and contribution to atmospheric volatile compound (VOC) emissions. Thus, environmentally-damaging solvents are being gradually replaced by the so-called ‘green’ solvents (Höfer, 2007). D-Limonene, a naturally occurring hydrocarbon, is a cyclic monoterpene, which is commonly found in the rinds of citrus fruits such as grapefruit, lemon, lime, and in particular, oranges. D-Limonene exhibits good biodegradability, hence it may be proposed as an interesting alternative to organic solvents. Furthermore, it has a similar molecular weight and structure to cyclohexane and toluene and therefore its solvent properties are similar, which makes D-limonene a promising material to replace those VOCs (Kerton, 2009).

The main goal of this Ph.D. Thesis was the formulation of a stable submicron D-limonene emulsion that can be applied in industrial formulations replacing traditional organic solvents. A non-ionic triblock copolymer, Pluronic PE9400, was used as emulsifier due to its low toxicity and expected irreversible adsorption at the D-limonene-water interface. Furthermore, a lyophilic biopolymer (rosin gum) was used to inhibit Ostwald ripening growth in these emulsions, which eventually led to highly stable colloidal systems.

This Ph.D. Thesis is formed of five chapters. The first chapter introduces the main concepts of emulsion science and technology as well as the state-of-the-art of D-limonene, Pluronics and Rosin gum in relation to their applications in colloidal systems.

The second chapter is devoted to the interfacial characterization of the non-ionic triblock copolymer surfactant, PE9400. Interfacial pressure isotherms, dilatational rheology and desorption measurements were carried out, allowing us to extract useful information regarding the adsorption and conformation of the emulsifier at the D-limonene-water interface.

The third chapter consists of a detailed study of the influence of two key variables for the formulation of emulsions; the disperse mass fraction, ϕ, and the surfactant/oil mass ratio, R, on the droplet size distribution (DSD) and stability of D-limonene-in-water-emulsions stabilized by Pluronic PE9400. By using a response surface methodology, an optimum value of both variables was obtained leading to a submicron emulsion, which can be prepared with just a one-step rotor/stator homogenization process. Nevertheless, this emulsion undergoes coalescence induced by the Ostwald ripening mechanism.

In the fourth chapter it is shown how the optimum formulation obtained in the previous chapter can be improved by the addition of a lipophilic gum (rosin gum). It is shown that at gum concentration above 10 wt% the Ostwald ripening is practically inhibited. Furthermore, from rheological measurements in combination with laser diffraction and multiple light scattering techniques the influence of surfactant concentration on the stability of the emulsions was explored.

Finally, the fifth chapter summarizes the main conclusions of this Ph.D. Thesis.

Resumen

Esta tesis está encuadrada dentro de la ejecución del proyecto “Caracterización Reológica y Estabilidad Física de Emulsiones Formuladas con Disolventes Verdes” (CTQ2011-27371) financiado por el Ministerio de Economía y Competitividad (MINECO) y con fondos de la Comisión Europea (Programa FEDER). La realización de esta tesis fue posible gracias a la concesión de la beca “IV Plan Propio Universidad de Sevilla” a Luis Mª Pérez Mosqueda.

El papel de los disolventes en la industria es cada vez más significativo. Muchos disolventes orgánicos han sido retirados, o se espera que sean prohibidos, en los próximos años debido a su toxicidad y a su contribución a las emisiones atmosféricas de compuestos orgánicos volátiles (VOC). De esta manera, los disolventes más dañinos para el medio ambiente están siendo sustituidos gradualmente por compuestos conocidos como “disolventes verdes” (Höfer, 2007). El D-limoneno, es un hidrocarbono natural, un monoterpeno cíclico, que se encuentra comúnmente en la cáscara de cítricos como pomelo, limón, lima y sobre todo en las naranjas. El D-limoneno presenta una buena biodegradabilidad y por este motivo puede ser presentado como una interesante alternativa a los disolventes orgánicos tradicionales. Además, presenta un peso molecular y estructura similar a la del ciclohexano y el tolueno, por lo que sus propiedades como disolvente son parecidas, haciéndole ser un prometedor candidato para sustituir a estos VOCs (Kerton, 2009).

El principal objetivo de esta tesis es la formulación de una emulsión submicrónica estable que puede ser empleada en formulaciones con potencial uso industrial sustituyendo los disolventes orgánicos tradicionales. El copolímero tribloque, PE 9400, se ha empleado como emulsificante debido a su baja toxicidad y a la esperada adsorción irreversible en la interfaz D-limoneno-agua. Además, la adición de un

biopolímero lipofílico (goma rosín) inhibe el crecimiento del tamaño de gota por Ostwald ripening obteniéndose un sistema coloidal altamente estable.

Esta tesis está formada por cinco capítulos. El primer capítulo introduce los principales concepto de la ciencia y tecnología de emulsiones así como el estado del arte de los principales compuestos empleados: D-limoneno, pluronics y goma rosín en relación con su aplicación en sistemas coloidales.

El segundo capítulo está dedicado a la caracterización interfacial del surfactante polimérico no-iónico, PE 9400. Se ha estudiado la isoterma de adsorción, reología dilatacional, y los procesos de desorción obteniendo información interesante respecto al proceso de adsorción y las conformaciones del surfactante en la interfaz D-limoneno-agua.

El tercer capítulo muestra detalladamente un estudio de la influencia de dos de las principales variables en emulsificación; la fracción de fase dispersa, ϕ, y la relación tensioactivo/aceite, R, en la distribución del tamaño de gota (DTG) y en la estabilidad física de emulsiones de D-limoneno en agua estabilizadas por el pluronic PE 9400. Usando metodología de superficie de respuesta se ha obtenido un óptimo de las dos variables llegando a tener una emulsión submicrónica en un proceso de homogenización de una etapa en un homogenizador rotor/stator. Sin embargo, esta emulsión sufre un rápido crecimiento del tamaño de partícula debido al proceso de Ostwald ripening.

En el cuarto capítulo de la tesis se muestra como el óptimo obtenido en la formulación en el capítulo previo puede ser mejorado por la adición de una goma lipofílica (goma rosín). Se muestra como una concentración de goma de en torno al 10% m/m inhibe casi completamente el proceso de Ostwald ripening. Además, la combinación de medidas reológicas, difacción láser y dispersión múltiple de luz

muestran la influencia de la concentración de surfactante en la estabilidad física de las emulsiones.

Finalmente, el quinto capítulo resume las principales conclusiones de la tesis.

1

Introduction

1.1 Emulsions

1.1.1 Definition

An emulsion is a type of disperse system which is formed by two immiscible liquids (usually a kind of oil and water). One of the liquids forms small spherical droplets in the other. The liquid which forms the droplets is known as the disperse phase and the liquid containing these droplets is the continuous phase. Several classes of emulsion could be distinguished depending on the relative spatial distribution of the oil and aqueous phase. A system which is formed by oil droplets dispersed in an aqueous phase is called an oil-in-water emulsion or O/W emulsion, such as milk, cream, dressings, mayonnaise, some beverages, different pharmaceuticals and cosmetics (Aulton, 2007; Troy, 2006). A system consisting of water droplets dispersed into an oil phase is called a water-in-oil or W/O emulsion, like margarine or butter (McClements, 2005; Tadros, 2009). In addition to the conventional O/W or W/O emulsions it is also possible to prepare various types of multiple emulsion as oil-in-water-in-oil (O/W/O) or water-in-oil-in-water (W/O/W) emulsions (Garti, 1997; Garti, 2004).

If we try to mix a pure organic phase with pure water a fast destabilization will be seen, since the attainment of a homogeneous solution is thermodynamically unfavorable (Israelachvili, 1992). Eventually, the phase with the lowest density (oil) will form a cream layer at the top, whereas at the bottom a water layer will appear. The system evolves to the state of minimal contact area between the two phases. This is because droplets tend to merge together, eventually leading to a complete phase separation (McClements, 2005). Nevertheless, it is feasible to create emulsions that are kinetically stable (metastable) with a time window useful for many industrial applications (ranging from a few days to months). To that end, the addition of an emulsifier is required. An emulsifier is a surface-active chemical that adsorbs at the

interface of freshly formed droplets and also plays an important role in long-term stability (Binks, 1998; Tadros, 2005; Tadros, 2009). A wide variety of molecules can be used as emulsifiers, such as: surfactants, proteins, polysaccharides, etc. In this Ph.D. Thesis a non-ionic triblock copolymer surfactant has been used as emulsifier.

Droplet concentration is usually defined as the disperse phase volume fraction (ϕ), which is the ratio between the volume occupied by all the droplets and the total volume of the emulsion ($\phi=V_D/V_E$) or as the disperse phase mass fraction (ϕ_m), which is the ratio between the mass of all emulsion droplets and the total mass of the emulsion ($\phi_m=m_D/m_E$). ϕ_m and ϕ are related according to (McClements, 2007):

$$\phi_m = \phi\left(\phi + (1-\phi)\frac{\rho_1}{\rho_2}\right)^{-1} \quad (1)$$

$$\phi = \phi_m\left(\phi_m + (1+\phi_m)\frac{\rho_1}{\rho_2}\right)^{-1} \quad (2)$$

where, ρ_1 and ρ_2 are the densities of the continuous and the disperse phase, respectively.

The process whereby two immiscible liquids form an emulsion is called homogenization. Normally, this process occurs in a device called a homogenizer, where this device supplies the necessary energy for the homogenization process.

1.1.2 Destabilization mechanism

The term “emulsion stability” usually refers to the ability of an emulsion to resist changes in its physicochemical properties over time (McClements, 2005). Several physicochemical mechanisms could take place to generate an unstable emulsion such as: gravitational separation (creaming/sedimentation), flocculation, coalescence, partial

coalescence, Ostwald ripening and phase inversion (Dickinson, 1992; Friberg, 2004; McClements, 2005).

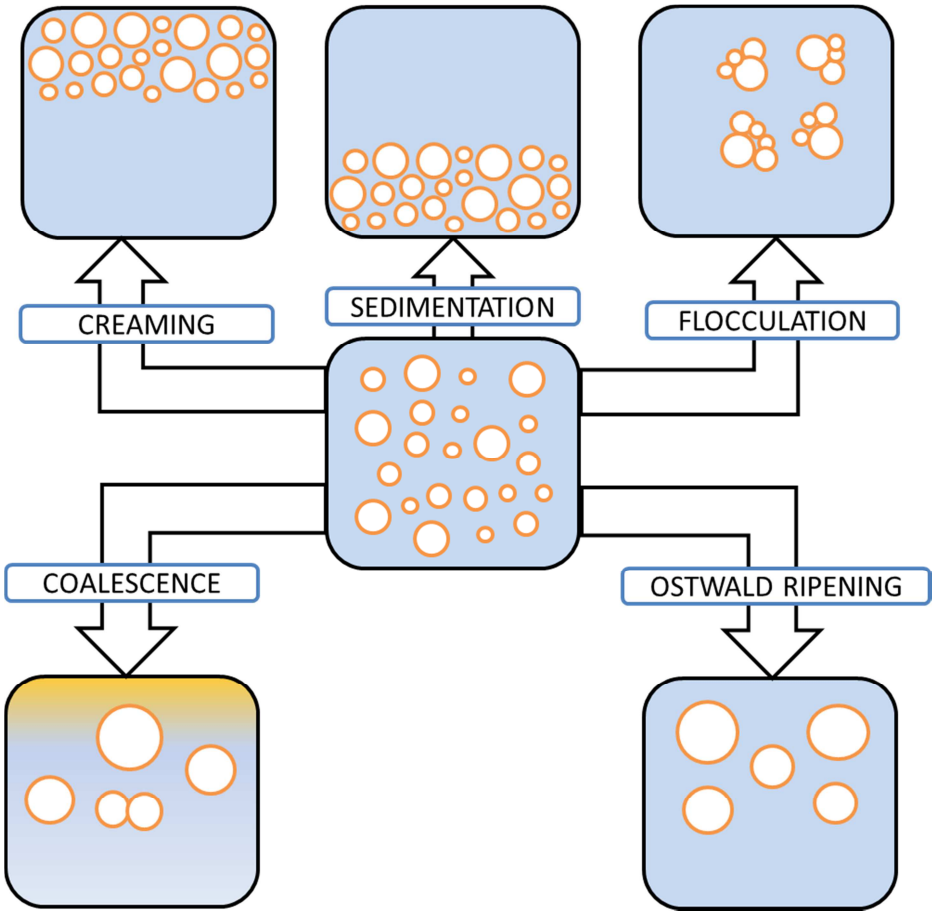

Figure 1. Destabilization processes for emulsions.

1.1.2.1 Gravitational separation

The density of the droplets in an emulsion is usually different from that of the liquid that surrounds them, and therefore a net gravitational force acts upon them (McClements, 2005; McClements, 2007).

On the one hand, if the liquid in the droplets has a lower density than the surrounding liquid, the droplets will tend to move upwards, a process known as creaming. On the other hand, if the liquid inside the droplets has a higher density than the surrounding liquid, the droplets will tend to move downwards, which is called sedimentation.

The rate of creaming or sedimentation depends on the balance force. The most famous mathematical model which describes the gravitational separation rate is Stoke's law. This approximation is only valid for an isolated rigid spherical particle drop in an ideal (Newtonian) liquid (McClements, 2007):

$$v_{stokes} = -\frac{2gr^2(\rho_2 - \rho_1)}{9\eta_1} \quad (3)$$

where v_{stokes} is the creaming velocity, r is the radius of the drop, g is the acceleration due to gravity, ρ, is the density, η, is the shear viscosity, and the numbers 1 and 2 refer to the continuous and the disperse phase, respectively. Although, this equation is valid only for ideal systems (a system is usually considered ideal when the volume disperse fraction is lower than 1%), the main factors influencing creaming/sedimentation rate, which are particle size, the viscosity of the disperse phase and differences between densities, also have to be taken into account for more concentrated emulsions. Furthermore, the polidispersity of the emulsion droplets as well as the likely occurrence of droplet flocculation have to be considered for more concentrated emulsions. Hence, in order to minimize the gravitational separation rate some strategies can be adopted such as minimizing the difference in densities between the phases, reducing the particle size, changing the rheology of the disperse phase, increasing the droplet concentration and/or avoiding flocculation (Bengoechea, 2006).

Chanamai (Chanamai, 2000a; Chanamai, 2000b) proposes dividing the creamed emulsion into three layers in order to quantify the extension of the creaming process: (a) a lower layer, where the concentration of droplets is very low or non-existent; (b) a middle layer, where the concentration of droplets is similar to the one in the original emulsion; and (c) an upper layer, where the concentration of droplets is higher than the initial one and they are closely packed. The trend of the droplets in most O/W emulsions, such as the ones studied in this Ph.D. Thesis, is to move upwards. It is observed that whereas the thickness of the lowest (H_L) and uppermost (H_U) layers increases over time, the thickness of the middle layer (H_M) decreases. In some cases, the middle layer disappears completely after a certain time (Figure 2), (Chanamai, 2000a; 2000b).

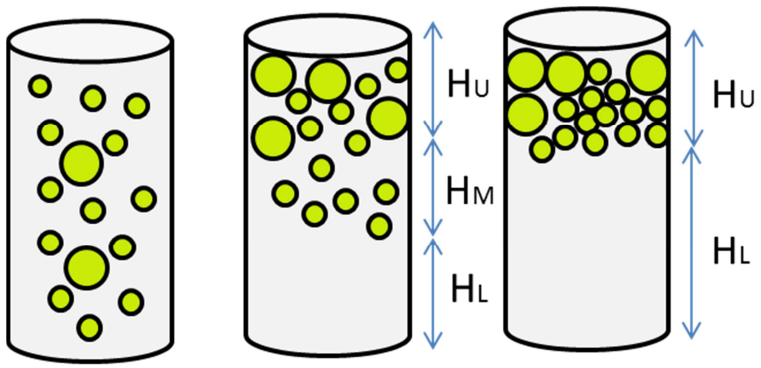

Figure 2. Creaming zones

1.1.2.2 Flocculation

This destabilization process occurs when several droplets suffer aggregation, forming larger entities but maintaining the integrity of the individual droplets. The interaction between droplets arises when the repulsion between them is not enough to avoid the van der Waals attraction (Tadros, 2009). Although this is a reversible destabilization process, it could drive the development of other destabilization processes such as coalescence.

One factor enhancing emulsion flocculation is the presence of non-adsorbing colloidal particles such as biopolymers or surfactant micelles. This destabilization mechanism is usually explained on the basis of the exclusion volume theory developed by Asakura and Osawa (1958). As shown in Figure 3, the surfactant micelles are excluded from a narrow region surrounding each droplet. This region extends from the droplet surface to a distance equal to that of the micelle radius. Hence an osmotic potential difference between the depletion zone and the bulk liquid is generated, whereby droplets tend to aggregate in order to reduce this difference (McClements, 2005; Pal, 2011; Quemada, 2002).

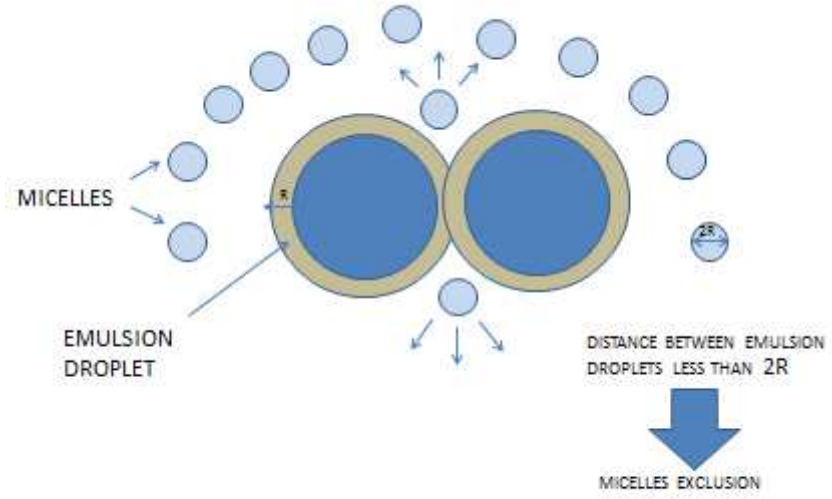

Figure 3. Depletion Flocculation scheme

1.1.2.3 Coalescence

This is an irreversible emulsion destabilization whereby two or more liquid droplets merge together to form a single, larger droplet (McClements, 2005). Interfacial elasticity of the adsorbed surfactant layer plays a key role in coalescence (Husband, 1997; Carrera-Sánchez, 2005). Emulsions which suffer coalescence evolve to a more

thermodynamically stable state because this process involves a decrease in the interfacial area between oil and water. In O/W emulsion, coalescence could lead to the formation of a layer of oil on the top of the sample, which is usually referred to as *oiling off*. In W/O emulsion, it leads to the accumulation of water at the bottom of the emulsion (McClements, 2005). Eventually, a complete separation of the emulsion into two distinct phases could take place (Tadros, 2009).

1.1.2.4 Ostwald ripening

The Ostwald ripening mechanism refers to the growth of larger droplets at the expense of smaller ones. This phenomenon can be explained due to the difference in chemical potential of the oil phase between different droplets arising from their different radii of curvature (Lifshitz, 1962; Wagner, 1961). The rate of droplet growth is likely to be determined by molecular diffusion across the continuous phase. A theoretical description of Ostwald ripening in two-phase systems is usually described in the LSW framework (Lifshitz, Slyozov and Wagner). Ostwald ripening rate is proportional to the cube of the radius. (Taylor, 1998; Kabalnov, 1992; Finsy, 2002):

$$\omega = \frac{dr_c^3}{dt} = \frac{8}{9}\frac{DC_\infty \gamma C}{\rho^2 RT} \tag{4}$$

where D is the diffusion coefficient of the dissolved disperse phase in the dispersion medium, C_∞ is the aqueous solubility of the dispersed phase, γ is the interfacial tension between the two phases, and M and ρ are the molar mass and density of the dispersed phase respectively, r_c is the critical radius of the system at any given time. The LSW theory assumes that: the mass transport is mainly governed by molecular diffusion through the continuous phase; the disperse phase particle is spherical; it is fixed in space; and there are no interactions between neighboring particles (Weers, 1998). The

particle size increase produced by Ostwald ripening is irreversible and may favor other destabilization processes such as creaming or flocculation.

1.1.3 Droplet size

Particle size plays a key role in many of the most important properties of emulsions, such as shelf- life, appearance or texture.

Emulsions are usually formed by droplets with a wide range of different sizes, which are known as *polydisperse* emulsions. If all the droplets of the emulsion had the same particle size it would be called *monodisperse (d)* emulsion. The droplet size of a monodisperse emulsion can be completely characterized by a single characteristic length such as diameter (*d*) or radius (*r*). Typically, real systems present a normal distribution of droplet sizes. Therefore, polydisperse emulsions are better defined by using the droplet size distribution (DSD) which is the volume percentage of the different diameters presented by the droplets in the emulsion.

Stable emulsions are usually associated with narrow droplet size distributions and small diameters (Dickinson, 1989).

1.2. Emulsification techniques

Production and control of submicron emulsions with narrow droplet size distribution are of wide interest and application in many fields, such as the food, pharmaceutical and cosmetic industry (Schultz, 2004; Jafari, 2008; Jafari, 2007). Droplet size distribution (DSD) and emulsion stability are very influenced by the homogenization process.

A first classification of homogenization processes can be to separate them into “high-energy emulsification” and “low-energy emulsification” methods.

In this Ph.D. Thesis only the "high-energy emulsification" methods are reviewed. The high energy methods include techniques such as *rotor/stator systems, high-pressure systems, ultrasonic systems, microfluidics systems, membrane systems* (Schultz, 2004; Urban, 2006). Many factors influence the choice of a particular homogenizer, including the available equipment, the volume of material to be homogenized, the desired throughput, the nature of the starting material and the desired droplet size distribution (McClements, 2005).

As a rule, high-energy homogenization processes are carried out in two steps in order to reduce the droplet size and to obtain a narrow distribution. The first step is the conversion of the separate phases into a coarse emulsion and it is usually carried out in a rotor/stator system. The second step involves the use of one of the other emulsification processes (high-pressure systems, ultrasonic systems, microfluidics systems, membrane systems).

Emulsification can also be produced in a single step by using a mixer or rotor/stator system. Nevertheless, it has been stated that it is not possible to achieve droplet size smaller than 1-2 µm with rotor/stator devices (McClements, 2005; Schultz, 2004). Hence, one of the attainments of this work is the achievement of stable submicrom emulsions by rotor/stator systems.

1.2.1 Rotor/stator systems

Rotor/stator devices are the most frequently used method for direct homogenization of emulsions (Loncin, 1979; Fellows, 2000). These homogenizers can be classified into gear-rim systems, which are devices suitable for work in batch processes, and colloid mills which are usually used for continuous processes (Urban, 2006; Jafari, 2008). Jafari defines rotor/stator devices as an assembly consisting of two

or more blades and a stator with vertical or slanted slots. The movement of the rotor generates the circulation of the liquids through the assembly producing the emulsification (Jafari, 2008; Maa, 1996).

There are several forces acting to reduce the droplet size. One of the most significant is the mechanical impingement against the wall due to the high acceleration of the fluid. Another key force is the shear stress produced in the gap between rotor and stator. The thickness of the gap can control the intensity of the shear stress. Furthermore, there are others factors which have a noticeable influence on droplet size reduction, such as the rotation speed (1000-25000), the kind of rotor (toothed surface, interlocking teeth) and the residence time of the emulsion in the vessel (McClements, 2005). This system is mainly used to produce a coarse emulsion for feeding other kinds of "high energy homogenizers".

1.2.2 High- pressure valve homogenizers

This is one of the most common methods used in the industry to produce emulsions. Normally, this technique is used to reduce the droplet size of a coarse emulsion produced by a *rotor/stator* system. The most commonly used high-pressure homogenizer is the radial diffuser system (Schultz, 2004). It consists of a pump that introduces the coarse emulsion into the compression chamber. The coarse emulsion is then compressed by a valve. As the coarse emulsion passes through the valve it experiences a combination of intense disruptive forces that cause the large droplets to be broken down into smaller ones (Phipps, 1985; Stang, 2001).

The standard way to work with a high pressure valve homogenizer is to pass the emulsion around the system several times to obtain the optimal droplet size. Emulsion droplets with diameters as low as 0.1 µm can be produced using this method.

1.2.3 Ultrasonic homogenizers

These devices have been used for a long time to produce emulsions (Gopal, 1968; Abismail, 1999). This apparatus uses high-intensity ultrasonic waves, generating intense shear and pressure gradients within a material, which disrupt the droplets mainly due to cavitational and turbulence effects.

Different methods are available to produce high-intensity ultrasonic waves but the most commonly used is a piezoelectric transducer.

These devices are well-suited for the production of small volume of emulsions and have therefore been widely used in lab-scale emulsion preparation.

1.2.4 Microfluidization

Microfluidizers can be divided into three parts: a liquid inlet, a pumping device, and an interaction chamber. Liquids are forced to flow through two channels that merge into one in the interaction chamber. Interaction chambers are designed with different shapes in order to optimize the emulsification process depending on the type of fluids that will be used. Normally, this technique is used to reduce the droplet size of a coarse emulsion produced by a *rotor/stator* system (Dickinson, 1988).

1.2.5 Membrane homogenizers

These homogenizers can form emulsions from the separate phases or can be used to reduce the droplet size of a coarse emulsion. The homogenization process is produced by obliging one non-miscible liquid (the disperse phase) into another non-miscible liquid (the continuous phase) through a solid membrane that contains small pores. This technology is suitable for the production of monodisperse emulsion, given that the membrane should contain pores with similar diameters (McClements, 2005).

1.3 Adsorption of surfactants

Surfactants play a fundamental role in emulsion formulation. They are amphiphilic molecules that tend to adsorb at interfaces, decreasing the interfacial tension and protecting the interface against destabilization processes such as coalescence.

The type and amount of surfactant in the emulsion is a key factor in obtaining the desired droplet size and stability. If particle size decreases the interfacial area between the two phases will increase. For a fixed concentration of oil, water, and emulsifier there is a maximum interfacial area that can be covered by the emulsifier (McClements, 2005):

$$r_{\min} = \frac{3\Gamma_{sat}\varphi}{c_s} = \frac{3\Gamma_{sat}\varphi}{c'_s(1-\phi)} \qquad (5)$$

where r_{sat} is the excess surface concentration of the emulsifier at saturation (kgm^{-2}), ϕ is the disperse phase volume fraction, c_s is the concentration of emulsifier in the emulsion (kgm^{-3}), and c'_s is the concentration of emulsifier in the continuous phase (kgm^{-3}).

Adsorption properties of surfactants are very influenced by their hydrophobicity. This is usually characterized by the hydrophilic lyophilic balance (HLB) which is defined as a number that gives an indication of the relative affinity of a surfactant molecule for the oil and aqueous phase (Davis, 1994; McClements, 2005).

A surfactant with high HLB has a predominant hydrophilic part and it is suitable to form O/W emulsion. On the other hand, in surfactants with low HLB, the hydrophobic groups predominate over the hydrophilic ones and W/O emulsions can be formed. Table 3 shows the usual application of surfactants according to their HLB values.

HLB	Application	Example
0-4	Antifoam	Oleic Acid (1,0) Etilen glycol mono-sterate (2,9)
4-6	Emulsificer W/O	Glycerol mono-sterate (3,8) Sorbed mono-stearate (4,7)
6-9	Emulsifier O/W Humectantes	PEG – 4 di-laurate (6,0) sucrose di-palmitate (7,4) sorbed monolaurate (8,6)
9-13	Emulsifier O/W	PEG – 4 monolaurate (9,8) polysorbate 61 (9,6) polysorbate 85 (11,0) PEG – 8 mono-estearate (11,6) octoxynol – 9 (12,8)
13-40	Emulsifier O/W, detergent	PEG – 8 mono-laurate (13,1) sucrose mono-laurate (15,0) Sodium oleate (18,0) Potasium oleate (20,0) Sodium lauril-sulfate (40)

Table 3. HLB Classification.

1.3.1 Interfacial tension

"*The change in free energy of a system that occurs when a surface-active solute is present manifests itself as a change in the interfacial tension, that is, in the amount of free energy required to increase the interfacial area between the water and the oil phases by a unit amount"* (McClements, 2005). The presence of an amphiphilic molecule decreases the interfacial tension because the hydrophobic portion is located in the oil (air) and the hydrophilic portion is located in the water phase and, as a result, the thermodynamically unfavorable contacts between the oil and water phase are decreased (McClements, 2005).

The interfacial tension is represented by γ, whereas the reduction of the interfacial tension by the presence of amphiphilic molecules could be referred to as *surface pressure:*

$$\Pi = \gamma_{o/w} - \gamma \quad (6)$$

where $\gamma_{o/w}$ is the interfacial tension of the pure oil-water (air-water) interface and γ is the interfacial tension in the presence of surfactants (Hiemenz, 1997).

The adsorption of surfactant at the interface is a dynamic process in which kinetics is very important, as, for example, in industrial processes (Torcello-Gómez, 2012). This process occurs in two steps. First, a diffusive process takes place, whereby surfactant molecules are transferred from the bulk phase to the interface. The concentration gradient is the driving force; this phenomenon is controlled by mass transfer. The second step is an adsorption/desorption process of the surfactants located at the interface. (Torcello-Gomez,2012).

It has been shown that there is an *induction time* for the adsorption of proteins and macromolecules. Hence, at the beginning of the adsorption process the interfacial tension does not decrease due to the high molar area of proteins and macromolecules (Miller, 2000; Maldonado-Valderrama, 2006).

Adsorption of surfactants is usually studied by equilibrium surface tension isotherms, i.e., plots of the equilibrium interfacial tension vs. surfactant bulk concentration $\gamma(c)$. For conventional surfactants three different regions are usually observed: first, at low concentrations the surfactant adsorption provokes a decrease in the interfacial tension. Once the interface has been saturated, a constant surface concentration value is attained and a linear decrease of interfacial tension versus the log of concentration is observed according to the Gibbs adsorption isotherm. Eventually, at high surfactant bulk concentration monomers start to aggregate producing micelles. Increasing the surfactant bulk concentration does not increase the number of monomers in solution and, therefore, a constant interfacial tension value is attained. The surfactant

bulk concentration at which micelles start to form is called critical micelle concentration, cmc.

However, for some polymeric surfactants, such as Pluronics or proteins, the interfacial tension isotherm shows a more complicated shape with intermediate regions of constant interfacial tension values, which are reported to be due to conformational changes of the adsorbed macromolecules (Ramírez, 2011; Ramírez, 2012; Pérez-Mosqueda, 2013)

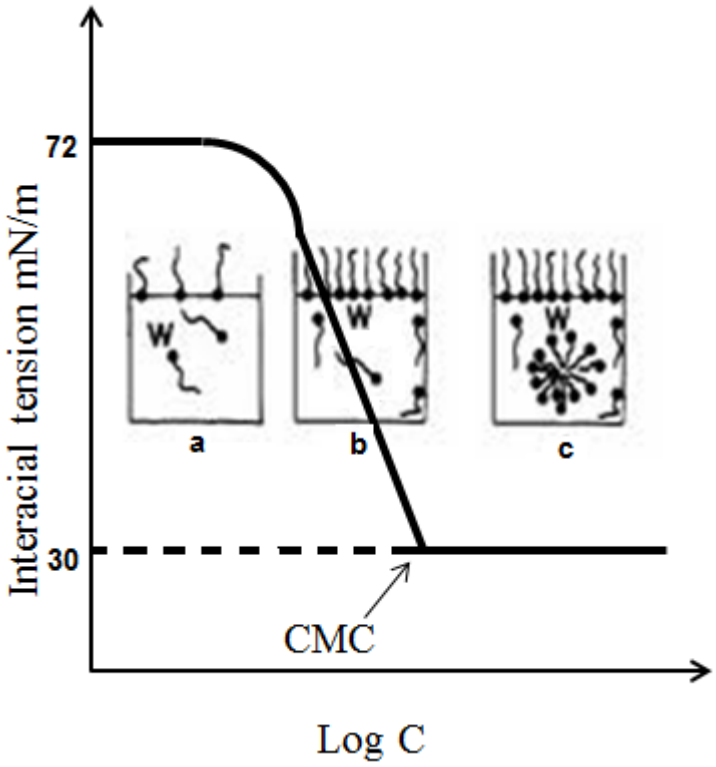

Figure 4. Structural region CMC

.

1.3.2 Interfacial rheology

"*Interfacial rheology is the science of the response of mobile two dimensional phases to deformation. Interfacial rheological properties are the main characteristics of the dynamic properties of a film*" (Sun 2011).

In many technological applications equilibrium values of the interfacial tension or cmc values are not enough to fully understand the interfacial properties of surfactants For example, the aim of this Ph.D. Thesis is the production of stable D-limonene emulsions, in these systems, the knowledge about how the interface will respond against any kind of interfacial perturbation is very important. This response will be conditioned by the composition of the molecules which are at the interface, and depends specially on the chemical structure of the molecules adsorbed, their conformation, concentration and interaction (Torcello-Gómez, 2012).

The interfacial rheological properties could be characterized by the interfacial shear and dilational viscoelasticity. However, it seems that dilational viscoelastic parameters are much larger than the shear ones and show a more direct correlation to emulsion stability (Wasan, 1982; Clint, 1981; Neustadter, 1981).

Gibbs defined the interfacial elasticity as the variation in the interfacial tension when a variation in the area is produced (Sun, 2011; Maldonado-Valderrama, 2006):

$$\varepsilon = \frac{d\gamma}{d\ln A} = \frac{d\gamma}{(dA/A)} \tag{7}$$

where ε is the dilational modulus, γ is the interfacial tension and A is the interfacial area. This expression gives a measure of the resistance of the interface to a change in the area. Usually the interfaces are not completely elastic because they could present some viscous behavior. This viscous process is related to relaxation processes, such as

the interchange of molecules between the bulk and the interface or molecular rearrangement processes in macromolecules (Williams, 1996; Maldonado-Valderrama, 2006). The dilatational modulus is formed in this case by an elastic component, called the storage modulus, and a viscous component, called the loss modulus:

$$\varepsilon = \varepsilon_d + i\omega\eta_d \tag{8}$$

where ε_d is the dilational elasticity or storage modulus and η_d is the dilational viscosity component or loss modulus that represents a combination of internal relaxation processes and relaxation due to transport of matter between the surface and the bulk.

Usually, the storage modulus and the loss modulus can be determined by dilatational rheology using oscillatory perturbations of the area. The oscillations have to be done in the linear viscoelastic range which implies less than 10% variation in the area. The response is a sinusoidal signal. The storage modulus is obtained from the ratio of amplitudes of the sinusoidal input signal and the sinusoidal output signal. The loss modulus can be determined by the lag phase between the two signals. This is determined by the phase angle parameter (φ) and is defined by the following expression:

$$\tan\varphi = \frac{\varepsilon_\eta}{\varepsilon_d} \tag{9}$$

If the $\varphi = 0^o$ the interfacial layer is purely elastic, otherwise if the $\varphi = 90^o$ the interfacial layer is completely viscous and if the phase angle is $0^o < \varphi < 90^o$ the interfacial layer is viscoelastic.

1.4. D-limonene

D-limonene (4-isopropenyl-1-methylciclohexane) is a natural occurring terpene with the following chemical structure:

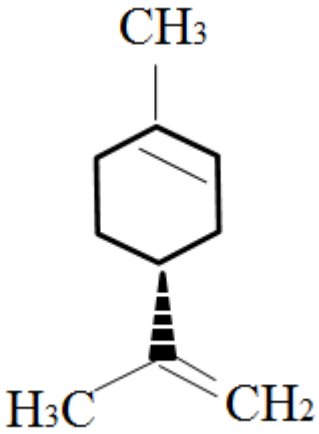

Figure 5. D-Limonene chemical formula.

This interesting bio-derived solvent can be obtained from citrus peels, especially from orange peel, by steam distillation, both at lab scale (Saleh, 2008) and an industrial scale. "*The vast majority of essential oils are produced from plant material in which they occur by different kinds of distillation or by cold pressing in the case of the peel oils from citrus fruits*" (Kubeczka, 2010). D-limonene gives citrus fruits their typical odor (Fahlbusch, 2003)

The option to obtain D-limonene from citrus peels could be an extra added value because it is possible to transform a by-product from the juice industry into an essential oil with interesting applications (Kerton, 2009).

Physical/chemical properties of D-limonene	
Molecular formula	$C_{10}H_{16}$
Molecular weight	136.2 g/mol
Physical state	Colorless liquid, with characteristic mild citrus odor
Melting point	-75 ºC
Boiling point	176 ºC
Solubility	13.8 mg/l at 25ºC
Density	0.84 g/ml

Table 2. Physical/Chemical properties of D-limonene

Limonene has a chiral center, i.e., an asymmetric carbon. There are two optical isomers. The IUPAC nomenclature for them is R-limonene and S-limonene. However, in this Ph.D. Thesis the most common nomenclature, D-limonene and L-limonene, is used. The two isomers present different properties; for example, the odor of D-limonene is lemon flavor and the odor of L-limonene is pine flavor (WHO, 1998). The D-limonene isomeric form is more abundantly present in plants than the racemic mixture and L-limonene isomeric form (Wichtel, 2002).

Usually, the purity of commercial D-limonene varies from 90% to 98%, the impurities usually being monoterpenes. D-limonene is likely to suffer a quick destabilization by oxidation. Hence, D-limonene should be stored in a cool, dry place without direct sunlight.

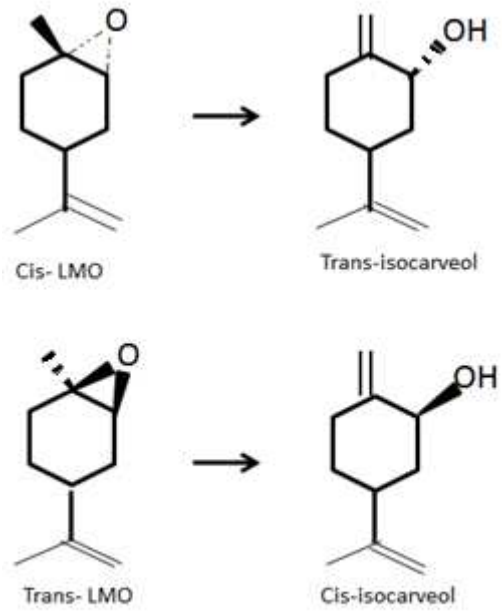

Figure 6. Product of D-limonene oxidation (Sonchick, 2003)

D-limonene is one of the most commonly used terpenes and the estimated worldwide limonene production is of $70 \cdot 10^6$ kg (Kerton, 2009). Due to its molecular weight and low miscibility in water, D-limonene has similar characteristic to classical volatile organic compounds (VOCs). Therefore, D-limonene is an interesting environmentally-friendly chemical which can replace these typical volatile organic compounds (VOCs), such as hexane, ciclohexane, acetone, toluene or xylene (Kerton, 2009).

D-limonene is widely used in household and personal cleaning products, fragrance additives and the food and cosmetic industries due to its characteristic lemon flavor. It is possible to use this solvent in other kinds of applications such as resins, paints, cooling fluids, pigments and, thanks to its low solubility in water, it is also employed as degreasing agent. Moreover, it has also been used as an insect repellent (Kerton, 2009).

Some studies have shown that D-limonene can act as an anticancer agent in some types of cancer, such as bladder (Xu, 2010) or colon cancer (Chidambara, 2012). Different researchers have proved that monoterpenes from dietary sources such as citrus are capable of inducing cytotoxicity in different human cancer cells (Crowell, 1999, Gould, 1995; 1997, Patil, 2010).

In this Ph.D. Thesis, we have used D-limonene as an ecofriendly oil phase in the O/W formulation with the goal of producing more environmentally-friendly emulsions with potential agrochemical use. D-limonene has a low solubility in water due to its hydrophobic character and in many applications the emulsified form is the best way to apply D-limonene. We have seen that D-limonene could be used as substitute for classical oils. There are numerous references from several authors concerning oil-in-water emulsions with D-limonene as the disperse phase: D-limonene is widely used in spray-drying encapsulation due to its flavor properties (Fisk, 2013; Marcuzzo, 2012; Jafari, 2007a; 2007b), and it is also used in the production of drug delivery systems because terpenes are not toxic to the skin (Abil, 2000; Sapra 2008). Another interesting application could be its use in the food industry as a preservative (Hai-Yan, 2012; Aissat, 2012; Chikhoune; 2013) due to its antimicrobial properties and because it is considered as safe (GRAS) for use as a flavoring agent and food preservative (Sun, 2007)

1.5. Pluronics

Pluronics are A-B-A triblock copolymer surfactants where the central chain is the hydrophobic part and is formed by PPO (poly propylene oxide) and the side chains are the hydrophilic parts and are formed by PEO (poly etoxi oxide). They are often denoted as (PEOx-PPOy-PEOx). Pluronics are also known as poloxamers, and kolliphor or Synperonic as commercial names. Due to the possibility of combining blocks,

surfactants with different molecular weights and HLB can be obtained, (from 2000 to 20000 Da and the range in PEO contents between 20-80% (Alexandridis, 1997), and the properties of the resulting polymers vary in a wide range.

This surfactant will present a different physical state at different temperatures, depending on the proportion between the PEO and PPO blocks. They are classified by a capital letter: F for flakes, P for Paste and L for Liquids. When a pluronic is named, the number which follows the capital letter provides information about the size and proportion of the different blocks: the first number (or the first two in a three-digit number) multiplied by 300 shows the approximate molecular weight of the hydrophobic part, and the last digit of the number multiplied by 10 gives the percentage of polyoxyethylene content (Pasquali, 2005). For example, we will focus on Pluronic PE9400, which is formed by the follow structure PPO_{21}-PEO_{50}-PPO_{21} and will be a paste at room temperature. The molecular weight of PPO will be around 9x300=2700 g/mol and each molecule will possess 60% of PEO. .

Normally, Pluronics adsorb at a liquid/liquid interface with the central chain (the hydrophobic PPO chain) at the hydrophobic interface while the two side chains (hydrophilic PEO chains) protrude into the water phase (Torcello-Gómez, 2012). An interesting property of Pluronics with respect to their use in emulsification processes is their interfacial behavior when dilatational perturbations take place. It is shown that the storage modulus is larger than the loss modulus and this fact means that the elastic contribution dominates the interfacial dilatational behavior and could preserve the emulsion droplets against instability processes such as coalescence.

It has been reported that pluronics at low concentration and small adsorption times present an induction time (Pérez-Mosqueda, 2013). These adsorption properties are typical for proteins and macromolecules.

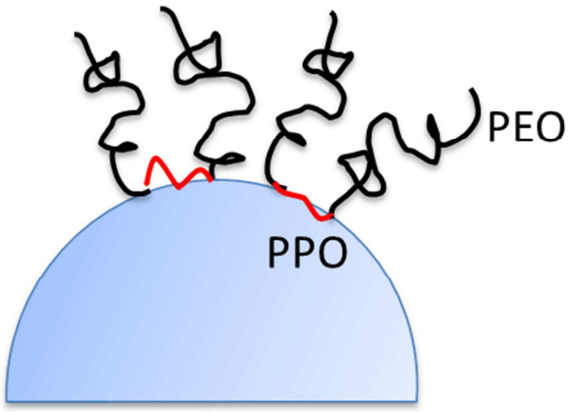

Figure 7. Pluronics at the interface.

This kind of surfactant has many applications in different fields such as cosmetics, the pharmaceutical industry, emulsification and foaming (Alexandridis, 2000; Berthier, 2010; Leal-Calderon, 2007; Schramm, 2005). Recently, Pluronics have been used in more complex systems. For example, the use of Pluronics in gene therapy is a promising area of research (Kabanov, 2002). Moreover, their use in delaying lipid digestion is being applied in the development of food products with satiating effects (Torcello-Gómez, 2011; Wulff-Pérez, 2012). The use of some pluronics in these applications is possible due to the fact that solutions of F-68 and F-127 have been approved as inactive ingredient for oral intake by the U. S. Food and Drug Administration (FDA)

1.6. Rosin gum

Sometimes the addition of other components to emulsion formulations is necessary, besides the oil, water and the emulsifier. Usually, these additives have the function of giving new properties to the formulation, such as to improve the physical

stability or modify the texture of the emulsion. The most classical additives are the well-known *thickening agents*, which have the function of increasing the viscosity of the aqueous phase of O/W emulsions (Mitchell, 1986; Williams, 2003). Others classical additives are *gelling agents*, which provoke a transition from a liquid-like aqueous phase to a gel (Morris, 1986; Ledward, 1986). On top of that, further useful additives are the so-called *weighting agents* which can delay creaming by reducing the difference between the densities of both phases (Tan, 2004). There is a long list of additives which have different functions: xanthan gum, seed gums, alginate, gellan gum, etc. In this Ph.D. Thesis we have employed a weighting agent; namely, rosin gum in our formulation in order to improve the physical stability of the emulsions studied.

Rosin gum is a natural polymer obtained from the pine tree. Its composition is a mixture of different rosin acids, which account for roughly 90%, and non-acidic compounds (Chang-Moon Lee, 2005). Yin proposes the following composition determined by HPLC for the rosin used in his work (Yin, 2000) (%): abietic acid 45.1, palustric acid 22.8, neoabietic acid 15.3, and others 16.8. This polymer is hydrophobic and fully insoluble in water, with a molecular weight of 306.53 g/mol and its density is 1.06 g/ml. Nevertheless, this gum has a good solubility in organic solvents and can be considered as a weighting agent when added to an oil phase of lower density.

Rosin gum and its various derivatives are widely used in paints, varnishes, printing inks, paper and wood products for their film forming properties. They are also used in chewing gum bases, dental varnishes and cosmetics. Studies reflect the biodegradation behavior for rosin gum (Prashant, 2003) and this is the key to its use in biocompatible systems as a coating agent, film-forming agent and coating material for drug delivery applications (Lee, 2004; Fulzele, 2004; Lee, 2005; Kumar, 2013). In some

of these applications rosin has been used without the presence of another surfactant. This fact suggests that the polymer is surface active.

References

Abismail, B., Canselier, J. P., Wilhelm, A. M., Delmas, H., & Gourdon, C. (1999). Emulsification by ultrasound: drop size distribution and stability. Ultrasonics Sonochemistry, 6(1), 75-83.

Alexandridis, P. (1997). Poly (ethylene oxide)/poly (propylene oxide) block copolymer surfactants. Current opinion in colloid & interface science, 2(5), 478-489.

Alexandridis, P., & Lindman, B. (2000). Amphiphilic block copolymers: self-assembly and applications. Elsevier.

Alahverdjieva, V. S., Fainerman, V. B., Aksenenko, E. V., Leser, M. E., & Miller, R. (2008). Adsorption of hen egg-white lysozyme at the air–water interface in presence of sodium dodecyl sulphate. Colloids and Surfaces A: Physicochemical and Engineering Aspects, 317(1), 610-617.

Alahverdjieva, V. S., Grigoriev, D. O., Fainerman, V. B., Aksenenko, E. V., Miller, R., & Möhwald, H. (2008). Competitive adsorption from mixed hen egg-white lysozyme/surfactant solutions at the air-water interface studied by tensiometry, ellipsometry, and surface dilational rheology. The Journal of Physical Chemistry B, 112(7), 2136-2143.

Asakura, S., & Oosawa, F. (1958). Interaction between particles suspended in solutions of macromolecules. Journal of Polymer Science, 33(126), 183-192.

Aulton A.B., Michael E., ed. (2007). Aulton's Pharmaceutics: The Design and Manufacture of Medicines (3rd ed.). Churchill Livingstone.

Asbill, C. S., El-Kattan, A. F., & Michniak, B. (2000). Enhancement of transdermal drug delivery: chemical and physical approaches. Critical Reviews™ in Therapeutic Drug Carrier Systems, 17(6).

Baser, K. H. C., & Buchbauer, G. (Eds.). (2010). Handbook of essential oils: science, technology, and applications. CRC Press.

Becher, P. (2001) Emulsions; theory and practice. Oxford University Press

Behrend, O., Ax, K., & Schubert, H. (2000). Influence of continuous phase viscosity on emulsification by ultrasound. Ultrasonics Sonochemistry, 7(2), 77-85.

Bengoechea, C. (2006) PhD. Universidad de Sevilla

Berthier, D. L., Schmidt, I., Fieber, W., Schatz, C., Furrer, A., Wong, K., & Lecommandoux, S. (2010). Controlled Release of Volatile Fragrance Molecules from PEO-b-PPO-b-PEO Block Copolymer Micelles in Ethanol− Water Mixtures. Langmuir, 26(11), 7953-7961.

Binks, B.P. (1998) Modern Aspects of Emulsion Science. The Royal Society of Chemistry Publication

Brooks, B.W., Richmon, H.N., Zerfa, M. (1998). Phase inversion and drop formation in agitated liquid-liquid dispersions in the presence of non-ionic surfactants, in Modern aspects of Emulsion Science, Binks, B.P., Ed., The Royal Society of Chemistry, UK, Chap 6

Chanamai, R., & McClements, D. J. (2000). Dependence of creaming and rheology of monodisperse oil-in-water emulsions on droplet size and concentration. Colloids and Surfaces A: Physicochemical and Engineering Aspects, 172(1), 79-86.

Chanamai, R., Herrmann, N., & McClements, D. J. (2000). Probing floc structure by ultrasonic spectroscopy, viscometry, and creaming measurements. Langmuir, 16(14), 5884-5891.

Chidambara Murthy, K. N., Jayaprakasha, G. K., & Patil, B. S. (2012). D-limonene rich volatile oil from blood oranges inhibits angiogenesis, metastasis and cell death in human colon cancer cells. Life sciences, 91(11), 429-439.

Chikhoune, A., Hazzit, M., Kerbouche, L., Baaliouamer, A., & Aissat, K. (2013). Tetraclinis articulata (Vahl) Masters essential oils: chemical composition and biological activities. Journal of Essential Oil Research, (ahead-of-print), 1-8.

Crowell, P. L. (1999). Prevention and therapy of cancer by dietary monoterpenes. The Journal of nutrition, 129(3), 775S-778S.

Davis, H. T. (1994). Factors determining emulsion type: Hydrophile—lipophile balance and beyond. *Colloids and Surfaces A: Physicochemical and Engineering Aspects*, *91*, 9-24.

Dickinson, E. (1992). Introduction to food colloids. Oxford University Press.

Dickinson, E., & Elvingson, C. (1988). The structure of aggregates formed during the very early stages of colloidal coagulation. Journal of the Chemical Society, Faraday Transactions 2: Molecular and Chemical Physics, 84(6), 775-789.

Dickinson, E., Flint, F. O., & Hunt, J. A. (1989). Bridging flocculation in binary protein stabilized emulsions. Food Hydrocolloids, 3(5), 389-397.

Donsì, F., Annunziata, M., Sessa, M., & Ferrari, G. (2011). Nanoencapsulation of essential oils to enhance their antimicrobial activity in foods. LWT-Food Science and Technology, 44(9), 1908-1914.

Eberth, K., & Merry, J. (1983). A comparative study of emulsions prepared by ultrasound and by a conventional method. Droplet size measurements by means of a Coulter Counter and microscopy. International Journal of Pharmaceutics, 14(2), 349-353.

Fahlbusch, Karl-Georg; Hammerschmidt, Franz-Josef; Panten, Johannes; Pickenhagen, Wilhelm; Schatkowski, Dietmar; Bauer, Kurt; Garbe, Dorothea; Surburg, Horst (2003). "Flavors and Fragrances". Ullmann's Encyclopedia of Industrial Chemistry. doi:10.1002/14356007.a11_141. ISBN 978-3-527-30673-2

Fainerman, V. B., Lucassen-Reynders, E. H., & Miller, R. (2003). Description of the adsorption behaviour of proteins at water/fluid interfaces in the framework of a two-dimensional solution model. Advances in Colloid and Interface Science, 106(1), 237-259.

Fisk, I. D., Linforth, R., Trophardy, G., & Gray, D. (2013). Entrapment of a volatile lipophilic aroma compound (D-limonene) in spray dried water-washed oil bodies

naturally derived from sunflower seeds (< i> Helianthus annus</i>). Food Research International, 54(1), 861-866.

Friberg, S.E.; Larsson, K., Sjoblom, J. (2004). Food emulsions, 4th ed. Marcel Dekker.

Frumkin, A. N. (1925). Surface tension curves of the higher fatty acids and the equation of condition of the surface layer. Z Phys Chem, 116, 466-483.

Fulzele, S.V., Satturwar, P.M., Kasliwal, R.H., Dorle, A.K.; Preparation and evaluation of microcapsules using polymerized rosin as a novel wall forming material, Journal of Microencapsulation 21 (1) , 83-89

Garti, N. (1997). Progress in stabilization and transport phenomena of double emulsions in food applications. LWT-Food Science and Technology, 30(3), 222-235.

Garti, N., & Benichou, A. (2004). Recent developments in double emulsions for food applications. Food emulsions, 353-412.

Gopal, E.S.R. (1968). Principles of Emulsion Formation, in Emulsion science, Sherman, P., ed, Academic Press, London, UK, Chap 1.

Gould, M. N. (1995). Prevention and therapy of mammary cancer by monoterpenes. Journal of Cellular Biochemistry, 59 (S22), 139-144.

Gould, M. N. (1997). Cancer chemoprevention and therapy by monoterpenes. Environmental Health Perspectives, 105(Suppl 4), 977.

Hernáiz, M. J., Alcántara, A. R., García, J. I., & Sinisterra, J. V. (2010). Applied biotransformations in green solvents. Chemistry-A European Journal, 16(31), 9422-9437.

Hiemenz, P.C., Rajagopalan, R. (1997). Principles of Colloid and Surface Chemistry, 3rd ed., Marcel Dekker, New York, NY.

Höfer, R., & Bigorra, J. (2007). Green chemistry—a sustainable solution for industrial specialties applications. *Green Chemistry*, *9*(3), 203-212.

Israelachvili, J.N. (1992). Intermolecular and Surface Forces, Academic Press, London, UK

Jafari, S. M., He, Y., & Bhandari, B. (2007). Effectiveness of encapsulating biopolymers to produce sub-micron emulsions by high energy emulsification techniques. Food research international, 40(7), 862-873.

Jafari, S. M., Assadpoor, E., Bhandari, B., & He, Y. (2008). Nano-particle encapsulation of fish oil by spray drying. Food Research International, 41(2), 172-183.

Jafari, S. M., Assadpoor, E., He, Y., & Bhandari, B. (2008). Re-coalescence of emulsion droplets during high-energy emulsification. Food Hydrocolloids, 22(7), 1191-1202.

Kabanov, A. V., Lemieux, P., Vinogradov, S., & Alakhov, V. (2002). Pluronic® block copolymers: novel functional molecules for gene therapy. Advanced drug delivery reviews, 54(2), 223-233.

Kabalnov, A. S., & Shchukin, E. D. (1992). Ostwald ripening theory: applications to fluorocarbon emulsion stability. Advances in Colloid and Interface Science, 38, 69-97.

Kabalnov (1998). Coalescence in emulsions, in Modern aspects of Emulsion Science, Binks, B.P., Ed., The Royal Society of Chemistry, UK, Chap 7.

Kandori, K. (1995). Applications of microporous glass membranes: membrane emulsification. Food Processing: Recent Developments, Elsevier, Amsterdam, 113-142.

Kerton, F. M., & Marriott, R. (2013). Alternative solvents for green chemistry (No. 20). Royal Society of chemistry.

Kim, S. I., & Lee, D. W. (2014). Toxicity of basil and orange essential oils and their components against two coleopteran stored products insect pests. Journal of Asia-Pacific Entomology, 17(1), 13-17.

Koyama, Y., Bando, H., Yamashita, F., Takakura, Y., Sezaki, H., & Hashida, M. (1994). Comparative analysis of percutaneous absorption enhancement by D-limonene and oleic acid based on a skin diffusion model. Pharmaceutical research, 11(3), 377-383.

Krishnaiah, Y. S. R., Satyanarayana, V., & Bhaskar, P. (2002). Influence of limonene on the bioavailability of nicardipine hydrochloride from membrane-moderated

transdermal therapeutic systems in human volunteers. International journal of pharmaceutics, 247(1), 91-102.

Kumar, S; Gupta, S. K.; (2013) Rosin: a naturally derived excipient in drug delivery systems. Polimery in medycynie 43 (1), 45-48

Leal-Calderon, F., Schmitt, V., & Bibette, J. (2007). Emulsion science: basic principles. Springer.

Ledward, D.A. (1986). Gelation of gelatin, in Functional Properties of Food Macromolecules, Mitchell, J.R., Ledward, D.A., Eds., Elsevier, London, UK, Chap 4.

Lee, C. M., Lim, S., Kim, G. Y., Kim, D., Kim, D. W., Lee, H. C., & Lee, K. Y. (2004). Rosin microparticles as drug carriers: Influence of various solvents on the formation of particles and sustained-release of indomethacin. Biotechnology and Bioprocess Engineering, 9(6), 476-481.

Lee, C. M., Lim, S., Kim, G. Y., Kim, D. W., Rhee, J. H., & Lee, K. Y. (2005). Rosin nanoparticles as a drug delivery carrier for the controlled release of hydrocortisone. Biotechnology letters, 27(19), 1487-1490.

Lifshitz, I. M., & Slyozov, V. V. (1961). The kinetics of precipitation from supersaturated solid solutions. Journal of Physics and Chemistry of Solids, 19(1), 35-50.

Lim, P. F. C., Liu, X. Y., Kang, L., Ho, P. C. L., Chan, Y. W., & Chan, S. Y. (2006). Limonene GP1/PG organogel as a vehicle in transdermal delivery of haloperidol. International journal of pharmaceutics, 311(1), 157-164.

Liu, S. X., & Mamidipally, P. K. (2005). Quality comparison of rice bran oil extracted with D-limonene and hexane. Cereal chemistry, 82(2), 209-215.

Lu, W. C., Chiang, B. H., Huang, D. W., & Li, P. H. (2014). Skin permeation of D-limonene-based nanoemulsions as a transdermal carrier prepared by ultrasonic emulsification. Ultrasonics sonochemistry, 21(2), 826-832.

Lu, H. Y., Shen, Y., Sun, X., Zhu, H., & Liu, X. J. (2013). Washing effects of limonene on pesticide residues in green peppers. Journal of the Science of Food and Agriculture.

Maldonado-Vaderrama, J. (2006) PhD. Universidad de Granada

Maldonado-Valderrama, J., Fainerman, V. B., Aksenenko, E., Jose Galvez-Ruiz, M., Cabrerizo-Vílchez, M. A., & Miller, R. (2005). Dynamics of protein adsorption at the oil–water interface: comparison with a theoretical model. Colloids and Surfaces A: Physicochemical and Engineering Aspects, 261(1), 85-92.

Maa, Y. F., & Hsu, C. (1996). Liquid-liquid emulsification by rotor/stator homogenization. Journal of controlled release, 38(2), 219-228.

Mamidipally, P. K., & Liu, S. X. (2004). First approach on rice bran oil extraction using limonene. European journal of lipid science and technology, 106(2), 122-125.

Marcuzzo, E., Debeaufort, F., Sensidoni, A., Tat, L., Beney, L., Hambleton, A., & Voilley, A. (2012). Release Behavior and Stability of Encapsulated D-Limonene from Emulsion-Based Edible Films. Journal of agricultural and food chemistry, 60(49), 12177-12185.

Marine, S. S., & Clemons, J. (2003). Determination of limonene oxidation products using SPME and GC-MS. Journal of chromatographic science, 41(1), 31-35.

Mason, T. J. (1999). Sonochemistry. New York, USA: Oxford University Press.

Mcclements, D. J. (2007). Critical review of techniques and methodologies for characterization of emulsion stability. Critical Reviews in Food Science and Nutrition, 47(7), 611-649.

Mcclements D.J. Food Emulsions Principles, Practices and Techniques. (2005) Boca Raton, Florida

McPartland T.Food grade insecticidal composition for repelling and killing ants, comprising D-limonene for controlling insect, non-toxic hydrophilic solvent and emulsifying agent to solubilize D-limonene in hydrophilic solvent. Patent Number: US2004092606-A1

Mitchell, J.R.; Ledward, D.A.; (1986), Funtional properties of Food Macromolecules, Elsevier, London, UK.

Miller, R., Fainerman, V. B., Makievski, A. V., Krägel, J., Grigoriev, D. O., Kazakov, V. N., & Sinyachenko, O. V. (2000). Dynamics of protein and mixed protein/surfactant

adsorption layers at the water/fluid interface. Advances in Colloid and Interface Science, 86(1), 39-82.

Miller, R., Fainerman, V. B., Aksenenko, E. V., Leser, M. E., & Michel, M. (2004). Dynamic surface tension and adsorption kinetics of β-Casein at the solution/air interface. Langmuir, 20(3), 771-777.

Morris, V.J., (1986). Gelation of polysaccharides, in Functional Properties of Food Macromolecules, Mitchell, J.R., Ledward, D.A., Eds., Elsevier, London, UK, Chap. 3

E. L. Neustadter, K. P. Whittingham and D. E. Graham, In Surface phenomena in enhanced oil recovery, ed. D. O. Shah, Plenum Press, New York, 1981, pp. 307–326.

Nguyen Hoang, T. K., La, V. B., Deriemaeker, L., & Finsy, R. (2002). Ostwald ripening of alkane in water emulsions stabilized by sodium dodecyl benzene sulfonate. Langmuir, 18(26), 10086-10090.

Pal, R. (2011). Rheology of simple and multiple emulsions. Current Opinion in Colloid & Interface Science, 16(1), 41-60.

Patil, J. R., Jayaprakasha, G. K., Murthy, K. N., Chetti, M. B., & Patil, B. S. (2010). Characterization of *Citrus aurantifolia* bioactive compounds and their inhibition of human pancreatic cancer cells through apoptosis. Microchemical Journal, 94(2), 108-117.

Pérez-Mosqueda, L. M., Maldonado-Valderrama, J., Ramírez, P., Cabrerizo-Vílchez, M. A., & Muñoz, J. (2013). Interfacial characterization of Pluronic PE9400 at biocompatible (air-water and limonene-water) interfaces. Colloids and Surfaces B: Biointerfaces.

Phipps, L. W. (1985). The high pressure dairy homogenizer (Vol. 6). National Institute for Research in Dairying.

Povey, M. J. W., & Mason, T. J. (1998). Ultrasound in food processing. New York, USA: Blackie Academic & Professional.

Quemada, D., & Berli, C. (2002). Energy of interaction in colloids and its implications in rheological modeling. Advances in colloid and interface science, 98(1), 51-85.

Ramírez, P., Muñoz, J., Fainerman, V. B., Aksenenko, E. V., Mucic, N., & Miller, R. (2011). Dynamic interfacial tension of triblock copolymers solutions at the water–hexane interface. Colloids and Surfaces A: Physicochemical and Engineering Aspects, 391(1), 119-124.

Reis, P., Miller, R., Kragel, J., Leser, M., Fainerman, V. B., Watzke, H., & Holmberg, K. (2008). Lipases at interfaces: unique interfacial properties as globular proteins. Langmuir, 24(13), 6812-6819.

Rizwan, M., Aqil, M., Ahad, A., Sultana, Y., & Ali, M. (2008). Transdermal delivery of valsartan: I. Effect of various terpenes. Drug development and industrial pharmacy, 34(6), 618-626.

Sainz, P., Sanz, J., Burillo, J., González-Coloma, A., Bailén, M., & Martínez-Díaz, R. A. (2012). Essential oils for the control of reduviid insects. Phytochemistry Reviews, 11(4), 361-369.

Schramm, L.L., (2005) Emulsions, Foams and Suspensions: Fundamentals and Applications, Wiley-VCH.

Schultz, S., Wagner, G., Urban, K., & Ulrich, J. (2004). High-Pressure Homogenization as a Process for Emulsion Formation. Chemical engineering & technology, 27(4), 361-368.

Sánchez, C. C., & Patino, J. M. R. (2005). Interfacial, foaming and emulsifying characteristics of sodium caseinate as influenced by protein concentration in solution. Food Hydrocolloids, 19(3), 407-416.

Sapra, B., Jain, S., & Tiwary, A. K. (2008). Percutaneous permeation enhancement by terpenes: mechanistic view. The AAPS journal, 10(1), 120-132.

Schröder, V., & Schubert, H. (1999). Production of emulsions using microporous, ceramic membranes. Colloids and Surfaces A: Physicochemical and Engineering Aspects, 152(1), 103-109.

Schultz, S., Wagner, G., Urban, K., & Ulrich, J. (2004). High-Pressure Homogenization as a Process for Emulsion Formation. Chemical engineering & technology, 27(4), 361-368.

Stang, M., Schuchmann, H., & Schubert, H. (2001). Emulsification in high-pressure homogenizers. Engineering in life sciences, 1(4), 151-157.

Strawbridge, K. B., Ray, E., Hallett, F. R., Tosh, S. M., & Dalgleish, D. G. (1995). Measurement of particle size distributions in milk homogenized by a microfluidizer: estimation of populations of particles with radii less than 100 nm. Journal of colloid and interface science, 171(2), 392-398.

Sun, J. (2007). D-Limonene: safety and clinical applications. Alternative Medicine Review, 12(3), 259.

Sun, H. Q., Zhang, L., Li, Z. Q., Zhang, L., Luo, L., & Zhao, S. (2011). Interfacial dilational rheology related to enhance oil recovery. Soft Matter, 7(17), 7601-7611.

Tadros, T. F. (2005). Applied surfactants: principles and applications. John Wiley & Sons.

Tadros, T. F. (2009). Emulsion science and technology: a general introduction. Emulsion science and technology. Wiley-VCH, Weinheim, 1-56.

Tadros, T. F. and Vincent B. (1993) in Enciclopedya of emulsion Technology (ed. Becher, P.) Marcel Deker, New York

Tan, C.T., Beverage emulsions, in Food Emulsions, 4th ed., Friberg, S., Larsson, K., Sjoblom, J., Eds., Marcel Dekker, New York, NY, Chap. 12

Taylor, P. (1998). Ostwald ripening in emulsions. Advances in Colloid and Interface Science, 75(2), 107-163.

Torcello-Gómez, A. (2012) PhD. Universidad de Granada

Torcello-Gómez, A., Maldonado-Valderrama, J., Martín-Rodríguez, A., & McClements, D. J. (2011). Physicochemical properties and digestibility of emulsified lipids in simulated intestinal fluids: influence of interfacial characteristics. Soft Matter, 7(13), 6167-6177.

Troy, D.A., Remington, J. P., Beringer, P., (2006). Remington: The Science and Practice of Pharmacy. Philadelphia: Lippincott Williams & Wilkins.

Vladisavljević, G. T., & Schubert, H. (2003). Preparation of Emulsions with a Narrow Particle Size Distribution Using Microporous α-Alumina Membranes. Journal of dispersion science and technology, 24(6), 811-819.

Vladisavljević, G. T., & Schubert, H. (2003). Influence of process parameters on droplet size distribution in SPG membrane emulsification and stability of prepared emulsion droplets. Journal of membrane science, 225(1), 15-23.

Wagner, C. (1961). Ostwald ripening theory. Ber. Bunsenges. Phys. Chem, 65, 581-591.

D. T. Wasan, F. S. Milos and P. E. DiNardo, In Interfacial phenomena in enhanced oil recovery, ed. D. T. Wasan and A. Payatakes, AIChE, New York, 1982, pp. 105–112.

J. Weers (1998). Molecular Diffusion in Emulsions and Emulsions Mixtures. in Modern aspects of Emulsion Science, Binks, B.P., Ed., The Royal Society of Chemistry, UK, Chap 6

Weiss, J., Gaysinsky, S., Davidson, M., & McClements, J. (2009). Nanostructured encapsulation systems: food antimicrobials. In IUFoST World Congress Book: Global Issues in Food Science and Technology (pp. 425-479).

Williams, P.A., Phillips, G.O. (2003). The use of hydrocolloids to improve food texture, in Texture in Flavours, Birch, G.G., Lindley, M.G., Eds., Elsevier, London, UK, p.1

Williams, A., & Prins, A. (1996). Comparison of the dilational behaviour of adsorbed milk proteins at the air-water and oil-water interfaces. Colloids and Surfaces A: Physicochemical and Engineering Aspects, 114, 267-275.

Wichtel, M. 2002. Teedrogen und Phytopharmaka. Stuttgart: Wissenschaftliche Verlagsgesellschaft. Yamaguchi, T.J. Caldwell, and P.B. Farmer

World Health Organization (1998).Concise international chemical assessment document nº5, Limonene.. Consultado el 23 de febrero de 2010

Wulff-Pérez, M., de Vicente, J., Martín-Rodríguez, A., & Gálvez-Ruiz, M. J. (2012). Controlling lipolysis through steric surfactants: New insights on the controlled degradation of submicron emulsions after oral and intravenous administration. International journal of pharmaceutics, 423(2), 161-166.

Zhang, Z., Vriesekoop, F., Yuan, Q., & Liang, H. (2014). Effects of nisin on the antimicrobial activity of D-limonene and its nanoemulsion. Food chemistry, 150, 307-312.

Zhao, K., & Singh, J. (1998). Mechanisms of percutaneous absorption of tamoxifen by terpenes: eugenol, D-limonene and menthone. Journal of controlled release, 55(2), 253-260.

2

Interfacial characterization of Pluronic PE9400 at biocompatible (air-water and limonene-water) interfaces.

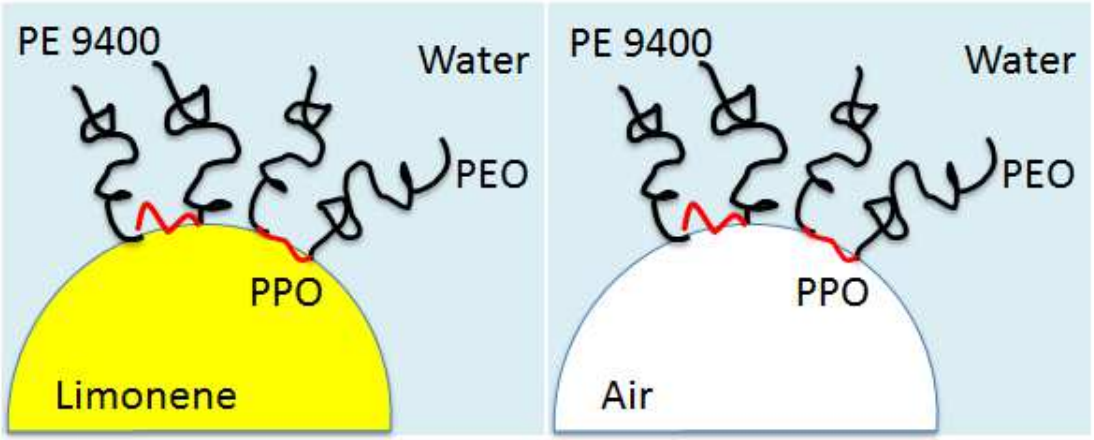

Abstract

In this work, we provide an accurate characterization of non-ionic triblock copolymer Pluronic PE9400 at the air-water and limonene-water interfaces, comprising a systematic analysis of surface tension isotherms, dynamic curves, dilatational rheology and desorption profiles. The surface pressure isotherms display two different slopes of the Π-c plot suggesting the existence of two adsorption regimes for PE9400 at both interfaces. Application of a theoretical model, which assumes the coexistence of different adsorbed states characterized by their molar areas, allows quantification of the conformational changes occurring at the adsorbed layer, indentifying differences between the conformations adopted at the air-water and the limonene-water interface. The presence of two maxima in the dilatational modulus vs. interfacial pressure importantly corroborates this conformational change from a 2D flat conformation to 3D brush one. Moreover, the dilatational response provides mechanical diferences between the interfacial layers formed at the two interfaces analysed. Dynamic surface pressure data were transformed into a dimensionless form and fitted to another model which considers the influence of the reorganization process on the adsorption dynamics. Finally, the desorption profiles reveal that Pluronic PE9400 is irreversibly adsorbed at both interfaces regardless of the interfacial conformation and nature of the interface. The systematic characterization presented in this work provides important new findings on the interfacial properties of pluronics which can be applied in the rational development of new products, such as biocompatible limonene-based emulsions and/or microemulsions.

2.1 Introduction

Pluronics are non-ionic triblock copolymers also known as polaxamers. They are formed by two hydrophilic side chains of poly(ethylene oxide), PEO, and a central hydrophobic chain of poly(propylene oxide), PPO. They are often denoted as (PEOx-PPOy-PEOx), where x and y are the repeating PEO and PPO units respectively. They have many applications in fields such as cosmetics, pharmaceutical industry, emulsification and foaming (Alexandridis, 2000; Berthier, 2010; Leal-Calderón, 2007; Li, 2010; Schramm, 2005; Tadros, 2003; Tadros, 2005; Tavano, 2010; Zoller, 2009; Bai, 2010). Recent investigations deal with the application of pluronics in the development of more complex systems. For example, the use of block copolymers in gene therapy is a promising area of research (Kabanov, 2002). In addition, their biocompatibility has boosted their application in the design of drugs with improved long-circulating properties (Torcello-Gómez, 2011a). Finally, their use in delaying lipid digestion is being applied in the development of food products with satiating effects (Torcello-Gómez, 2011b; Wulff-Pérez, 2010; Wulff-Pérez, 2012). All these applications involve events occurring at the interface and hence, an improved understanding of the surface properties of pluronics is important in order to rationally design biotechnological systems.

The surface properties of some pluronics have been studied in the literature by means of different techniques such as dynamic and equilibrium surface tension, ellipsometry, surface rheology and neutron reflectivity at the air-water and hexane-water interfaces (Blomqvist, 2005; Hambardzumyan, 2004; Kim, 2003; Monroy, 2009; Muñoz, 2000a; Muñoz, 2000b; Noskov, 2000; Noskov, 2006; Noskov, 2010; Sedev, 2002; Vieira, 2002; Ramírez, 2011; Torcello-Gómez, 2012; Llamas, 2013). Some of these studies show the occurrence of conformational changes within the adsorbed layer

of Pluronics at the interface when increasing the amount of adsorbed polymer, suggesting that the conformation of Pluronic molecules changes from a 2D flat conformation to a 3D brush/mushroom one at the interface (Blomqvist, 2005; Hambardzumyan, 2004; Muñoz, 2000a). Traditionally, scaling theories have been used to explain the conformation of the adsorbed polymer. Only recently, the equilibrium surface pressure isotherms have been fitted with thermodynamic theories which take into account this reorganization process (Ramírez, 2011; Torcello-Gómez, 2012; Llamas, 2013). Nevertheless, the morphology of pluronic interfacial layers remains to be fully understood, especially with respect to applications in emulsification processes. Also, recent studies on the dynamic adsorption of the Pluronics triblock copolymer have revealed that a slow reorganization process at the interface has to be considered along with diffusion (Muñoz, 2000b). These studies deal with model interfaces and the properties of pluronics still need to be validated at more realistic interfaces. This work presents a systematic characterization of the Pluronic PE9400 at the air-water and limonene-water interfaces. Limonene is an interesting bio-derived solvent which has been used in food (Jafari, 2012; Marcuzzo, 2012; Klein, 2010) and pharmaceutical applications (Murali, 2013), and in the formulation of biocompatible microemulsions (Papadimitriou, 2008). Furthermore, limonene is an interesting candidate to be used as (bio)solvent, replacing more polluting solvents such as hexane or xylene (Kerton, 2009) in agrochemical formulations. Hence, the interfacial characterization of PE9400 at the limonene/water interface validates the previous work in a more realistic and practical scenario. The experimental results have been analysed in the framework of a previously reported model originally developed for protein adsorption which has recently been used as a model for Pluronics adsorption at the hexane-water interface (Ramírez, 2012). Hence, this work provides a systematic study showing a sequence of surface, dynamic,

rheological and desorption (Torcello-Gómez, 2012; Svitova, 2005)] properties of Pluronics. The combination of measurements along with the theoretical fitting of the experimental curves provides a thorough characterization, complementing work in the literature on pluronics and enabling the interpretation of interfacial conformation at a molecular level. These new findings can have applications concerning the rational design of biotechnological complex systems with different applications.

2.2 Materials, methods and models

2.2.1. Material

The triblock copolymer Pluronic PE9400 (PEO_{21}-PPO_{50}-PEO_{21}, Mw = 4600 $gmol^{-1}$ and HLB = 12-18) was kindly provided by BASF and used as received. The hydrophilic-lipophilic balance value of PEO-PPO-PEO non-ionic triblock copolymers is defined as HLB = 20 $M_{w,PEO}/M_w$, where $M_{w,PEO}$ is the molecular weight of the hydrophilic PEO units and M_w is the total molecular weight.

D-Limonene (4-isopropenyl-1-methylciclohexane) is an organic compound widely used as an industrial solvent. It is obtained from the peel of citrus fruit, mainly from oranges and lemons. D-Limonene 97% was purchased from Sigma-Aldrich® and purified with Florisil® resins (Fluka, 60-10 mesh) prior to use by following the procedure used elsewhere (Maldonado-Valderrama, 2005; Maldonado-Valderrama, 2010). Namely, a mixture of oil and Florisil® in proportion 2:1 w/w was shaken gently for 3 h and then filtered with Millex® filters (0.1μm PDVF) and stored under nitrogen in the dark. The interfacial tension of the purified limonene oil-water interface was measured before every experiment, in order to confirm the absence of surface-active contaminants, yielding values of 44.0±0.5 mN m-1 at 20°C.

Ultrapure water, cleaned using a Milli-Q water purification system (0.054 μS), was used. All glassware was washed with 10% Micro-90 cleaning solution and exhaustively rinsed with tap water, isopropanol, deionized water, and ultrapure water in this sequence. All other chemicals used were of analytical grades and used as received. All measurements were carried out at 20^0C. The reproducibility of the experiments was tested by performing at least three replicate measurements in all cases, obtaining values for the standard deviation within (0.5 mN/m).

2.2.2 Drop profile tensiometry

The OCTOPUS, a drop profile analysis tensiometer based on axisymmetric drop shape analysis (ADSA), which has been fully designed and developed at the University of Granada, was used in this study (Cabrerizo-Vilchez, 1999). The image capturing, the micro-injector and the ADSA algorithm are managed by a Windows integrated program (DINATEN®). The solution droplet is formed at the tip of a double capillary which is inside a thermostated cuvette at 20ºC containing the less dense phase (air or limonene). The interfacial tension, γ, and the interfacial area, A, are calculated by fitting the drop profiles to the Young–Laplace equation of capillarity. The surface pressure is defined as $\Pi = \gamma_0 - \gamma$, where γ is the interfacial tension of the polymer solution against air or limonene, and γ_0 is the interfacial tension of the pure interface (γ_0 = 72,8±0.2 mNm^{-1} for the air-water interface and γ_0 = 44.0±0.5 mNm^{-1} for the limonene-water interface at 20ºC).

The dilatational rheology of the adsorbed Pluronic films was studied by small harmonic oscillations of the interfacial area in order to avoid excessive perturbation of the interface (<5% ΔA). The system records the response of the surface tension to this

area deformation (Myrvold 1998). In a general case, the dilatational modulus (*E*) is a complex quantity that contains a real and an imaginary part:

$$E(i\omega) = E' + iE'' \quad (1)$$

where the real part, *E'*, is called the storage modulus and coincides with the dilatational interfacial elasticity, and the imaginary part, *E''*, is called the loss modulus and it is related to the dilatational interfacial viscosity.

Finally, the double capillary allows us to carry out desorption studies by exchanging the subphase of the drop by pure buffer as explained elsewhere (Cabrerizo-Vilchez, 1999). The initial volume of the drop was replaced 80 times to ensure the complete removal of the polymer in the subphase while monitoring the interfacial tension.

2.2.3 Theoretical models

2.2.3.1 Equilibrium isotherm

The theoretical model used to fit the experimental data of adsorption was developed by Fainerman and co-workers originally to explain the experimental surface properties of adsorbed proteins (Fainerman, 2003; Miller, 2004; Maldonado-Valderrama, 2005; Alahverdjieva, 2005). This model has been applied recently to fit the experimental surface pressure isotherm of several Pluronics at the hexane-water interface assuming that polymers can adsorb in different adsorbed states characterized by their molar area, ω (Ramírez, 2011). In order to proceed with the fitting accurately the authors distinguish two behavioural regions in the isotherm: the "pre-critical" and the "post-critical" ones, the critical point being defined by the critical surface pressure, Π^*, which corresponds to the two-dimensional condensation onset.

Pre-critical regime

In both regimes the relevant physical parameters are: ω_m, the maximum molar area occupied by the adsorbed molecules, ω_1, the molar area at high surface coverage and ω_0, the molar area of the solvent or the molar area of one segment of the polymer molecule. The number of adsorbed states, n, is given by:

$$n = \frac{(\omega_m - \omega_1)}{\omega_0} + 1 \tag{2}$$

The equation of state is given by:

$$\Pi = -\frac{RT}{\omega_0}\left[\ln(1-\Gamma\omega) + \Gamma(\omega-\omega_0) + a(\Gamma\omega)^2\right] \tag{3}$$

where $\Pi = \gamma_0 - \gamma$, is the surface pressure, R is the Boltzmann constant, T the temperature and a reflects the interaction between the adsorbed molecules. Γ, is the total surface concentration which is the sum of the molecules adsorbed in each state, Γ_i, ($\Gamma = \sum_{i=1}^{n} \Gamma_i$) and ω is the mean molar area and is defined as: $\omega\Gamma = \sum_{i=1}^{n} \omega_i \Gamma_i$ where the partial adsorption in each state, Γ_i, is:

$$\Gamma_i = \Gamma \frac{(1-\Gamma\omega)^{\frac{\omega_i-\omega_1}{\omega}} \exp\left[\left(\frac{\omega_i-\omega_1}{\omega}\right)(2a\Gamma\omega)\right]}{\sum_{i=1}^{n}(1-\Gamma\omega)^{\frac{\omega_i-\omega_1}{\omega}} \exp\left[\left(\frac{\omega_i-\omega_1}{\omega}\right)(2a\Gamma\omega)\right]} \tag{4}$$

The adsorption isotherm for each state is given by:

$$b_i c = \frac{\Gamma_i \omega}{(1-\Gamma\omega)^{\omega_i/\omega}} \exp\left[-2a\left(\frac{\omega_i}{\omega}\right)\Gamma\omega\right] \tag{5}$$

where c is the surfactant bulk concentration and b_i is the adsorption equilibrium constant of the polymer in the state i. It is assumed that the adsorption equilibrium values are constant for all the states, hence the total adsorption constant is: $b = \sum_{i=1}^{n} n b_i$.

Post-critical regime

In this regime three additional parameters are used: the compressibility coefficient, ε, the number of multilayers, m, and the adsorption coefficient for the adsorption of the second and subsequent layers, b_2. ε is introduced to account for the decrease in the area occupied per molecule due to condensation. From this parameter a new auxiliary variable is defined:

$$\Psi = \frac{\Gamma}{\Gamma^*} \exp\left(\varepsilon \frac{\Pi - \Pi^*}{RT} \omega \right) \tag{6}$$

where, Π^* and Γ^* are the values of the critical surface pressure and critical surface concentration, respectively. Therefore, the adsorption isotherm and the equation of state become:

$$b_i c = \frac{\Gamma_i \omega \exp\left[-\frac{\omega_i}{\omega \Psi} (2a\Gamma\omega) \right]}{(1 - \Gamma\omega)^{\omega_i / \omega\Psi}} \tag{7}$$

$$\Pi = -\frac{RT}{\Psi \omega_0} \left[\ln(1 - \Gamma\omega) + \Gamma(\omega - \omega_0) + a(\Gamma\omega)^2 \right] \tag{8}$$

It is assumed that surface pressure values are not affected by the adsorption of the subsequent layers and the coverage of the multilayers is proportional to an adsorption coefficient b_2 and the preceding surface concentration. So, as a rough approximation the surface concentration of the second and subsequent layers, Γ_Σ, is given by:

$$\Gamma_{\Sigma} = \Gamma \sum_{i=1}^{m} \left(\frac{b_2 c}{1 + b_2 c} \right)^{i-1} \quad (9)$$

The software package Protein M, (Aksenenko, 2012) has been used to fit surface pressure isotherm data to the model explained above.

2.2.3.2 Dilatational rheology

According to the diffusional model (Zholob, 2009; Lucassen, 1972) the interfacial elasticity, which is directly linked to the dilatational modulus, *E* can be calculated by the following equation:

$$E = \frac{E_0}{\sqrt{1 + 2\zeta + 2\zeta^2}} \quad (10)$$

where E_0 is the limiting elasticity which is defined as:

$$E_0 = \left(\frac{d\Pi}{d \ln \Gamma} \right)_{eq} \quad (11)$$

the parameter ζ is defined as:

$$\zeta = \sqrt{\frac{\omega_0}{\omega}} \quad (12)$$

where ω is the angular frequency of the measurement and ω_0 is the characteristic frequency of the diffusion process and can be written as:

$$\omega_0 = \left(\frac{dC_S}{d\Gamma} \right)^2 \frac{D}{2} \quad (13)$$

C_s being the bulk concentration and *D* the diffusion coefficient.

2.2.3.3 Adsorption kinetics

The experimental data (surface tension vs. time) have been transformed into the dimensionless variables, θ and *t'*, according to the scaling argument for diffusion controlled adsorption proposed by Ferri et al. (Ferri, 2000):

$$\theta = \frac{\gamma(t) - \gamma_{eq}}{\gamma_0 - \gamma_{eq}} \tag{14}$$

$$t' = \frac{t}{\tau_D} \tag{15}$$

where $\gamma(t)$, γ_0 and γ_{eq} are the surface tension, the surface tension of the pure interface and the equilibrium surface tension, respectively. τ_D is the characteristic time scale for the diffusion process and is a function of the diffusion coefficient, *D*, and the adsorption depth, *h*:

$$\tau_D = \frac{h^2}{D} \tag{16}$$

The adsorption depth can be calculated from mass balance on a differential area, *dA*:

$$\Gamma_{eq} dA = C_0 h dA \rightarrow h = \frac{\Gamma_{eq}}{C_0} \tag{17}$$

where Γ_{eq} stands for the equilibrium surface concentration and C_0 is the surfactant bulk concentration.

In order to fit the experimental dynamic surface tension values a model which combines the diffusion of the polymer to the interface with the subsequent reorientation has been used (Serrien, 1992). The proposed equation for the dimensionless dynamic surface tension reads as follows:

$$\theta(t') = \left[(1-B) \exp\left[-\left(\frac{4}{\pi} t' \right)^{1/2} \right] + B \right] \exp(-At') \tag{18}$$

where $B = \frac{\beta}{\gamma_0 - \gamma_{eq}}$ and $A = \frac{\tau_D}{\tau_R}$. β and τ_R are the amplitude and characteristic time of the reorganization process, respectively. When $\beta = 0$ and $\tau_R >> \tau_D$ equation (18) reduces to a pure diffusional process:

$$\theta(t') = \exp\left[-\left(\frac{4}{\pi}t'\right)^{1/2}\right] \quad (19)$$

This model has been previously used to explain the adsorption kinetics of other Pluronics (Muñoz, 2000b).

2.3 Results and Discussion

2.3.1 Equilibrium surface pressure isotherms

Figures 1A and 1B show the interfacial pressure isotherms (Π-c) obtained for Pluronic PE9400 adsorbed at the air-water interface and the limonene-water interface respectively. The interfacial pressure values plotted in Figures 1A and 1B were obtained after 3 hours of adsorption at constant interfacial area. After this period, the interfacial layer has settled and the changes of interfacial tension remain below 5%. Both figures show a non-monotonous increase in the interfacial pressure as a function of bulk concentration. Namely, Figures 1A and 1B show two separate regions: first an increase in the interfacial pressure as the bulk concentration increases and finally a constant value once the interfacial layer is saturated, accounting for a critical aggregation concentration, cac. Within the first region we can also distinguish two regimes (pre-critical and post-critical) which differ in the slope of the increasing tendency of Π. This type of behaviour has previously been reported for pluronics adsorbed at the air-water interface and at the hexane–water interfaces but not at the limonene-water interface (Muñoz, 2000a; Ramírez, 2011). The occurrence of this kink before the cmc is likely to be due to a conformational change at the interface in which the polymer changes its orientation from 2D flat conformation to a 3D brush or mushroom one as reported in the literature for other Pluronics (Muñoz, 2000a; Muñoz, 2000b; Ramírez, 2011; Ramírez, 2012; Torcello-Gómez, 2012; Llamas, 2013). Figures 1A and 1B reveal that adsorption

in a flat conformation leads to a higher slope in the Π-c isotherm due to the high interfacial area occupied by each molecule leading to larger changes in the interfacial coverage, and hence, in the interfacial pressure. Once the interface is saturated with flat molecules the increase of Π is less pronounced. Further adsorption at the post-critical regime could lead to the formation of multilayers, condensation of the adsorbed polymer layer, aggregation within the interfacial layer and/or penetration into the oil phase. Interestingly, these regimes appear at both the air-water and the limonene-water interface. The main difference is the length of the first adsorption regime (2D-flat conformation) which is larger at the limonene-water interface (Figure 1B). This already suggests structural differences in the adsorbed layer of PE9400 at air-water and limonene-water interfaces. Furthermore, the interfacial pressure of a saturated interface appears higher for PE9400 at the limonene-water interface, hence demonstrating a higher adsorption recorded at the oil-water interface as compared to the adsorption at the air-water interface (Maldonado-Valderrama, 2005). The cac of PE9400 is slightly higher at the limonene-water interface ($cac_{limonene\text{-}water}$ = 0,05 $molm^{-3}$ > $cac_{air\text{-}water}$ = 0,01 $molm^{-3}$) also accounting for this feature.

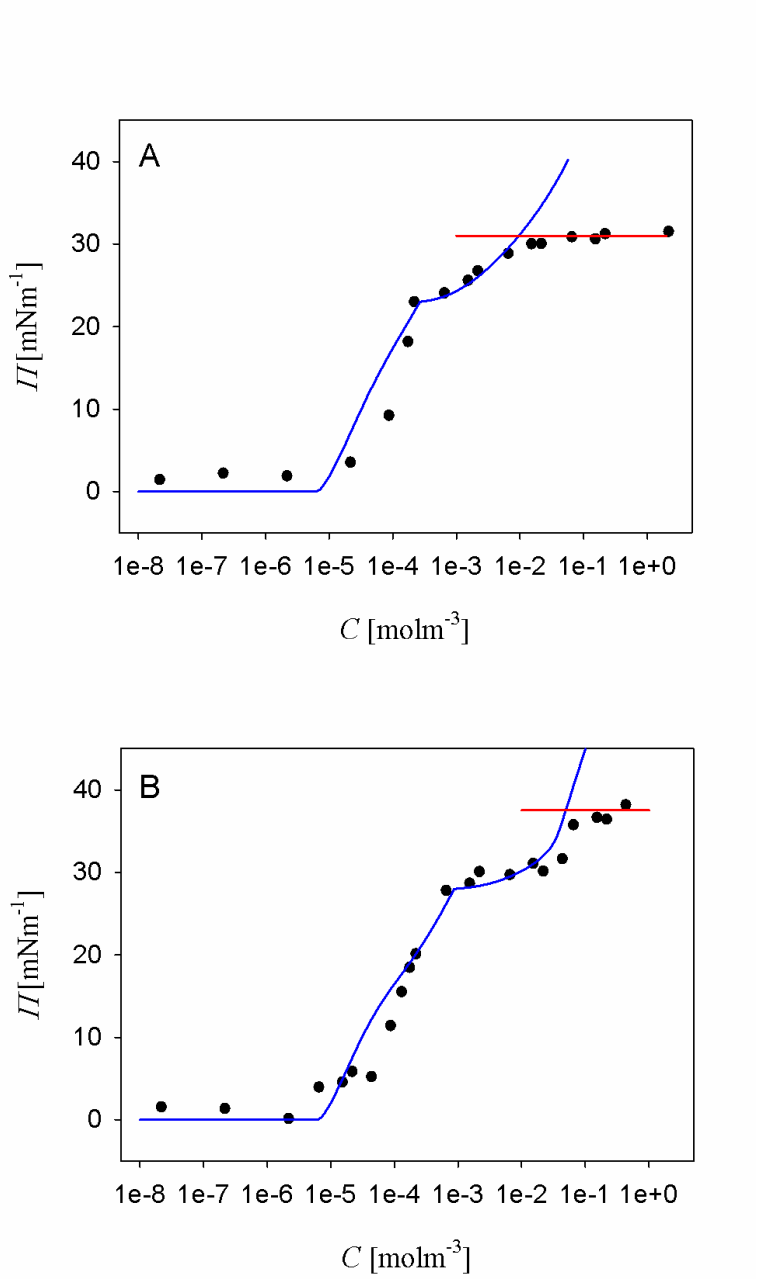

Figure 1. A) Surface pressure isotherm for Pluronic PE9400 at the air-water interface at T = 25ºC. B) Surface pressure isotherm for Pluronic PE9400 at the air-water interface at T = 25ºC. The blue line is the best fit to the protein adsorption model with the values of the parameters given in Table 1. The crossing of the blue line with the red line indicates the value of the cac. The standard deviation of each data point is ±0.5 mN/m.

In order to gain further insight into the different conformation and condensation of the interfacial layer of PE9400 at the air-water and the limonene-water interface we applied the theoretical model explained above to the experimental data

displayed in Figures 1A and 1B. The lines in Figures 1A and 1B are the best fit of the experimental data obtained with parameters given in Table 1. Since there are many adjusting parameters the experimental data can be fitted with a high number of different combinations of them. In order to obtain a meaningful physical result, two of the parameters, ($\omega_0 = 2{,}4\cdot 10^5 \ \frac{m^2}{mol}$, $\omega_m = 3{,}0\cdot 10^7 \ \frac{m^2}{mol}$), have been fixed according to the values given in a previous work for the adsorption of the same polymer at the hexane-water interface (Ramírez, 2011). Hence, we consider that the molar area occupied by a segment of the polymer, ω_0, and the maximum molar area, ω_m, are intrinsic properties of the polymer and do not depend on the nature of the non-polar phase. Accordingly, the only fitting parameters are: ω_1, the minimum molar area (this parameter can be different since it is likely that the hydrophobic segments of the polymer can dissolve or penetrate into the oil phase while this is not possible at the air-water interface), a, the interaction parameter, ε, the condensation parameter and when multilayer formation is considered, b_2 and m in the post-critical regime.

Table 1 shows a lower value of ω_1 of PE9400 at the limonene-water interface than that obtained at the air-water. This agrees with the experimental findings discussed above suggesting the formation of a more compact layer at the limonene-water interface at high interfacial coverage. This could be the result of PPO segments penetrating into the limonene in agreement with recent work which demonstrates the penetration of PPO segments into the hexane phase by ellipsometric measurements (Ramírez, 2012). The same value of a at both interfaces indicates that the attractive interaction between adsorbed polymer molecules is similar at the air-water and the limonene-water interface. Conversely, the value of ε appears much higher at the limonene-water interface. This accounts for an increased compressibility of the PE9400 at the oil-water interface that

would possibly promote higher interfacial coverage and lead to higher condensation of the interfacial layer. In general, the higher condensation of the adsorbed layer of PE9400 at the limonene-water interface, which was already inferred from the experimental Π-c isotherms, is corroborated and rationally quantified by the outcome of the fitting procedure. Moreover, the numerical values displayed in Table 1 importantly quantify this increased condensation by means of the lower molar area (ω_1), the higher saturation Π and the higher compressibility (ε) of the molecule at the limonene-water interface. The values of the interfacial pressure isotherm are not affected by introducing the parameters of multilayer formation. However, they are given in Table 1 since they affect the fitting of the dilatational rheology, as will be explained in next section (Maldonado-Valderrama, 2005).

2.3.2 Interfacial dilatational rheology

In order to explore in more detail the interfacial behaviour of the copolymer at the air-water and the limonene-water interfaces the dilatational rheology of these systems was measured (Figures 2A and 2B). The dilatational modulus was obtained by imposing harmonic perturbations to the interface at a frequency of 0,1 Hz after equilibration of the interfacial layer. Figures 2A and 2B show the dilatational modulus measured at the end of the adsorption process recorded for each of the bulk concentrations shown in Figures 1A and 1B. Also, since it has been reported previously that the interfacial elasticity of these copolymers is a unique function of the interfacial pressure (i.e. interfacial coverage) (Blomqvist, 2005; Torcello-Gómez, 2012), harmonic oscillations were performed throughout the whole adsorption process for a given concentration of PE9400 in the bulk. These values are also plotted in Figures 2A and 2B, hence confirming that *E* is directly linked to the interfacial pressure rather than the polymer bulk concentration.

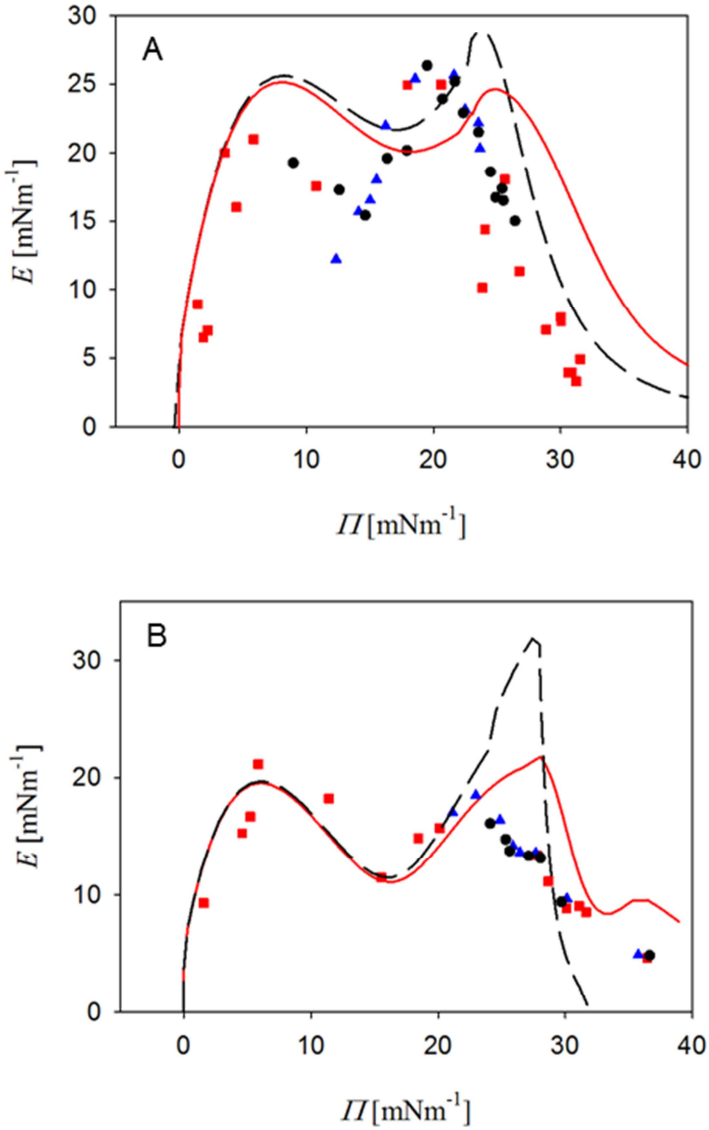

Figure 2. A) Surface dilatational elasticity vs. surface pressure for Pluronic PE9400 at the air-water interface. B) Interfacial dilatational elasticity vs. interfacial pressure for Pluronic PE9400 at the limonene-water interface. Black circles are the surface elasticity calculated once the final surface pressure was reached for each bulk concentration. Red squares and blue triangles are two independent measurements of the surface elasticity for a given bulk concentration ($2{,}2 \cdot 10^{-3}$ $molm^{-3}$) at different adsorption times. Solid and dashed lines correspond to a theoretical dilatational modulus calculated via equation (10) for a harmonic perturbation of 0,1 Hz and a diffusion coefficient of $1 \cdot 10^{-10}$ m^2s^{-1} (air-water) and $2 \cdot 10^{-10}$ m^2s^{-1} (limonene-water) with the equilibrium model parameters of Table 1 and m = 2 (bilayer, solid line) and m = 1 (monolayer, dashed line), respectively. The standard deviation of each data point is ± 0.5 mN/m.

The existence of two maxima in the elasticity of the interfacial layer was expected in the literature owing to the conformational transition taking place (Torcello-Gómez, 2012; Muñoz, 2003) but very few works specifically report two maxima (Blomqvist, 2005; Noskov, 2006; Ramírez, 2012; Muñoz, 2003). Recently, the occurrence of three maxima (two of them at low surface pressure) was reported for a more hydrophilic Pluronic F68 at the air/water interface by means of electrocapillary wave and quasi-elastic light scattering, a technique capable of measuring at very high frequencies (up to $1 \cdot 10^6$ Hz) (Llamas, 2013). The first maximum, located at low interfacial pressures, i.e. low interfacial coverage, corresponds to the 2D conformation of the molecules which lie fully extended at the interface (Blomqvist, 2005). This conformation provides similar elasticity values (20 mN/m) regardless of the nature of the interface. This is consistent with the theoretical analysis which provides the same maximum molar area (ω_{max}) and interaction parameter (a) at both interfaces (Table 1) and only shows differences in the molecular conformation at high interfacial pressures, i.e. when the interaction is maximized. The second maximum would correspond to a 3D brush conformation of the polymer in which the PPO segment protrudes into the oil phase. Interestingly, this maximum appears displaced to higher interfacial pressures at the limonene-water interface, importantly corroborating the higher interfacial coverage attained at the oil-water interface.

Figures 2A and 2B also show theoretical predictions of E as a function of Π. The theoretical values were obtained via equation (10). The limiting elasticity, E_0 and characteristic frequency are related to the equilibrium properties of the adsorbed film by equations, (11-13).

Therefore, with the equilibrium model parameters (Table 1) the only adjusting parameter is the diffusion coefficient. The solid lines in Figures 2A and 2B show the

best fit to the experimental data at air-water and limonene-water interfaces with diffusion coefficients of $1 \cdot 10^{-10}$ m^2s^{-1} and $2 \cdot 10^{-10}$ m^2s^{-1}, respectively. Diffusion coefficients of similar Pluronics determined by different techniques such as dynamic surface tension, time-resolved ellipsometry and dynamic quasielastic light-scattering measurements at the air-water interface have been reported to be in the range 0,6-$1{,}5 \cdot 10^{-10}$ m^2s^{-1} (Muñoz 2000b) in concordance with our result. Furthermore, in a recent paper the dynamic surface tension of Pluronic PE9400 and similar Pluronics at the hexane-water interface was calculated between 1,5-$3{,}5 \cdot 10^{-10}$ m^2s^{-1} (Ramírez, 2011), which is slightly higher than the diffusion coefficient obtained at the limonene-water interface in the present work. Figures 2A and 2B also show the theoretical predictions considering either a monolayer or a bilayer adsorption. It is seen that considering bilayer adsorption at the air-water interface does not significantly enhance the agreement with the experimental data whereas it importantly improves the fitting at the limonene-water interface. Application of the theoretical model in this way provides important new information about the interfacial conformation of pluronics at interfaces.

2.3.4 Adsorption kinetics

Figures 3A and 4A show the adsorption kinetics of PE9400 at the air-water and the limonene-water interface, respectively. For the sake of clarity only three concentrations have been plotted in each figure. The original data were transformed into a dimensionless form according to equation 11 and 12. Hence, Figures 3B and 4B show the θ vs. t' plot, where $\theta = (\gamma(t)-\gamma_{eq})/(\gamma_0-\gamma_{eq})$ and $t'=t/\tau_{D,}$ (see section 2.3 for a detailed explanation of the parameters). Whereas γ_{eq}, γ_0, γ and t are experimental values, τ_D has to be calculated. The diffusion time scale, τ_D, is determined from the diffusion

coefficient, *D*, and the adsorption depth, *h*, as described in equations 13 and 14. Since *h* is determined by the equilibrium adsorption isotherm, a τ_D value for each concentration can be calculated from the experimental data, depending only on the value of the diffusion coefficient, *D*. In order to obtain the *D* values the theoretical dependence of θ vs. *t'* for a pure diffusion process (equation 16), which gives a unique curve, are plotted in Figures 3B and 4B (blue line). Hence, *D* values that best fit the theoretical plot are selected (ca. $1 \cdot 10^{-10}$ m^2s^{-1} for air-water interface and $2 \cdot 10^{-10}$ m^2s^{-1} for limonene-water interface). The values used agree with the previously reported ones which are in the range 0,6-3,5$\cdot 10^{-10} m^2s^{-1}$ (Muñoz, 2000b; Ramírez, 2011). It is seen that at the air water interface the experimental data agree well with a diffusion-controlled adsorption. On the contrary, at the limonene-water interface the experimental data deviate from the behaviour of a pure diffusion adsorption. Previous works show the occurrence of a slower reorganization process which follows the first diffusion step in the adsorption kinetic of Pluronics at fluid and solid interfaces (Muñoz, 2000b; Guzmán, 2011). In order to take into account this slower process a theoretical model developed elsewhere (Serrien 1992) was used. Two extra parameters, accounting for the amplitude, *B*, and time scale, *A*, of the reorganization process, are included, (see equation 18, section 2.3). Hence, a more favourable interaction between the polymer and limonene rather than air, in agreement with the discussion of the adsorption behaviour and the dilatational curves, is also inferred from adsorption kinetics measurements.

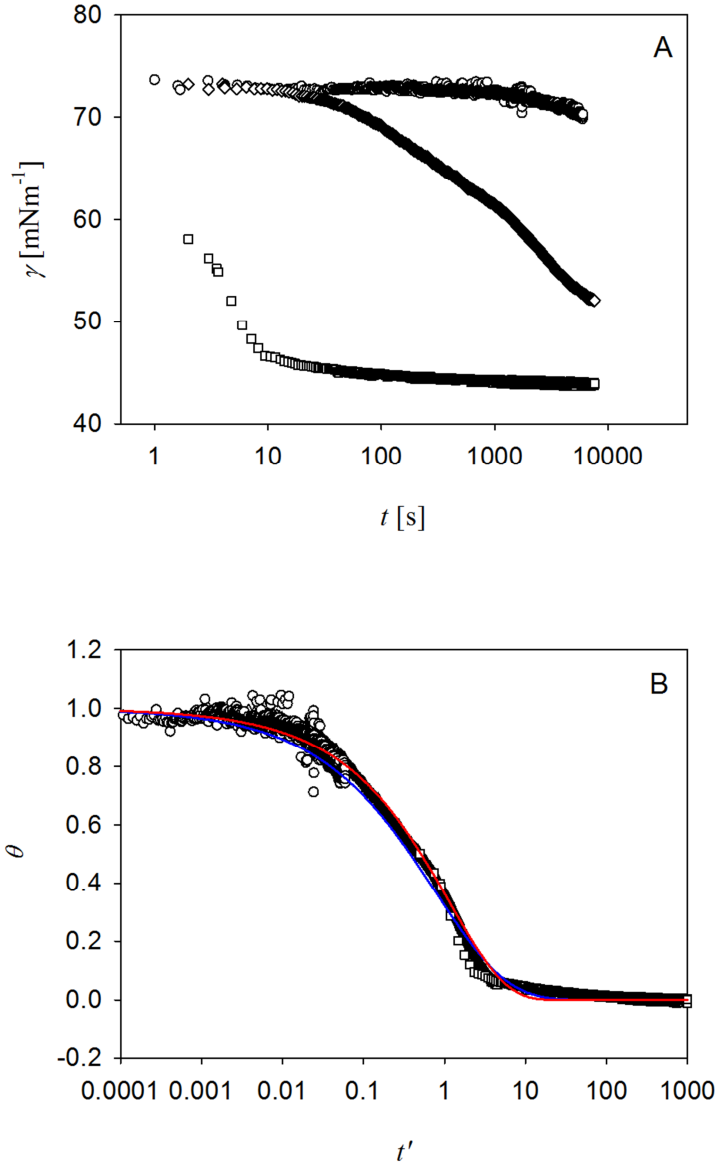

Figure 3. A) Dynamic surface tension for Pluronic PE9400 at the air-water interface for the following polymer bulk concentrations: $2{,}7\cdot10^{-5}$ molm^{-3} (circles); $1{,}7\cdot10^{-4}$ molm^{-3} (diamonds) and $6{,}5\cdot10^{-3}$ (squares). B) Dimensionless dynamic surface tension plot from the experimental data of Figure 3A as explained in the text. The blue line is the theoretical dependence according to a purely diffusional process. The standard deviation of each data point is ± 0.5 mN/m.

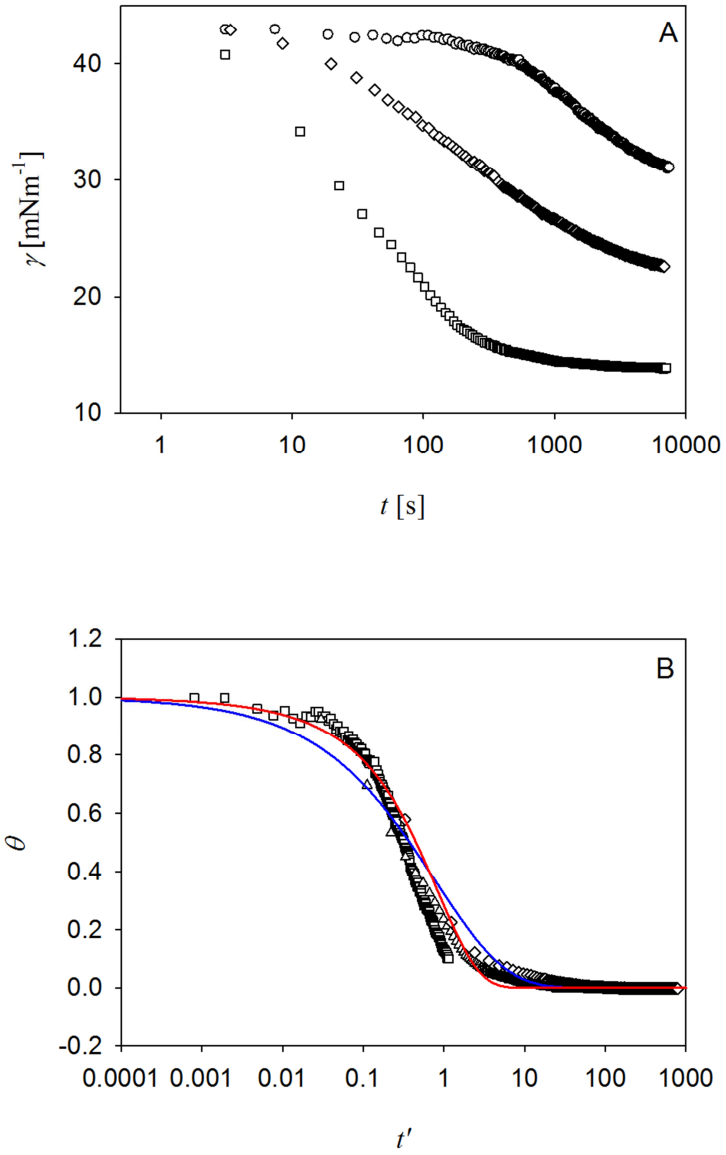

Figure 4. A) Dynamic surface tension for Pluronic PE9400 at the limonene-water interface for the polymer bulk concentrations: 8,7·10^{-5} molm^{-3} (circles); 2,2·10^{-4} molm^{-3} (diamonds) and 1,5·10^{-3}molm^{-3} (squares). B) Dimensionless dynamic surface tension plot from the experimental data of Figure 4A as explained in the text. The blue line is the theoretical dependence according to a purely diffusional process, whereas the red line is the theoretical dependence when a reorganization process is also considered. The standard deviation of each data point is ± 0.5 mN/m.

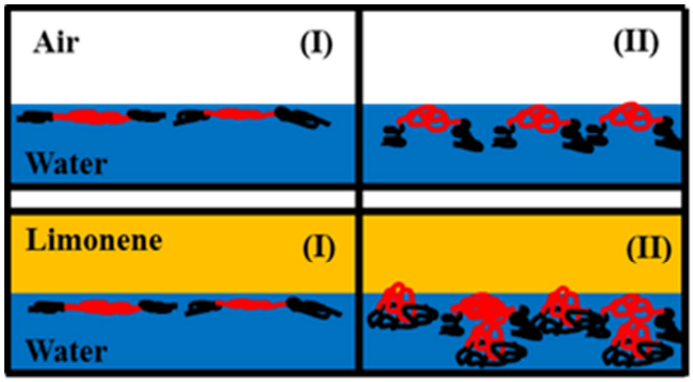

Figure 5. Sketch of the different conformational changes occurring as long as the polymer adsorbs at the interface. The red segment stands for PPO units, whereas the black one represents the PEO units. The oil phase is orange and the aqueous phase is blue. (I) represents the flat 2D conformation at low Π values, whereas (II) are the 3D conformation for high Π values.

2.3.5 Desorption process

Finally, the desorption behaviour of PE9400 from the air-water interface and the limonene-water interface was studied. This is done by exchanging the bulk solution for that of a buffer, hence depleting the subphase of the drop of polymer. This methodology allows the investigation of the reversibility of the adsorption process and the desorption profile. Figure 5 shows the evolution of the interfacial tension throughout the whole exchange process for two different concentrations at both interfaces (air-water and limonene-water). The solid lines in Figure 5 mark the beginning of the exchange of the bulk solution once a stable layer had adsorbed at the interface. It can be seen that the interfacial tension remains constant for the lower concentrations at both interfaces (Figure 5A), whereas a slight increase (about 2 mNm^{-1}) is observed for the higher concentration of PE9400, also at both interfaces. These results importantly complement the findings of Svitova (Svitova, 2005) and Torcello Gómez et al (Torcello-Gómez, 2012) for the adsorption/desorption of Pluronic F68, demonstrating that Pluronic PE9400 is adsorbed irreversibly at both interfaces. Moreover, the desorption profile

obtained also reveals that this anchoring at the interface is independent of the conformation of the polymer at the interface, planar or mushroom/brush as well as of the nature of the non-polar phase.

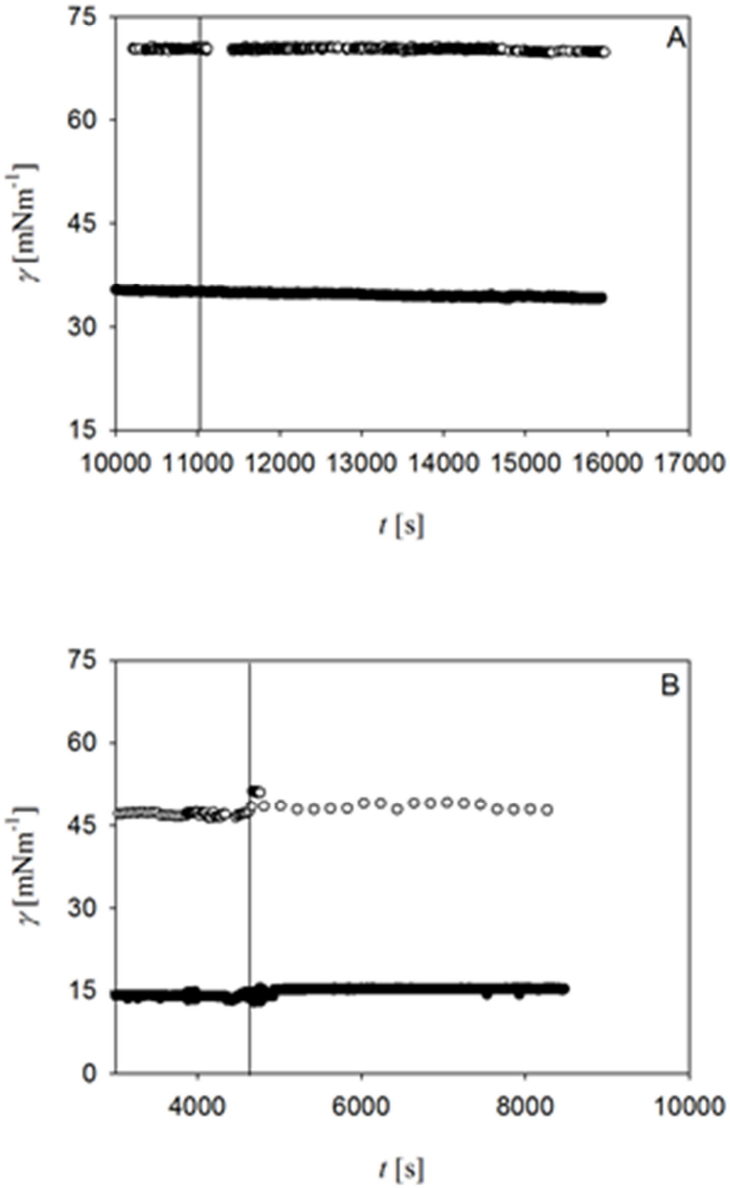

Figure 6. Dynamic surface tension for the bulk solution exchange experiments. Open circles and filled circles stand for air-water and limonene-water, respectively. A) Polymer bulk concentration: 2,2·10^{-5} molm^{-3}; B) Polymer bulk concentration: 2,2·10^{-3} molm^{-3}. The standard deviation of each data point is ±0.5 mN/m.

2.4. Conclusions

A systematic surface characterization has been carried out on the equilibrium, dynamics, interfacial rheology and desorption profile of Pluronic PE9400 at the air-water and limonene-water interface in order to fully characterize the properties of the adsorbed layers. The equilibrium surface pressure isotherm displays two adsorption regimes in the pre-critical region which are characterized by two slopes in the Π-c plot. These regimes are related to a conformational transition of the adsorbed polymer layer from a 2D flat conformation to a 3D brush one which takes place at both the air-water and the limonene-water interface. The theoretical model provides quantitative information on this transition showing that Pluronic PE9400 has a lower minimum molar area and higher internal compressibility at the limonene-water interface than at the air-water interface, suggesting a more compressible layer formed at the former. Dilatational rheology offers further evidence of the two conformations at the interface by showing two maxima as a function of the surface pressure and the application of the theoretical model to these data provides good agreement, importantly confirming the reliability of the proposed model. Moreover, the dilatational response confirms the structural differences between adsorbed molecules at high interfacial coverage. Also, the model indicates that the adsorption proceeds in the form of a bilayer at higher interfacial coverage at the limonene-water interface. In general, the higher condensation of the adsorbed layer of PE9400 at the limonene-water interface is corroborated and rationally quantified by the outcome of the fitting procedure. Figure 6 displays a sketch of the transition from 2D flat conformation to a 3D brush structure when augmenting the surface pressure in both air/water and limonene/water interfaces showing the enhanced compressibility and the likely bilayer formation of the adsorbed PE9400 at the limonene/water interface. Analysis of the adsorption kinetics by transforming the

original data into a dimensionless form yields a unique curve for the dynamic surface tension at different concentrations, which is fitted to a model involving the diffusion time scale and the amplitude and the time scale of the reorganization process. Realistic diffusion coefficients were obtained at both interfaces and a more favourable interaction between PE9400 and limonene again inferred from the adjusting parameters. Finally, the desorption profile of PE9400 was studied at the air-water and the oil-water interface. These experimental results importantly demonstrate that Pluronic PE9400 is irreversibly adsorbed at the interface regardless of the nature of the interface and the conformation of the polymer, providing important functional information concerning the adsorbed layer.

References

Aksenenko, E.V., http://www.thomascat.info/Scientific/AdSo/AdSo.htm (accessed December 2012).

Alahverdjieva, V. S., Fainerman, V. B., Aksenenko, E. V., Leser, M. E., & Miller, R. (2008). Adsorption of hen egg-white lysozyme at the air–water interface in presence of sodium dodecyl sulphate. Colloids and Surfaces A: Physicochemical and Engineering Aspects, 317(1), 610-617.

Alexandridis, P., & Lindman, B. (2000). Amphiphilic block copolymers: self-assembly and applications. Elsevier.

Bai, Z., & Lodge, T. P. (2010). Pluronic micelle shuttle between water and an ionic liquid. Langmuir, 26(11), 8887-8892.

Berthier, D. L., Schmidt, I., Fieber, W., Schatz, C., Furrer, A., Wong, K., & Lecommandoux, S. (2010). Controlled Release of Volatile Fragrance Molecules from PEO-b-PPO-b-PEO Block Copolymer Micelles in Ethanol− Water Mixtures. Langmuir, 26(11), 7953-7961.

Blomqvist, B. R., Wärnheim, T., & Claesson, P. M. (2005). Surface rheology of PEO-PPO-PEO triblock copolymers at the air-water interface: Comparison of spread and adsorbed layers. Langmuir, 21(14), 6373-6384.

Fainerman, V. B., Lucassen-Reynders, E. H., & Miller, R. (2003). Description of the adsorption behaviour of proteins at water/fluid interfaces in the framework of a two-dimensional solution model. Advances in Colloid and Interface Science, 106(1), 237-259.

Ferri, J. K., & Stebe, K. J. (2000). Which surfactants reduce surface tension faster? A scaling argument for diffusion-controlled adsorption. Advances in colloid and interface science, 85(1), 61-97.

Guzmán, E., Ortega, F., Baghdadli, N., Luengo, G. S., & Rubio, R. G. (2011). Effect of the molecular structure on the adsorption of conditioning polyelectrolytes on solid substrates. Colloids and Surfaces A: Physicochemical and Engineering Aspects, 375(1), 209-218.

Hambardzumyan, A., Aguié-Béghin, V., Daoud, M., & Douillard, R. (2004). β-Casein and symmetrical triblock copolymer (PEO-PPO-PEO and PPO-PEO-PPO) surface properties at the air-water interface. Langmuir, 20(3), 756-763.

Jafari, S. M., Beheshti, P., & Assadpoor, E. (2012). Rheological behavior and stability of d-limonene emulsions made by a novel hydrocolloid (Angum gum) compared with Arabic gum. Journal of Food Engineering, 109(1), 1-8.

Kabanov, A. V., Lemieux, P., Vinogradov, S., & Alakhov, V. (2002). Pluronic® block copolymers: novel functional molecules for gene therapy. Advanced drug delivery reviews, 54(2), 223-233.

Kerton, F. M. (2009) Alternative solvents for green chemistry, RSC Publishing,

Kim, C., & Yu, H. (2003). Surface rheology of monolayers of triblock copolymers of PEO and PPO: surface light scattering studies at the air/water interface. Langmuir, 19(10), 4460-4464.

Klein, M., Aserin, A., Svitov, I., & Garti, N. (2010). Enhanced stabilization of cloudy emulsions with gum Arabic and whey protein isolate. Colloids and Surfaces B: Biointerfaces, 77(1), 75-81.

Leal-Calderon, F., Schmitt, V., & Bibette, J. (2007). Emulsion science: basic principles. Springer.

Li, X., Zhang, Y., Fan, Y., Zhou, Y., Wang, X., Fan, C., ... & Zhang, Q. (2011). Preparation and evaluation of novel mixed micelles as nanocarriers for intravenous delivery of propofol. Nanoscale research letters, 6(1), 1-9.

Llamas, S., Mendoza, A. J., Guzmán, E., Ortega, F., & Rubio, R. G. (2013). Salt effects on the air/solution interfacial properties of PEO-containing copolymers: Equilibrium, adsorption kinetics and surface rheological behavior. Journal of colloid and interface science, 400, 49-58.

Lucassen, J., & Van Den Tempel, M. (1972). Dynamic measurements of dilational properties of a liquid interface. Chemical Engineering Science, 27(6), 1283-1291.

Maldonado-Valderrama, J., Fainerman, V. B., Gálvez-Ruiz, M. J., Martín-Rodriguez, A., Cabrerizo-Vílchez, M. A., & Miller, R. (2005). Dilatational rheology of β-casein adsorbed layers at liquid-fluid interfaces. The Journal of Physical Chemistry B, 109(37), 17608-17616.

Maldonado-Valderrama, J., Miller, R., Fainerman, V. B., Wilde, P. J., & Morris, V. J. (2010). Effect of gastric conditions on β-lactoglobulin interfacial networks: Influence of the oil phase on protein structure. Langmuir, 26(20), 15901-15908.

Maldonado-Valderrama, J., Fainerman, V. B., Aksenenko, E., Jose Galvez-Ruiz, M., Cabrerizo-Vílchez, M. A., & Miller, R. (2005). Dynamics of protein adsorption at the oil–water interface: comparison with a theoretical model. Colloids and Surfaces A: Physicochemical and Engineering Aspects, 261(1), 85-92.

Marcuzzo, E., Debeaufort, F., Sensidoni, A., Tat, L., Beney, L., Hambleton, A., ... & Voilley, A. (2012). Release Behavior and Stability of Encapsulated d-Limonene from Emulsion-Based Edible Films. Journal of agricultural and food chemistry, 60(49), 12177-12185.

F. Monroy, F. Ortega, R.G. Rubio, B.A. Noskov, in R. Miller and L. Liggieri (2009) (Eds.), Interfacial Rheology, Brill, Leiden, , Chapter 6.

Muñoz, M. G., Monroy, F., Ortega, F., Rubio, R. G., & Langevin, D. (2000). Monolayers of symmetric triblock copolymers at the air-water interface. 1. Equilibrium properties. Langmuir, 16(3), 1083-1093.

Munoz, M. G., Monroy, F., Ortega, F., Rubio, R. G., & Langevin, D. (2000). Monolayers of symmetric triblock copolymers at the air-water interface. 2. Adsorption kinetics. Langmuir, 16(3), 1094-1101.

Muñoz, M. G., Monroy, F., Hernández, P., Ortega, F., Rubio, R. G., & Langevin, D. (2003). Anomalous damping of the capillary waves at the air-water interface of a soluble triblock copolymer. Langmuir, 19(6), 2147-2154.

Murali, R., Karthikeyan, A., & Saravanan, R. (2013). Protective Effects of d-Limonene on Lipid Peroxidation and Antioxidant Enzymes in Streptozotocin-Induced Diabetic Rats. Basic & clinical pharmacology & toxicology, 112(3), 175-181.

Myrvold, R., & Hansen, F. K. (1998). Surface elasticity and viscosity from oscillating bubbles measured by automatic axisymmetric drop shape analysis. Journal of colloid and interface science, 207(1), 97-105.

Noskov, B. A., Akentiev, A. V., Loglio, G., & Miller, R. (2000). Dynamic surface properties of solutions of poly (ethylene oxide) and polyethylene glycols. The Journal of Physical Chemistry B, 104(33), 7923-7931.

Noskov, B. A., Lin, S. Y., Loglio, G., Rubio, R. G., & Miller, R. (2006). Dilational viscoelasticity of PEO-PPO-PEO triblock copolymer films at the air-water interface in the range of high surface pressures. Langmuir, 22(6), 2647-2652.

Noskov, B. A. (2010). Dilational surface rheology of polymer and polymer/surfactant solutions. Current Opinion in Colloid & Interface Science, 15(4), 229-236.

Papadimitriou, V., Pispas, S., Syriou, S., Pournara, A., Zoumpanioti, M., Sotiroudis, T. G., & Xenakis, A. (2008). Biocompatible microemulsions based on limonene: formulation, structure, and applications. Langmuir, 24(7), 3380-3386.

Ramírez, P., Muñoz, J., Fainerman, V. B., Aksenenko, E. V., Mucic, N., & Miller, R. (2011). Dynamic interfacial tension of triblock copolymers solutions at the water–hexane interface. Colloids and Surfaces A: Physicochemical and Engineering Aspects, 391(1), 119-124.

Ramírez, P., Stocco, A., Muñoz, J., & Miller, R. (2012). Interfacial rheology and conformations of triblock copolymers adsorbed onto the water–oil interface. Journal of colloid and interface science, 378(1), 135-143.

Schramm, L. L. (2006). Emulsions, foams, and suspensions: fundamentals and applications. John Wiley & Sons.

Sedev, R., Steitz, R., & Findenegg, G. H. (2002). The structure of PEO–PPO–PEO triblock copolymers at the water/air interface. Physica B: Condensed Matter, 315(4), 267-272.

Serrien, G., Geeraerts, G., Ghosh, L., & Joos, P. (1992). Dynamic surface properties of adsorbed protein solutions: BSA, casein and buttermilk. Colloids and surfaces, 68(4), 219-233.

Svitova, T. F., & Radke, C. J. (2005). AOT and Pluronic F68 coadsorption at fluid/fluid interfaces: a continuous-flow tensiometry study. Industrial & engineering chemistry research, 44(5), 1129-1138.

Tadros, T.; in Holmberg, K. (Ed.). (2003). Novel Surfactants: Preparation Applications And Biodegradability, Revised And Expanded. Crc Press. Chapter 16

Tadros, T. F. (2005). Applied surfactants: principles and applications. John Wiley & Sons.

Tavano, L., Muzzalupo, R., Trombino, S., Cassano, R., Pingitore, A., & Picci, N. (2010). Effect of formulations variables on the in vitro percutaneous permeation of Sodium Diclofenac from new vesicular systems obtained from Pluronic triblock copolymers. Colloids and Surfaces B: Biointerfaces, 79(1), 227-234.

Torcello-Gómez, A., Santander-Ortega, M. J., Peula-García, J. M., Maldonado-Valderrama, J., Gálvez-Ruiz, M. J., Ortega-Vinuesa, J. L., & Martín-Rodríguez, A. (2011). Adsorption of antibody onto Pluronic F68-covered nanoparticles: link with surface properties. Soft Matter, 7(18), 8450-8461.

Torcello-Gómez, A., Maldonado-Valderrama, J., Martín-Rodríguez, A., & McClements, D. J. (2011). Physicochemical properties and digestibility of emulsified lipids in simulated intestinal fluids: influence of interfacial characteristics. Soft Matter, 7(13), 6167-6177.

Torcello-Gómez, A., Jódar-Reyes, A. B., Maldonado-Valderrama, J., & Martín-Rodríguez, A. (2012). Effect of emulsifier type against the action of bile salts at oil–water interfaces. Food Research International, 48(1), 140-147.

Vieira, J. B., Li, Z. X., & Thomas, R. K. (2002). Adsorption of triblock copolymers of ethylene oxide and propylene oxide at the air/water interface: The surface excess. The Journal of Physical Chemistry B, 106(21), 5400-5407.

Wulff-Pérez, M., Gálvez-Ruíz, M. J., De Vicente, J., & Martín-Rodríguez, A. (2010). Delaying lipid digestion through steric surfactant Pluronic F68: A novel in vitro approach. Food research international, 43(6), 1629-1633.

Wulff-Pérez, M., de Vicente, J., Martín-Rodríguez, A., & Gálvez-Ruiz, M. J. (2012). Controlling lipolysis through steric surfactants: New insights on the controlled degradation of submicron emulsions after oral and intravenous administration. International journal of pharmaceutics, 423(2), 161-166.

Zholob,S.A, Kovalchuk, V.I., Makievski,A.V., Krägel,J., Fainerman,V.B., Miller,R., in Miller, R., and L. Liggieri (2009) (Eds.), Interfacial Rheology, Brill, Leiden, , Chapter 3.

Zoller, U. (Ed.). (2009). Handbook of detergents, part E: applications. CRC Press.

3

Optimum formulation of D limonene emulsions by response surface methodology

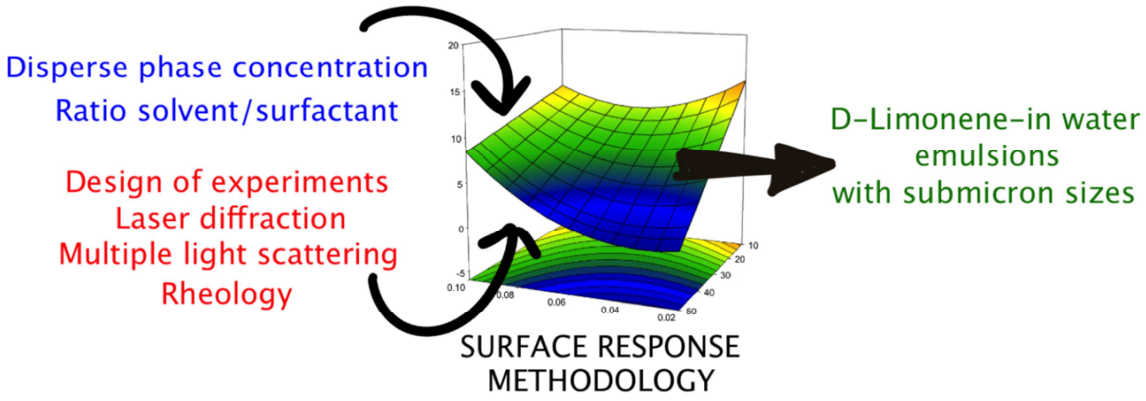

Abstract

D-limonene is a naturally occurring solvent that can replace more polluting chemicals in agrochemical formulations.

In the present work, a comprehensive study of the influence of disperse phase mass fraction, ϕ, and of the surfactant/oil ratio, R, on the emulsion stability and droplet size distribution of D-limonene-in-water emulsions stabilized by a non-ionic triblock copolymer surfactant has been carried out.

An experimental full factorial design 3^2 was conducted in order to optimize the emulsion formulation. These emulsions were mainly destabilized by both creaming and Ostwald ripening. Therefore, initial droplet size, creaming rate, normalized Ostwald ripening rate and turbiscan stability index, were used as dependent variables. The optimal formulation, involving minimum droplet size and maximum stability was achieved at ϕ = 50 wt%; R = 0.062.

The combination of these experimental findings with the rheological characterization of the emulsions allowed us to gain a deeper insight into the stability of these emulsions, which can be applied to the rational development of new formulations with potential applications in agrochemical formulations.

3.1 Introduction

The role of solvents in the agrochemical industry is becoming increasingly important. More than 25% of all pesticides contain high concentrations of organic solvents, which represent a fire hazard, may be toxic and contribute to atmospheric volatile compound (VOC) emissions (Höfer, 2007). Thus, many of the classical solvents are being gradually replaced by so-called 'green' solvents. D-limonene, a naturally occurring hydrocarbon, is a cyclic monoterpene which is commonly found in the rinds of citrus fruits such as grapefruit, lemons, limes and, in particular, oranges. Limonene exhibits good biodegradability, and it may therefore be proposed as an interesting alternative to organic solvents, meeting the ever-increasing safety and environmental demands of the 21st Century (Kerton, 2013).

D-Limonene is the major flavour compound in several citrus oil, such as orange oil, lemon or mandarin (Brud, 2010) and it is widely used as flavour additive in cosmetics, food and pharmaceutical applications (Jafari, 2012; Lu, 2013; Marcuzzo, 2012; Murali, 2013). It has been reported that D-limonene had bactericide, antioxidant and therapeutic activities (Gerhäuser, 2003). Given that D-limonene is not soluble in water, emulsification is an interesting alternative to solubilize and protect D-limonene from oxidative degradation (Soottitantawat, 2003), in order to keep the lemon-like flavor and be active in those areas of food (Li, 2013)

In order to emulsify D-limonene, non-ionic polymeric surfactants, Pluronics, have been used. Their chemical structure is denoted by PEOx-PPOy-PEOx, where PEO and PPO stands for poly(ethylene) oxide and poly(propylene) oxide, respectively. The HLB can be modulated depending on the number of PEO and PPO units. They have been used as foam and emulsions stabilizers in industrial applications (Alexandridis, 2000; Tadros, 2010). Furthermore, these polymeric surfactants are promising materials

for many technological applications such as drug delivery, gene therapy and the development of foods that provide specific physiological responses, such as control of lipid digestion or satiety (Batrakov, 2008; Kabanov, 2002; Torcello-Gómez, 2011a, 2011b, 2013, 2014). Recently, the interfacial properties of Pluronic PE9400 adsorbed at the limonene-water interface have been reported by Pérez-Mosqueda (2013) showing that PE9400 is irreversibly adsorbed at this interface, thereby making it a potential candidate to prevent emulsion coalescence.

Emulsions are thermodynamically unstable colloidal dispersions that are destabilized by several mechanisms, such as flocculation, coalescence, gravitational separation (sedimentation or creaming) and Ostwald ripening. It has been shown that orange oil suffers from creaming and Ostwald ripening (Lim, 2011). It is known that both destabilization processes, creaming and Ostwald ripening, depend on the disperse mass fraction, ϕ, and surfactant concentration (Abeynake, 2012; Chanamai, 2000; Neogi, 2001; Weiss, 2000). Therefore, a correct selection of composition and physicochemical formulation is essential to improve the emulsification process (Cuellar, 2005; Salager, 2003). Multivariate statistical techniques, such as response surface methodology (RSM), have been shown to be an interesting tool for the optimization of emulsions and nanoemulsions (Bueno, 2009; Maher, 2011; Musa, 2013; Soleimanpour, 2013). With this approach, a mathematical model connecting the response variables to the process ones is obtained with a minimum number of experiments. Hence, the development of new formulations becomes more effective (Montgomery, 2001).

The most common emulsification methods are based on mechanical energy input to the system by an external source. As a rule, emulsions are prepared in two steps; the aim of the first (primary homogenization) is to create droplets of disperse phase such that a coarse emulsion is formed. The goal of the second step is to reduce the size of

pre-existing droplets, which usually involves the use of a different homogenizer, such as an ultrasonic probe, a high-pressure valve homogenizer or a microfluidizer (Jafari, 2007; Urban, 2006).

Nevertheless, in the present study a single-step rotor/stator homogenizer was used in order to obtain monomodal submicron emulsions with a disperse mass fraction in the range from dilute to slightly concentrated emulsions (ϕ = 10-50 wt%) and with a low ratio of wt% surfactant over wt% solvent (R < 0.1). An experimental full factorial design 3^2 was conducted in order to optimize the emulsion formulation.

3.2 Materials and methods

3.2.1. Materials

D-Limonene (4-isopropenyl-1-methylciclohexane) was used as disperse phase in the emulsion formulation. It is mainly obtained from the peel of citrus fruit, principally from oranges and lemons. D-Limonene 97% was purchased from Sigma-Aldrich® and purified with Florisil® resins (Fluka, 60-10 mesh) prior to use by following the procedure used elsewhere (Maldonado-Valderrama, 2005; Maldonado-Valderrama, 2010). Namely, a mixture of oil and Florisil® in proportion 2:1 w/w was shaken gently for 3 h and then separated by decanting.

The triblock copolymer Pluronic PE9400 (PEO_{21}-PPO_{50}-PEO_{21}, Mw = 4600 $g \cdot mol^{-1}$ and HLB = 12-18) was kindly provided by BASF and used as received.

Ultrapure water, cleaned using a Milli-Q water purification system was used. All glassware was washed with 10% Micro-90 cleaning solution and exhaustively rinsed with tap water, isopropanol, deionized water, and ultrapure water in this sequence.

3.2.2 Emulsion preparation

The aqueous phase was first prepared by dissolving the correct amount of surfactant with magnetic stirring for 15 min at 300 rpm. The emulsion was then formed using a batch process. The oil phase was added over the continuous phase while homogenizing at 17500 rpm for 60 seconds using a rotor/stator system (Ultra Turrax T-25/KV11, IKA Instruments, Germany). The final emulsion weight was 50 g.

3.2.3 Droplet size measurements

Droplet size distribution (DSD) was determined by using laser diffraction measurements performed with a Mastersizer X (Malvern) particle size analyzer. The mean droplet diameter was expressed as the Sauter diameter, $d_{3,2}$:

$$d_{3,2} = \frac{\sum_i N_i D_i^3}{\sum_i N_i D_i^2} \quad (1)$$

where N_i is the number of droplets with a diameter, D_i. Measurements were done in triplicate.

3.2.4 Creaming stability

Multiple light scattering measurements with a Turbiscan Expert LabMeasuring were used in order to study the creaming of the emulsions (Chanamai and McClements, 2000). This instrument is capable of detecting creaming before it is visible to the naked eye[31]. The extent of creaming was quantified using a creaming index (McClements, 2007), *CI:*

$$CI = \frac{H_S}{H_E} \times 100 \quad (2)$$

where, H_S is the height of the serum layer at given time (12 hours) and H_E is the total height of the emulsion. The height of the serum layer was obtained from the width of the peak at the bottom part of the cell of the backscattered light in reference mode, i.e. the backscattering flux at time t = 12 h minus the initial backscattering flux.

3.2.5 Ostwald ripening

The evolution of the Sauter diameter with time was monitored using laser diffraction measurements (Mastersizer X, Malvern). A linear variation of the plot of r^3/r^3_0 vs. t was obtained following the LSW theory (Lifshitz, 1961), where r and r_0 are the droplet radius at a given time and the initial droplet radius, respectively. The normalized Ostwald ripening rate (k_{OR}) was calculated from the slope of these plots.

3.2.6. Overall destabilization index (Turbiscan Stability Index)

In order to quantify simultaneously the destabilization processes in our emulsions the Turbiscan Stability Index (TSI) was used. This index is a statistical factor and its value is calculated as the sum of all the destabilization processes in the measuring cell (Lesaint et al, 2009) and it is given by:

$$TSI = \sum_j \left| scan_{ref}(h_j) - scan_i(h_j) \right| \qquad (3)$$

where $scan_{ref}$ and $scan_i$ are the initial backscattering value and the backscattering value at a given time respectively, h_j is a given height in the measuring cell and TSI is the sum of all the scan differences from the bottom to the top of the vial.

3.2.7. Rheology of emulsions

Flow curves were carried out using a rheometer from Haake Thermo Scientific (Germany), a Mars controlled-stress rheometer with a sandblasted Z20 coaxial cylinder sensor system (Ri=1cm, Re/Ri=1.085). All rheological measurements were performed

at 25ºC ± 0.1ºC, using a C5P Phoenix circulator (Thermo-Scientific) for sample temperature control. The results represent the mean of three measurements. Equilibration time prior to rheological tests was 180 s.

3.2.8. Design of experiments

In order to rationally develop an optimal formulation of D-limonene-in-water emulsions prepared with a rotor/stator homogenizer, a second-order experimental design and mathematical model was required. In the present work, the two process variables selected were: surfactant/oil ratio, *R*, and disperse mass fraction, ϕ. With only two factors, a full factorial design 3^2 with three replications of the center point was selected. The quadratic model is given below:

$$Y = \beta_0 + \beta_1 R + \beta_2 \emptyset + \beta_{11} R^2 + \beta_{22} \emptyset^2 + \beta_{12} R\emptyset \quad (4)$$

Each factor is measured at three levels which were coded to take the value -1 when the factor is at its low level, 0 when at its medium level and +1 when at its high level. The lowest value for *R* (0.02) was chosen such that the minimum size of stable droplets that can be theoretically produced was 1 μm, according to the following equation (McClements, 2005):

$$d_{\min} = \frac{6\Gamma_{sat}\phi}{C_s} \quad (5)$$

where C_s is the surfactant concentration in the emulsion and Γ_{sat} is the excess surface concentration of the surfactant at saturation. A value of Γ_{sat} = 3 mg·m^{-2} was used[16]. The highest limit was set as 5 times the lowest one, so *R* varied in the range 0.02 – 0.1. ϕ was studied in the range 10 – 50 wt%, from dilute to slightly concentrated emulsion.

It has been reported that emulsion droplet size is a function of the processing conditions; homogenization rate and emulsification time (Franco, 1998) in addition to the formulation used. The optimal processing conditions were found to be 17500 rpm and 60 seconds of homogenization rate and emulsification time respectively, as shown in Figure 1 for the center point (R= 0.06, ϕ = 30 wt%).

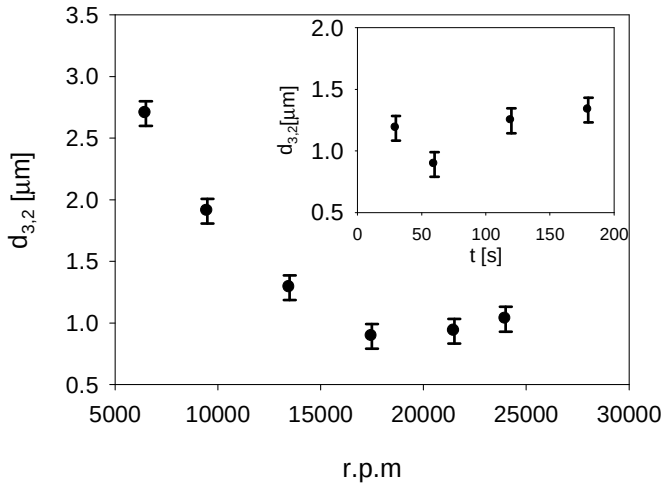

Figure 1. Sauter mean diameter as a function of homogenization rate for D-limonene-in-water emulsion with R = 0.06 and ϕ = 30%. Emulsions were produced by Ultraturrax T-25 at room temperature. The inset shows the influence of emulsification time on droplet size for the optimal homogenization rate (17500 rpm). Symbols are the mean of three replicates and the error bars show the standard deviation of the measurements.

The effect of the two independent variables, surfactant/oil ratio (R) and disperse mass fraction (ϕ) on emulsion mean droplet size, $d_{3,2}$, and on the destabilization processes: creaming index, *CI*, Ostwald ripening rate k_{OR} and the overall destabilization index *TSI* (Turbiscan Stability Index) of D-limonene-in-water emulsion was studied using a 3^2 experimental factorial design. Experiments were randomly carried out in

order to minimize the effects of random error in the observed responses. The center point in the design was determined in triplicate to calculate the repeatability of the method[27] and to check the fitting quality of the mathematical model (Khuri, 1996).

The quadratic terms of the response surface models were obtained by the least squared method. For model construction, terms with $p > 0.05$ were removed and the analysis was recalculated without these terms. The suitability of the models was determined by using the coefficient of determination (R^2) and the lack of fit test (F_{lof}). Joklegar and May proposed that R^2 should be higher than 0.80 to obtain a good fitting (Jokeglar, 1987). F_{lof} is the ratio between mean squares due to lack of fit and mean squares for pure error. This F_{lof} value must be compared with a table value of F_{crit} for α level of significance and the degrees of freedom of the mean squares employed. It was assumed that the proposed model did not exhibit lack of fit at α level of significance when F_{crit} exceeded F_{lof}.

3.3 Results and discussions

3.3.1. Surface response analysis

The variation of each response variable was initially assessed as a quadratic function of surfactant/oil ratio and disperse mass fraction (Table 1). The lack of fit shown by the fittings of creaming index and turbiscan stability index was solved by adding a new cubic interaction term in these models: $\beta_{122}\ R^*\phi^2$. The results indicated that the models employed were adequate, showing no significant lack of fit ($F_{crit} > F_{lof}$ with $\alpha = 0.05$) and very satisfactory values of R^2 for all responses. The R^2 values for droplet size, creaming index, Ostwald ripening rate and turbiscan stability index were found to be 0.959, 0.998, 0.967 and 0.991 respectively. Comparison between predicted and actual values for the response variables also indicated that the polynomial

regression models were suitable to determine optimum formulation for preparing D-limonene-in-water emulsions with maximum stability (Fig. 2).

Regression coefficients	**$d_{3,2}$ (μm)**	**C.I. (%)**	**k_{OR} (h^{-1})**	**TSI**
β_0	0.936667	2.49224	0.236833	5.78167
β_1	-0.348333	0.50695	0.262155	4.025
β_2	-0.1216667	-2.3496	0.230378	-4.63667
β_{11}	0.248333	1.48822	0.0923217	3.085
β_{22}	- (p > 0.05)	1.77868	-(p > 0.05)	-(p > 0.05)
β_{12}	- (p > 0.05)	2.6975	0.209317	2.5125
β_{122}	---	-1.47425	---	-3.6275
F_{lof}	1.45	2.81	1.51	3.05
F_{crit}	9.01	9.55	9.12	9.28
R^2	0.959	0.998	0.967	0.991
Adj-R^2	0.943	0.997	0.948	0.983

Table 1. Regression coefficients of the fitting models

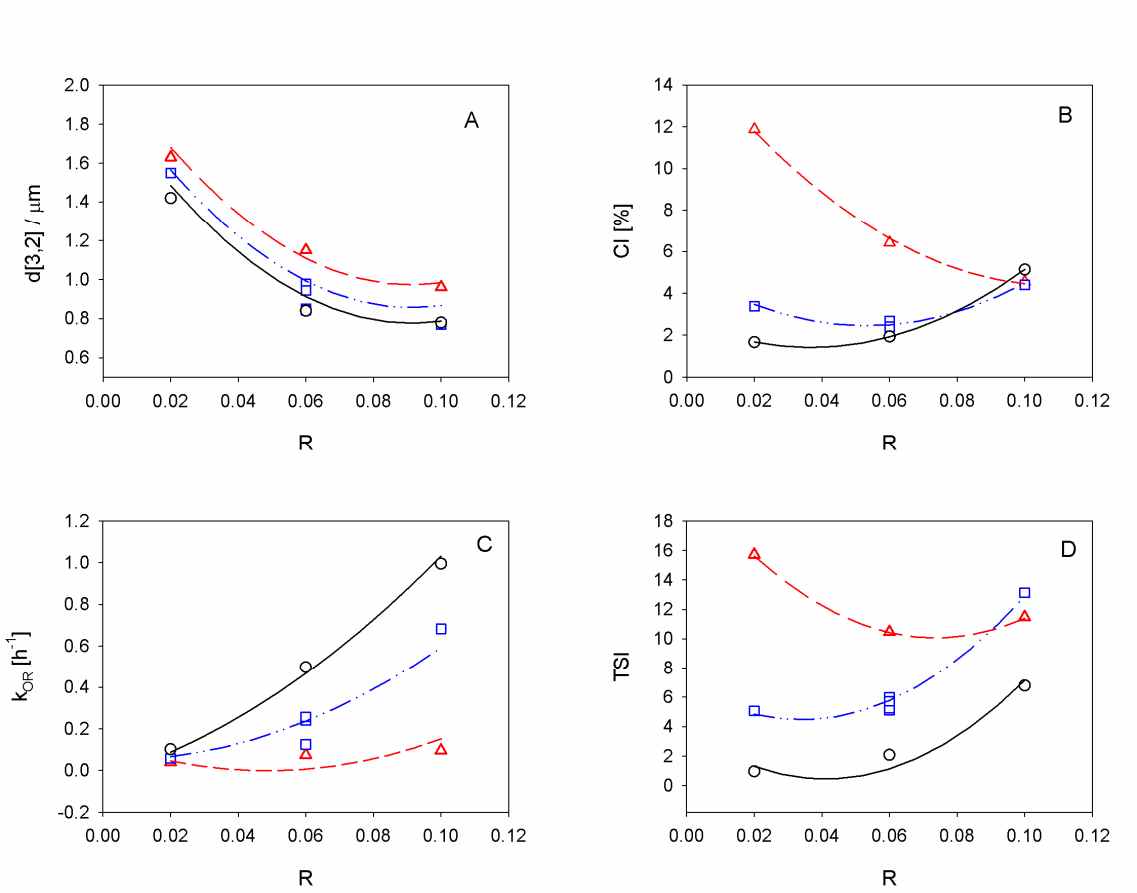

Figure 2 A) Sauter mean diameter at t = 0 vs. surfactant/oil ratio, R. B) Creaming index (CI) as a function of R. C) Normalized Ostwald ripening rate (k_{OR}) vs. R and D) Turbiscan stability index (TSI) vs. R. Symbols correspond to experimental measurements: triangles (ϕ = 10%), squares (ϕ = 30%) and circles (ϕ = 50%). Lines are the theoretical values obtained by the surface response models by using the parameters in Table 1.

3.3.2 Emulsion droplet size

Droplet size is a key variable to study emulsion stability (McClements, 2005). Destabilization processes, such as creaming or Ostwald ripening growth, depend greatly on droplet size. It was therefore particularly important to determine the droplet size in order to characterize our system.

From full factorial design we deduced that the most significant factors affecting droplet size in our system were the linear and quadratic terms of surfactant/oil ratio and the linear term of disperse mass fraction (Table 1). The equation of the fitted model was:

$$d_{3,2} = 0.94 - 0.35*R - 0.12*\phi + 0.25*R^2 \quad (6)$$

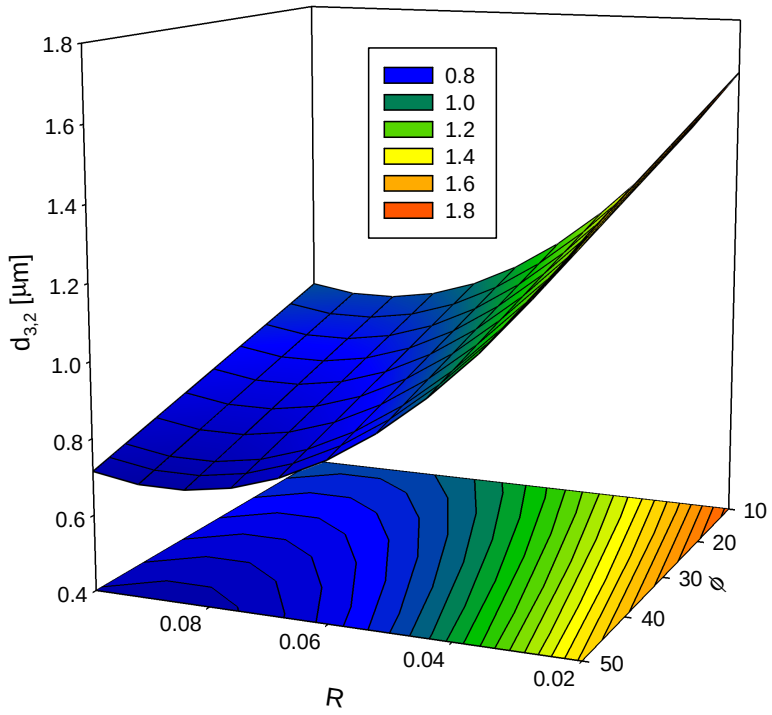

Figure 3 Response surface 3D plot of the Sauter mean diameter as a function of the process variables R and ϕ. The color scale indicates the Sauter mean diameter values ranging from 0.8 μm to 1.8 μm.

Figure 3 shows the surface response of the effect of variables R and ϕ on the $d_{3,2}$. For a given disperse mass fraction, increasing R yielded a decrease in the droplet size until it reached a minimum value. This $d_{3,2}$ variation was to be expected since more emulsifier was available to fully cover the O/W interface with smaller droplets as R was

increased. However, once a certain ratio was achieved a further increase of surfactant did not result in smaller droplets. The limiting factor may be a) the actual emulsification process, which was not capable of generating enough energy to further reduce the droplet size, and/or b) the fact that the emulsifier did not adsorb fast enough to form a protective layer to prevent recoalescence phenomena (McClements, 2005).

On the other hand, the influence of ϕ on the droplet size was certainly more striking. The lack of major differences in $d_{3,2}$ with ϕ was to be expected. However, a clear tendency to decrease $d_{3,2}$ with increasing ϕ was observed. For a given surfactant/oil ratio (R) if the amount of oil (disperse phase) is increased, the surfactant concentration in the continuous phase is also increased, enhancing the viscosity of the continuous phase, η_c. It has been reported that the viscosity of the continuous phase influences the droplet size diameter obtained in rotor/stator homogenizers. It is stated that an increase in η_c will lead to higher turbulent eddies which can be larger than the smaller droplets and therefore emulsification will proceed via a turbulent viscous regime producing smaller droplets (Vankova, 2007).

3.3.3 Destabilization processes

It was seen that all emulsions were affected by both gravitational separation and increase in droplet size in a very short time (within 12 hours). Since the disperse phase is less dense than the continuous one the oil droplets tend to move towards the top, which is known as creaming. As an example, Figure 4 shows the droplet size distribution (A-C) and the backscattering profiles (D-F) for emulsions with R = 0.06. Depending on ϕ, two different behaviors were detected: for ϕ = 10 and 30 wt% both destabilization processes, creaming and increase of the droplet size were readily noticeable. Nevertheless, for emulsions with ϕ = 50 wt% creaming was not easily

perceived whereas the increase in the droplet size was very marked. Eventually, this emulsion was also affected by creaming, probably due to the increase in droplet size.

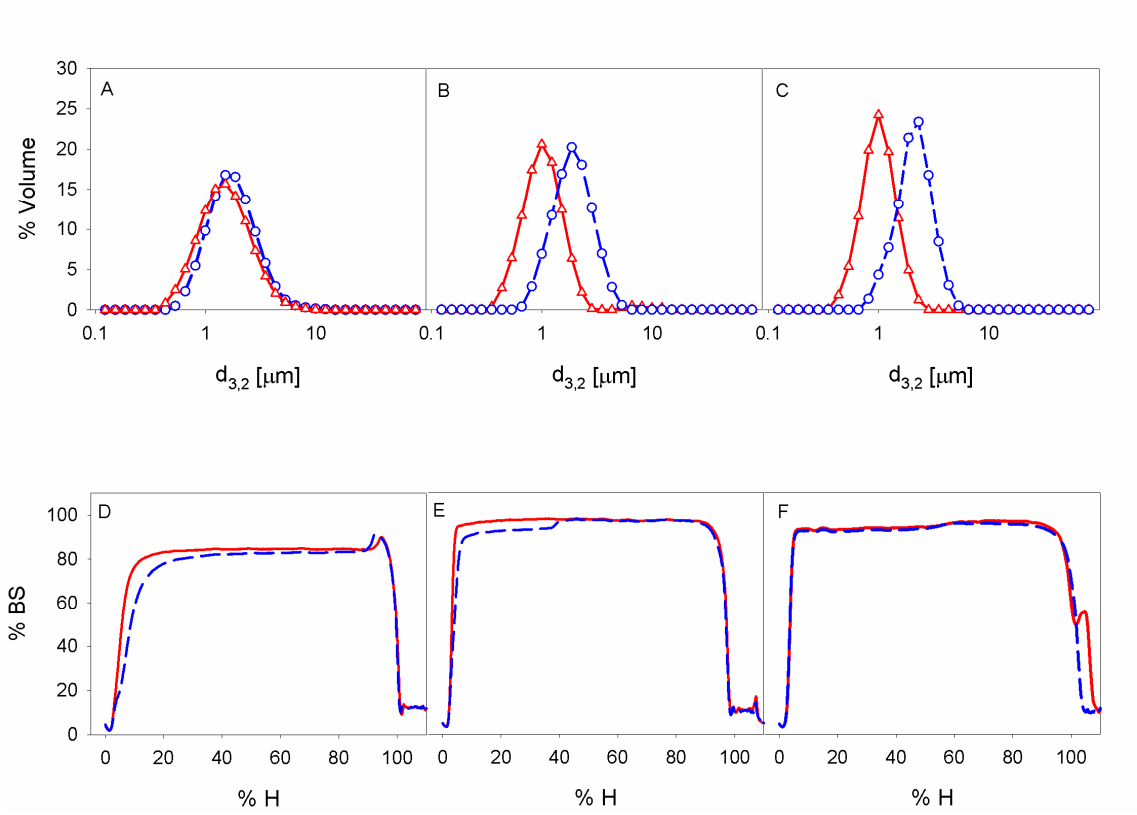

Figure 4. A-C: Droplet size distribution for emulsions with R = 0.06 and ϕ = 10 wt% (A), ϕ = 30 wt% (B) and ϕ = 50 wt% (C). t = 0 (Squares and solid lines) and t = 12 h (Circles and dashed lines). D-F: Backscattering profiles as a function of the measuring cell height for emulsions with R = 0.06 and ϕ = 10 wt% (A), ϕ = 30 wt% (B) and ϕ = 50 wt% (C). t = 0 (solid lines) and t =12 h (dashed lines).

In order to gain a deeper knowledge of the destabilization processes a 3^2 full factorial design was used, *R* and ϕ being the process variables. The dependent variables studied were creaming index (*CI*) to analyze gravitational separation, normalized Ostwald ripening rate (k_{OR}) for droplet size growth and turbiscan stability index (*TSI*) as an overall destabilization parameter.

3.3.4 Creaming Index (CI)

Due to the lack of fit of the quadratic model the addition of a cubic interaction was considered, R*ϕ^2. Hence, the model equation was:

$$CI = 2.5 + 0.51*R - 2.3*\phi + 1.5*R^2 + 1.8*\phi^2 + 2.7*R*\phi - 1.5*R*\phi^2 \qquad (7)$$

The high value of the coefficient of determination, R^2 (0.998) indicates that experimental measurements agree well with the model.

Figure 5 shows the surface response of the effect of process variables *R* and ϕ on the *CI*. The *CI* variation as a function of *R* was quite dependent on disperse mass fraction, ϕ. Hence, at ϕ = 10 wt% *CI* decreased with *R*, whereas for the highest ϕ = 50 wt% the opposite behavior was observed.

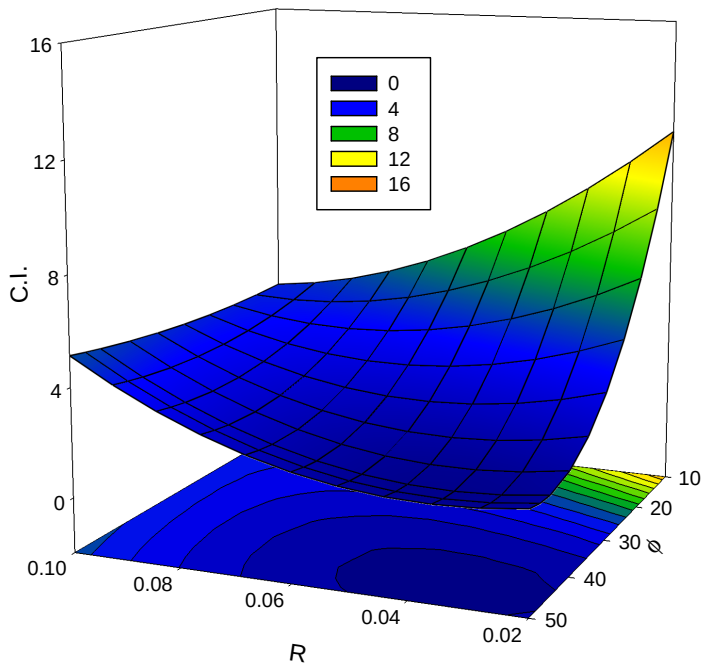

Figure 5. Response surface 3D plot of the creaming index (CI) as a function of the process variables R and ϕ. The color scale indicates the creaming index values ranging from 0 to 16.

From *CI* values, the creaming velocity (V_c) can be calculated as follow:

$$V_c = \frac{(CI \cdot H_e)}{100 \cdot 12} \quad (8)$$

where H_e is the total height of the emulsions in mm and 12 is the total time of measurement in hours, therefore V_c is in mm·h^{-1}. Figure 6 shows the creaming velocity as a function of the squared radius of the droplets r^2. A linear variation was observed for emulsions containing 10 wt% D-limonene. For non-dilute emulsions (ϕ > 2 wt%) hydrodynamics interactions between particles are expected to slow down the velocity of the gravitational separation as expressed by Stokes' law. If droplet flocculation is negligible a kind of Stokes' law equation can be used to predict the creaming velocity (McClements, 2005).

$$V_c = -\frac{2gr^2(\rho_2 - \rho_1)}{9\eta_e} \quad (9)$$

where g is the acceleration due to gravity, r is the radius of the droplet, ρ_1 and ρ_2 are the densities of the continuous and disperse phases respectively and η_e is the viscosity of the emulsion. As shown in Figure 7A the emulsions with ϕ = 10 wt% are Newtonian and the viscosity for all the emulsions was around 2 mPa·s. By using equation (9) with η_e = 2 mPa·s, g = 9.81 ms^{-2}, ρ_1 = 1000 kg·m^{-3} and ρ_2 = 841 kg·m^{-3} creaming velocities very close to experimental values were obtained as seen in Figure 6.

For ϕ values above 10 wt% the systems became more complex and it was likely that droplet-droplet interactions lead to droplet flocculation. Therefore, creaming velocity was not a linear function of r^2.

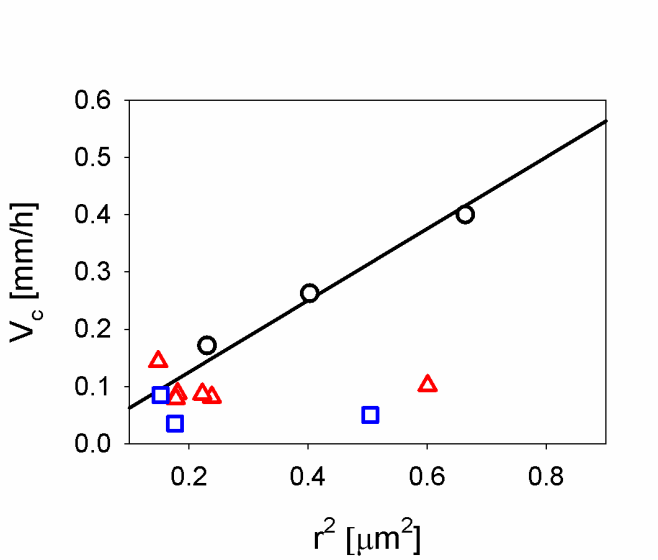

Figure 6. Creaming velocity (V_c) as a function of the droplet radius squared for D-limonene-in-water emulsions with ϕ = 10 wt% (circles), ϕ = 30 wt% (triangles) and ϕ = 50 wt% (squares). The solid line is the creaming velocity dependence with r^2 calculated via equation (8) with the parameters values given in the text.

Rheological measurements were carried out to gain a deeper insight into the creaming destabilization. Figure 7A shows the flow curves for emulsions containing 10 wt% D-limonene. All curves showed Newtonian behavior, whatever the droplet size or surfactant concentration. The viscosity obtained for these emulsions was around 2 mPa·s. For emulsions with ϕ = 30 wt% a transition from Newtonian to shear-thinning behavior was observed as shown in Figure 7B. This transition can be attributed to the onset of flocculation due to the excess of surfactant in solution (Derkach, 2009; Manoj, 1998; Pal, 2011). Nevertheless, the increase in the creaming index at the highest *R* value pointed to the occurrence of flocculation which led to an enhanced gravitational separation. For emulsions at ϕ = 50 wt% (Figure 7C) all the systems were shear-thinning. The increase in the shear-thinning behavior was probably due to the flocculation induced by micelles in solution (depletion flocculation) as explained for emulsions with ϕ = 30 wt%.

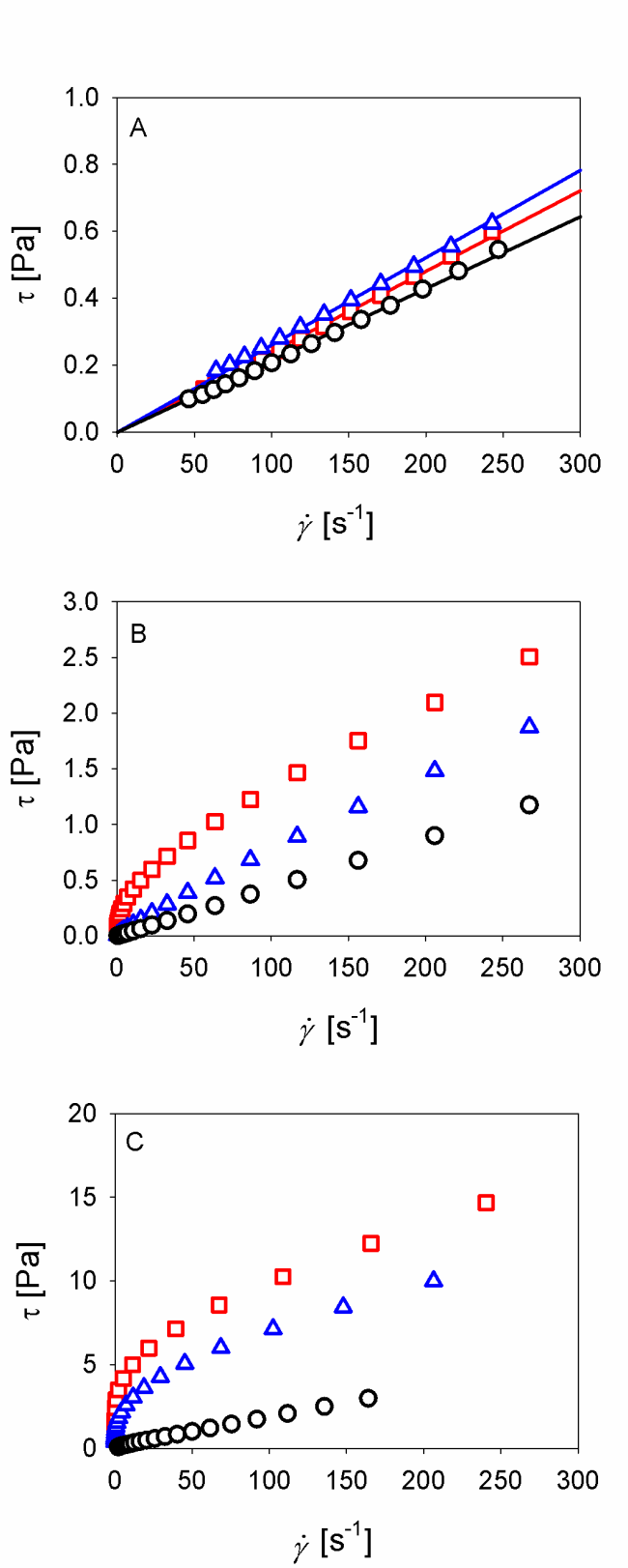

Figure 7. Flow curves shown as shear stress vs. shear rate for the D-limonene-in-water emulsions. Figure 7A, ϕ = 10 wt% ; Figure 7B, ϕ = 30 wt% and Figure 7C, ϕ = 50 wt%. Circles (R = 0.02), triangles (R = 0.06) and squares (R = 0.1).

3.3.5. Ostwald ripening

As shown in Figure 4, by using both multiple light scattering and laser diffraction techniques, emulsions also underwent an increase in droplet size. Two destabilization mechanisms were likely to occur, coalescence and/or Ostwald ripening. On the one hand, if coalescence is the leading destabilization process a linear plot of $1/r^2$ vs. t will be shown (Kabalnov, 1998); on the other hand, a linear plot of r^3 vs. t will be obtained if Ostwald ripening is the main destabilization process (Weers, 1998). In all the systems studied a linear variation of r^3 with time was observed confirming the occurrence of Ostwald ripening. Figure 8 shows the time evolution of the cube of the normalized droplet radius. From the slope of these plots the Ostwald ripening rate (k_{OR}) was calculated. This rate constant was used to evaluate the influence of the process variables R and ϕ in the Ostwald ripening.

As shown in Table 1 the only factor that is not significant is the quadratic term of ϕ. Hence, the model equation was:

$$k_{OR} = 0.24 + 0.26*\phi + 0.23*R + 0.092*R^2 + 0.21*R*\phi \quad (10)$$

The high value of the coefficient of determination, R^2 (0.967) indicates that experimental measurements agree well with the model.

Figure 9 shows the surface response of the Ostwald ripening rate as a function of R and ϕ. At the lowest R value the k_{OR} was close to zero, whatever the disperse mass fraction. k_{OR} increased with R for all ϕ values. Nevertheless, the rise became steeper with increasing ϕ.

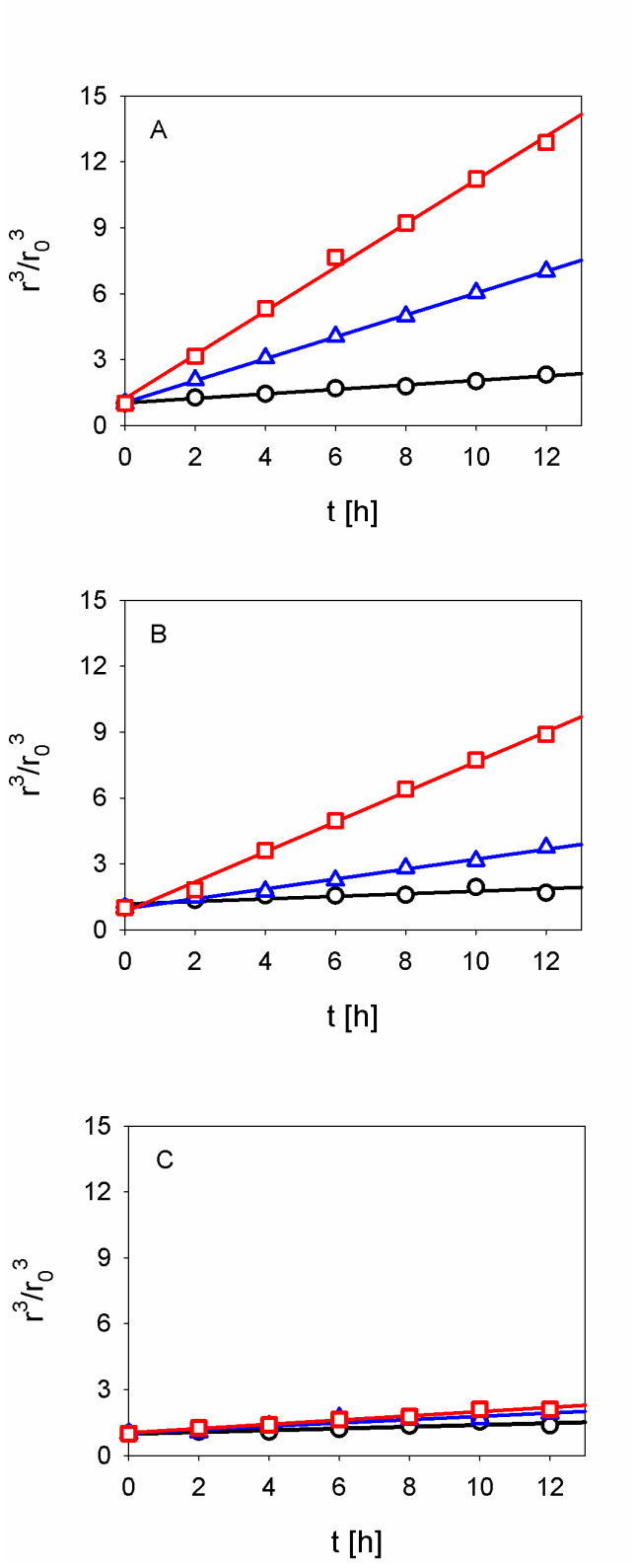

Figura 8. Normalized radius cubed vs. time. Figure 8A, ϕ = 10 wt% ; Figure 8B, ϕ = 30 wt% and Figure 8C, ϕ = 50 wt%. Circles (R = 0.02), triangles (R = 0.06) and squares (R = 0.1). Lines are the best linear fit to experimental data. From the slopes the normalized Ostwald ripening rate (k_{OR}) was determined.

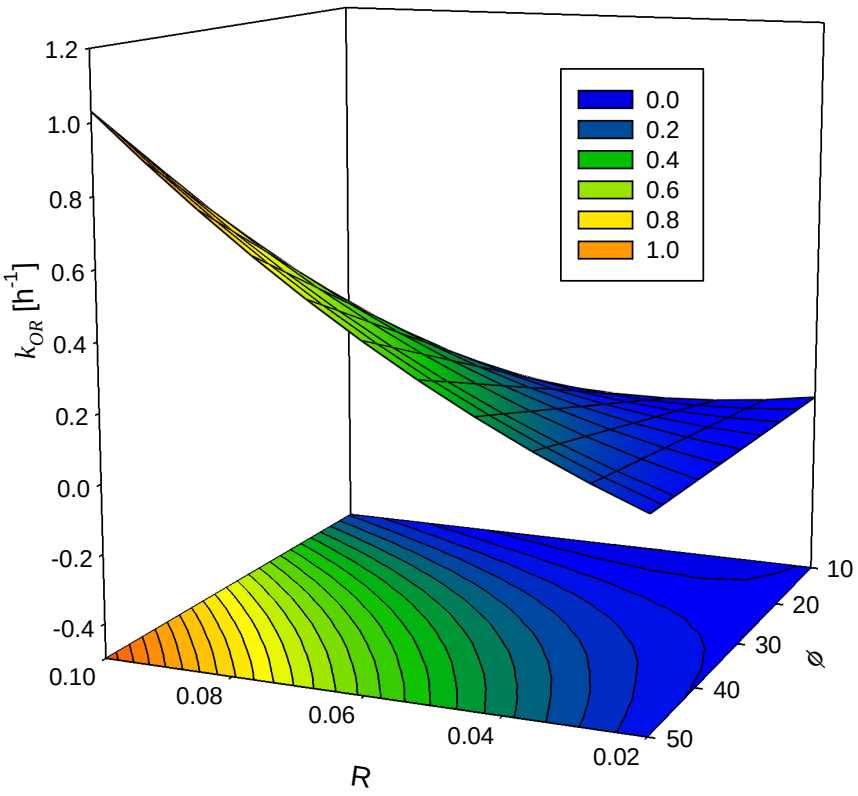

Figure 9. Response surface 3D plot of the normalized Ostwald ripening rate (k_{OR}) as a function of the process variables R and ϕ. The color scale indicates the Ostwald ripening rate values ranging from 0 h^{-1} to 1 h^{-1}.

3.3.6. Turbiscan Stability Index (TSI)

Taking into account that the emulsions were destabilized simultaneously by both processes, creaming and Ostwald ripening, the influence of *R* and ϕ in the global destabilization parameter, TSI, was studied. A good correlation was obtained between experimental data and the model proposed as shown in Figure 2. The model equation was:

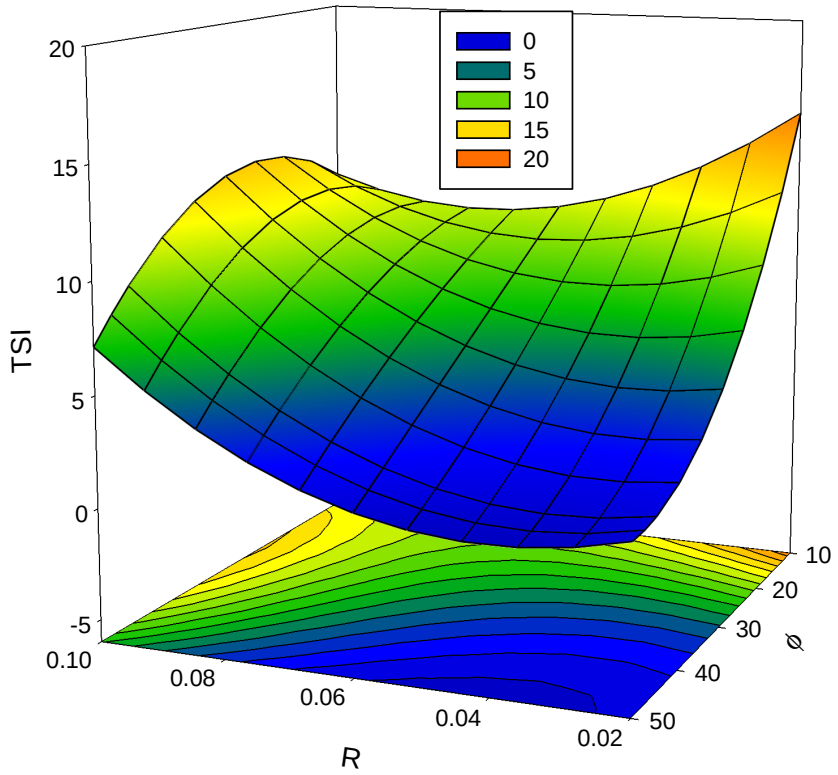

Figure 10. Response surface 3D plot of the Turbiscan Stability Index (TSI) as a function of the process variables R and ϕ. The color scale indicates the Turbiscan Stability Index values ranging from 0 to 20

$$TSI = 5.8 - 4.6*\phi + 4.0*R + 3.1*R^2 + 2.5*R*\phi - 3.6*R*\phi^2 \quad (11)$$

Figure 10 shows the dependence of TSI as a function of both, *R* and *ϕ*. It is worth noting the existence of an area with TSI values close to zero, for *R* values in the range 0.03-0.05 and for the highest *ϕ* value (50 wt%). Hence, an optimum process condition can be set for emulsions of submicron size with minimum destabilization. Figure 11 shows the normalized values of TSI and droplet size for the emulsions containing 50 wt% of disperse phase as a function of surfactant/oil ratio. The

intersection of both curves gave an optimal value with minimum destabilization and droplet size for R = 0.062.

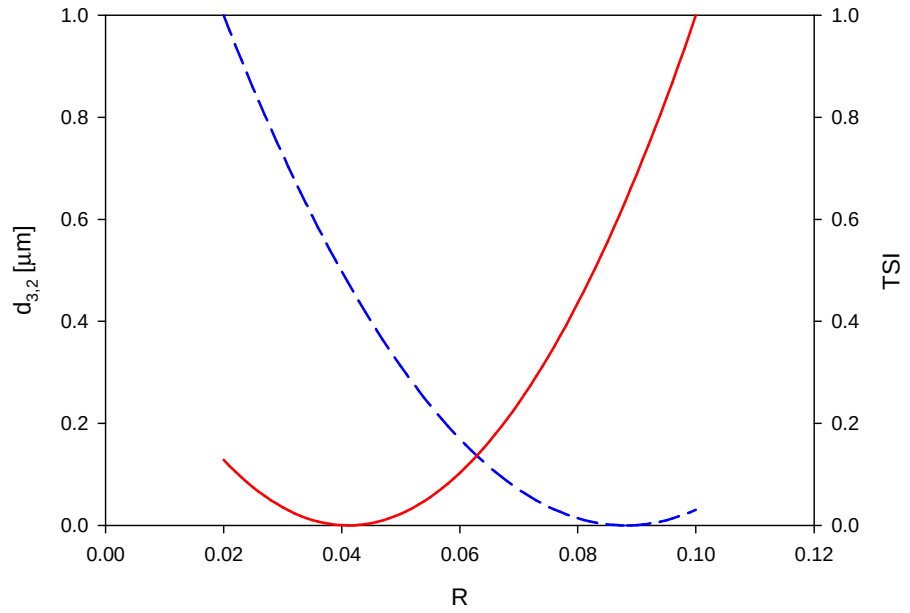

Figure 11. Normalized Sauter mean diameter vs R (dashed line) and normalized Turbiscan Stability Index vs. R (solid line) for emulsions with ϕ = 50 %wt. The intersection of both curves indicates the optimum formulation.

3.4 Conclusions

Monomodal, submicron D-limonene-in-water emulsions were obtained by rotor/stator homogenizer by using pluronic PE9400 as emulsifier. In order to gain a deeper knowledge of the droplet size distribution and stability of the emulsions as a function of the variables, surfactant/oil ratio (*R)* and disperse mass fraction (*ϕ)* a surface response methodology has been implemented. The mathematical models obtained from the full factorial design gave an adequate fit between the experimental and actual values.

D-limonene-in-water emulsions were destabilized by both, creaming and Ostwald ripening growth. The former was more marked for dilute emulsions, whereas the latter was faster at higher ϕ values. Furthermore, creaming destabilization of dilute emulsions (ϕ = 10 wt%) can be quantified using a kind of Stokes' law by substituting the viscosity of the continuous phase for that of the emulsion.

From rheological measurements the transition from Newtonian to shear-thinning behavior of the emulsions pointed to the occurrence of flocculation induced by surfactant micelles.

In order to take into account the influence of both destabilization processes a global destabilization parameter, the turbiscan stability index (TSI), has been used. An optimal formulation, with minimum TSI and minimum droplet size values, was obtained for R = 0.062 and ϕ = 50 wt%.

References

Abeynaike, A., Sederman, A. J., Khan, Y., Johns, M. L., Davidson, J. F., & Mackley, M. R. (2012). The experimental measurement and modelling of sedimentation and creaming for glycerol/biodiesel droplet dispersions. Chemical Engineering Science, 79, 125-137.

Alexandridis, P., & Lindman, B. (2000). Amphiphilic block copolymers: self-assembly and applications. Elsevier.

Batrakova, E. V., & Kabanov, A. V. (2008). Pluronic block copolymers: evolution of drug delivery concept from inert nanocarriers to biological response modifiers. Journal of Controlled Release, 130(2), 98-106.

Baser, K. H. C., & Buchbauer, G. (Eds.). (2009). Handbook of essential oils: science, technology, and applications. CRC Press.

Bueno, A. S., Pereira, C. M., Menegassi, B., Arêas, J. A. G., & Castro, I. A. (2009). Effect of extrusion on the emulsifying properties of soybean proteins and pectin mixtures modelled by response surface methodology. Journal of food engineering, 90(4), 504-510.

Chanamai, R., & McClements, D. J. (2000). Dependence of creaming and rheology of monodisperse oil-in-water emulsions on droplet size and concentration. Colloids and Surfaces A: Physicochemical and Engineering Aspects, 172(1), 79-86.

Cuellar, I., Bullón, J., Forgarini, A. M., Cardenas, A., & Briceno, M. I. (2005). More efficient preparation of parenteral emulsions or how to improve a pharmaceutical recipe by formulation engineering. Chemical engineering science, 60(8), 2127-2134.

Derkach, S. R. (2009). Rheology of emulsions. Advances in colloid and interface science, 151(1), 1-23.

Franco, J. M., Raymundo, A., Sousa, I., & Gallegos, C. (1998). Influence of processing variables on the rheological and textural properties of lupin protein-stabilized emulsions. Journal of Agricultural and Food Chemistry, 46(8), 3109-3115.

Gerhäuser, C., Klimo, K., Heiss, E., Neumann, I., Gamal-Eldeen, A., Knauft, J., ... & Frank, N. (2003). Mechanism-based in vitro screening of potential cancer chemopreventive agents. Mutation Research/Fundamental and Molecular Mechanisms of Mutagenesis, 523, 163-172.

Höfer, R., & Bigorra, J. (2007). Green chemistry—a sustainable solution for industrial specialties applications. Green Chemistry, 9(3), 203-212.

Jafari, S. M., He, Y., & Bhandari, B. (2007). Production of sub-micron emulsions by ultrasound and microfluidization techniques. Journal of Food Engineering, 82(4), 478-488.

Jafari, S. M., Beheshti, P., & Assadpoor, E. (2012). Rheological behavior and stability of d-limonene emulsions made by a novel hydrocolloid (Angum gum) compared with Arabic gum. Journal of Food Engineering, 109(1), 1-8.

Joglekar, A. M., & May, A. T. (1987). Product excellence through experimental design. Food Product and Development: From Concept to the Marketplace, 211-30.

Kabalnov A, (1998).Coalescence in emulsions, in Modern Aspects of Emulsions Science, ed. by Binks, Royal Society of Chemistry, pp. 205-260

Kabanov, A. V., Lemieux, P., Vinogradov, S., & Alakhov, V. (2002). Pluronic® block copolymers: novel functional molecules for gene therapy. Advanced drug delivery reviews, 54(2), 223-233.

Kerton, F. M., & Marriott, R. (2013). Alternative solvents for green chemistry (No. 20). Royal Society of chemistry.

Khuri, A. I., & Cornell, J. A. (1996). Response surfaces: designs and analyses (Vol. 152). CRC press.

Lesaint, C., Glomm, W. R., Lundgaard, L. E., & Sjöblom, J. (2009). Dehydration efficiency of AC electrical fields on water-in-model-oil emulsions. Colloids and Surfaces A: Physicochemical and Engineering Aspects, 352(1), 63-69.

Li, Y., Zhang, Z., Yuan, Q., Liang, H., & Vriesekoop, F. (2013). Process optimization and stability of d-limonene nanoemulsions prepared by catastrophic phase inversion method. Journal of Food Engineering, 119(3), 419-424.

Lifshitz, I. M., & Slyozov, V. V. (1961). The kinetics of precipitation from supersaturated solid solutions. Journal of Physics and Chemistry of Solids, 19(1), 35-50.

Lim, S. S., Baik, M. Y., Decker, E. A., Henson, L., Michael Popplewell, L., McClements, D. J., & Choi, S. J. (2011). Stabilization of orange oil-in-water emulsions: a new role for ester gum as an Ostwald ripening inhibitor. Food Chemistry, 128(4), 1023-1028.

Lu, H. Y., Shen, Y., Sun, X., Zhu, H., & Liu, X. J. (2013). Washing effects of limonene on pesticide residues in green peppers. Journal of the Science of Food and Agriculture, 93(12), 2917-2921.

Maher, P. G., Fenelon, M. A., Zhou, Y., Haque, K., & Roos, Y. H. (2011). Optimization of β-Casein Stabilized Nanoemulsions Using Experimental Mixture Design. Journal of food science, 76(8), C1108-C1117.

Maldonado-Valderrama, J., Fainerman, V. B., Gálvez-Ruiz, M. J., Martín-Rodriguez, A., Cabrerizo-Vílchez, M. A., & Miller, R. (2005). Dilatational rheology of β-casein adsorbed layers at liquid-fluid interfaces. The Journal of Physical Chemistry B, 109(37), 17608-17616.

Maldonado-Valderrama, J., Miller, R., Fainerman, V. B., Wilde, P. J., & Morris, V. J. (2010). Effect of gastric conditions on β-lactoglobulin interfacial networks: Influence of the oil phase on protein structure. Langmuir, 26(20), 15901-15908.

Manoj P, Watson AD, Hibberd DJ, Fillery-Travis AJ and Robins MM, (1998). *Characterization of a depletion-flocculated polydisperse emulsion. II. Steady-state rheological investigations.* Journal of Colloid and Interface Science **207**: 294-302

Marcuzzo, E., Debeaufort, F., Sensidoni, A., Tat, L., Beney, L., Hambleton, A.,& Voilley, A. (2012). Release Behavior and Stability of Encapsulated d-Limonene from Emulsion-Based Edible Films. Journal of agricultural and food chemistry, 60(49), 12177-12185.

McClements DJ, (2005) *Food Emulsions. Principles, Practices and Techniques*. CRC Press, Boca Raton

Mcclements, D. J. (2007). Critical review of techniques and methodologies for characterization of emulsion stability. Critical reviews in food science and nutrition, 47(7), 611-649.

Mengual, O., Meunier, G., Cayre, I., Puech, K., & Snabre, P. (1999). TURBISCAN MA 2000: multiple light scattering measurement for concentrated emulsion and suspension instability analysis. Talanta, 50(2), 445-456.

Montgomery DC, (2001) *Design and analysis of experiments*. Wiley, New York.

Murali, R., Karthikeyan, A., & Saravanan, R. (2013). Protective Effects of d-Limonene on Lipid Peroxidation and Antioxidant Enzymes in Streptozotocin-Induced Diabetic Rats. Basic & clinical pharmacology & toxicology, 112(3), 175-181.

Musa, S. H., Basri, M., Masoumi, H. R. F., Karjiban, R. A., Malek, E. A., Basri, H., & Shamsuddin, A. F. (2013). Formulation optimization of palm kernel oil esters

nanoemulsion-loaded with chloramphenicol suitable for meningitis treatment. Colloids and Surfaces B: Biointerfaces, 112, 113-119.

Neogi, P., Narsimhan, G., (2001). Ostwald ripening of oil drops in a micellar solution. Chemical Engineering Science, 56(14), 4225-4231.

Pal, R., (2011). Rheology of simple and multiple emulsion. Current Opinion in Colloid and Interface Science 16, 41-60.

Pérez-Mosqueda, L. M., Maldonado-Valderrama, J., Ramírez, P., Cabrerizo-Vílchez, M. A., Muñoz, J., (2013). Interfacial characterization of Pluronic PE9400 at biocompatible(air–water and limonene–water) interfaces. Colloids Surf. B, 111 171-178.

Salager, J. L., Anton, R. E., Briceño, M. I., Choplin, L., Marquez, L., Pizzino, A., Rodriguez, M. P., (2003). The emergence of formulation engineering in emulsion making—transferring know-how from research laboratory to plant. Polymer international, 52(4), 471-478.

Soleimanpour, M., Koocheki, A., Kadkhodaee, R., (2013). Influence of main emulsion components on the physical properties of corn oil in water emulsion: Effect of oil volume fraction, whey protein concentrate and *Lepidium perfoliatum* seed gum. Food Research International, 50(1), 457-466.

Soottitantawat, A., Yoshii, H., Furuta, T., Ohkawara, M., Linko, P. (2003). Microencapsulation by spray drying: influence of emulsion size on the retention of volatile compounds. Journal of Food Science, 68(7), 2256-2262.

Torcello-Gómez, A., Santander-Ortega, M. J., Peula-García, J. M., Maldonado-Valderrama, J., Gálvez-Ruiz, M. J., Ortega-Vinuesa, J. L., Martín-Rodríguez, A. (2011a). Adsorption of antibody onto Pluronic F68-covered nanoparticles: link with surface properties. Soft Matter, 7(18), 8450-8461.

Torcello-Gómez, A., Maldonado-Valderrama, J., Martín-Rodríguez, A., McClements, D. J., (2011b). Physicochemical properties and digestibility of emulsified lipids in simulated intestinal fluids: influence of interfacial characteristics. Soft Matter, 7(13), 6167-6177.

Torcello-Gómez, A., Maldonado-Valderrama, J., Jódar-Reyes, A. B., Foster, T. J., (2013). Interactions between Pluronics (F127 and F68) and Bile Salts (NaTDC) in the Aqueous Phase and the Interface of Oil-in-Water Emulsions. Langmuir, 29(8), 2520-2529.

Torcello-Gómez, A., Maldonado-Valderrama, J., Jódar-Reyes, A. B., Cabrerizo-Vílchez, M. A., Martín-rodríguez, A., (2014). Pluronic-covered oil-water interfaces under simulated duodenal conditions. Food Hydrocolloids, 34, 54-61.

Urban, K., Wagner, G., Schaffner, D., Röglin, D., & Ulrich, J. (2006). Rotor-Stator and Disc Systems for Emulsification Processes. Chemical engineering & technology, 29(1), 24-31.

Vankova, N., Tcholakova, S., Denkov, N. D., Ivanov, I. B., Vulchev, V. D., Danner, T., 2007. Emulsification in turbulent flow. 1. Meand and maximum drop diameters in inertial and viscous regimes, Journal of colloid and interface science, 312, 363-380.

Weers, J.G., 1998. Ostwald ripening in emulsions, in Binks (Ed.), Modern Aspects of Emulsions Science, Royal Sociaty of Chemistry, Cambridge, pp. 292-327.

Weiss, J., Canceliere, C., McClements, D. J., 2000. Mass transport phenomena in oil-in-water emulsions containing surfactant micelles: Ostwald ripening. Langmuir, 16(17), 6833-6838.

4

Influence of emulsifier concentration on the rheology, microstructure and physical stability of D-limonene emulsions stabilized by a lipophilic biopolymer

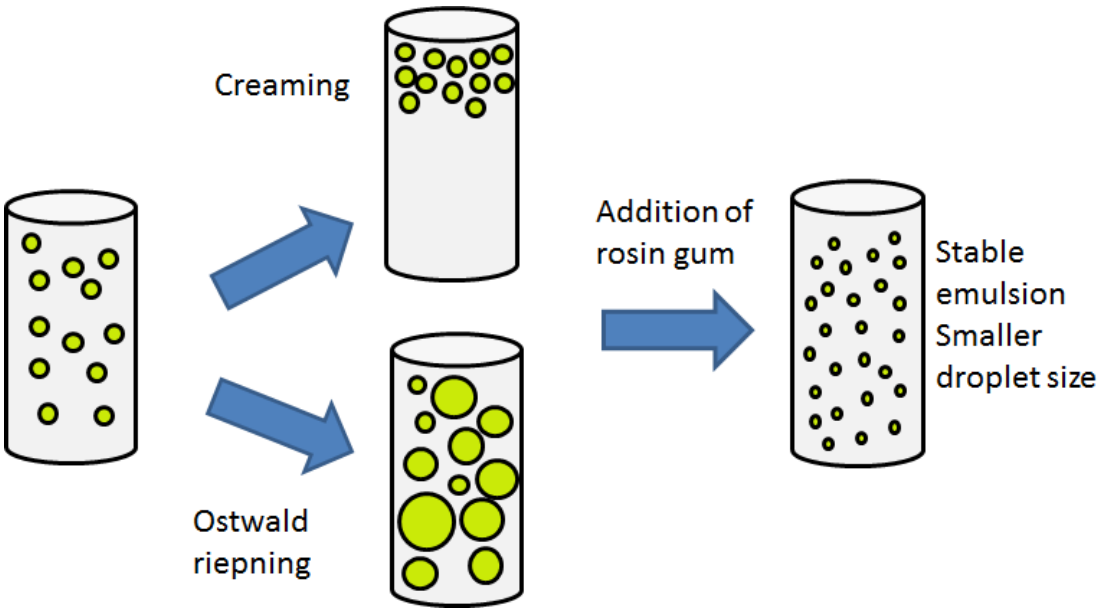

Abstract

Stable sub-micron D-limonene-in-water emulsions have been obtained by means of a single-step rotor/stator homogenising process. The formulation comprises the use of a naturally occurring lipophilic biopolymer (rosin gum) dissolved in the disperse phase and a non-ionic triblock copolymer as emulsifier (Pluronic PE9400).

The addition of rosin gum highly increases the stability of Pluronic-covered emulsions by reducing the Ostwald ripening growth of the emulsion droplets. A full Ostwald ripening inhibition was obtained for rosin gum concentrations above 10 wt%. Furthermore, it has been observed that rosin gum adsorbs at the interface, reducing the interfacial tension and leading to lower droplet sizes.

Emulsions were classified in three different regions as a function of Pluronic PE9400 concentration. Region I: from 1 wt% to 3 wt% the surfactant available was not enough to achieve the minimum droplet size that can be obtained under the operating conditions. Region II: from 3 wt% to 6 wt% the droplet size reached a constant value and highly stable emulsions were obtained. Region III: from 6 wt% to 8 wt% an excess of surfactant in solution provoked a depletion flocculation process, which eventually led to the creaming of the emulsion.

This chapter is a contribution to the development of sustainable product engineering by scouting the applications of green solvents in model agrochemical emulsions.

4.1 Introduction

D-limonene is an interesting bio-derived solvent which can be obtained from citric peels. This organic compound presents interesting applications in different fields such as cosmetics, food, pesticide applications and pharmaceutical industries (Brud, 2010, Caballero-Gallardo, 2011; Jafari, 2012; Marcuzzo, 2012; Klein, 2010; Murali, 2012). Furthermore, D-limonene is a good candidate to be used as a (bio-)solvent in the design of novel agrochemical products, replacing more pollutant chemicals (Kerton, 2009).

The formulation of the disperse phase was completed with rosin gum as stabilizer. Rosin gum is a natural polymer obtained from pine trees. It is chiefly composed of 90% rosin acids (abietic acid, palustric acid, neoabietic acid, and others) and is 10% non-acidic. There exist several papers which comment on the application of rosin gum in biocompatible systems such as drug delivery (Lee 2004 and 2005, Kumar 2013) or microencapsulation (Fulzele 2004).

The emulsifier function was carried out by an ABA block copolymer, Pluronic PE 9400, where A and B stand for poly(ethylene) oxide and poly(propylene) oxide respectively. These surfactants have found many industrial applications as foam and emulsion stabilizers (Alexandridis, 2000; Tadros, 2005). On the other hand, these polymeric surfactants have been employed recently in more sophisticated technological applications such as drug delivery, gene therapy and the developing of foodstuffs that provide specific physiological responses, such as control of lipid digestion or satiety (Batrakova, 2008; Kabanov, 2002; Torcello-Gómez, 2011a, 2011b, 2013 & 2014, Wulff-Perez 2012, Jódar-Reyes 2010).

Emulsions are thermodynamically unstable colloidal dispersions which are destabilized by several mechanisms such as flocculation, coalescence, gravitational

separation (sedimentation or creaming) and Ostwald ripening. Production of stable submicron emulsions is a key achievement in several fields such as food, pharmaceutical and agrochemicals (McClements, 2005; Leal-Calderon, 2007; Tadros, 2009).

Two-step emulsification processes are commonly used to obtain submicron emulsion. First a coarse emulsion is usually produced by means of a rotor/stator system. Then high pressure homogenizer or ultrasonication devices are used to decrease the droplet size to a submicron level. Nevertheless, in the present work emulsions with volumetric diameters of ca. 0.5 μm were produced by using a single-step rotor/stator emulsification process.

One of the critical parameters that have to be carefully controlled in emulsion formulation is the emulsifier concentration. A minimum surfactant bulk concentration is required to fully cover the available interfacial area created during the emulsification process. However, an excess of surfactant in solution will lead to the formation of a large number of micelles. It is well-known that non-adsorbed surfactant micelles could induce the flocculation of the emulsion droplets due to a depletion mechanism. Although flocculation is a reversible process, it could develop irreversible destabilization processes such as creaming and/or coalescence (Bibette, 1991; Dickinson, 2000; Dimitrova, 1999; McClements, 1994; Radford, 2004; Shields, 2001).

This work provides a systematic study concerning the development and physicochemical characterization of fine emulsions by means of fundamental principles of colloid and interface science. These new findings can have applications concerning the rational design of eco-friendly emulsions with promising applications in agrochemical formulations.

4.2 Materials and methods

4.2.1 Materials

D-Limonene (4-isopropenyl-1-methylciclohexane) is an organic compound widely used as an industrial solvent. It is obtained from the peel of citrus fruit, mainly from oranges and lemons. D-Limonene (97%) was purchased from Sigma-Aldrich® and purified with Florisil® resins (Fluka, 60-10 mesh) prior to use by following the procedure used elsewhere (Maldonado-Valderrama, 2005; Maldonado-Valderrama, 2010) Namely, a mixture of oil and Florisil® in proportion 2:1 w/w was shaken gently for 3 h and then separated by decanting.

Rosin gum is an exudate gum which is solid at room temperature. It is a mixture of different acids such as abiatic acid, palaustric acid, neoabetic acid. Its molecular weight is 302.45 $gmol^{-1}$ and its density at 20ºC is 1.06 gmL^{-1}

The triblock copolymer Pluronic PE9400 (PEO_{21}-PPO_{50}-PEO_{21}, Mw = 4600 $gmol^{-1}$ and HLB = 12-18) was kindly provided by BASF and used as received.

Ultrapure water, cleaned using a Milli-Q water purification system was used. All glassware was washed with 10% Micro-90 cleaning solution and exhaustively rinsed with tap water, isopropanol, deionized water, and ultrapure water in this sequence. All measurements were carried out at 20^0C.

4.2.2 Emulsification methods

First, an excess of the required amount of rosin gum was dissolved in purified D-limonene by gently stirring overnight. This solution was filtered in order to remove the insoluble fraction of the rosin gum and then D-limonene was added to the filtered solution, reaching a final rosin gum concentration of 30 wt%.

The continuous phase was produced by dissolving PE9400 surfactant using a magnetic stirrer for 15 minutes at 300 r.p.m.

The emulsion was then formed by using a batch process; the oil phase (70 wt% Dlimonene and 30 wt% rosin gum) was added over the continuous phase and homogenized for 60 s at 17500 r.p.m. using a rotor/stator system Ultraturrax T-25/KV11. The mass disperse fraction ϕ = 50 wt% and the final emulsion weight was 50 g. The influence of Pluronic PE9400 concentration on the stability and physicochemical properties of the emulsions was studied in the range from 1 to 8 wt%.

4.2.3 Emulsion droplet size analysis

Droplet size distribution (DSD) was determined by a laser diffraction technique using a Mastersizer X (Malvern Instruments). These measurements were carried out after 1, 7, 15, 30, 45 and 75 days aging time to analyze the time evolution of the DSD. All measurements were carried out in triplicate.

The mean droplet diameter was expressed as the Sauter diameter ($d_{3,2}$) and volume mean diameter ($d_{4,3}$).

$$d_{m,n} = \frac{\sum_i N_i D_i^m}{\sum_i N_i D_i^n} \quad (1)$$

where N_i is the number of droplets with a diameter, D_i. To determine the distribution width of droplet sizes, “span” was used, calculated by the following formula:

$$Span = \frac{D(v,0.9) - D(v,0.1)}{D(v,0.5)} \quad (2)$$

where, *D(v,0.9), D(v,0.5), D(v,0.1)* are diameters at 90%, 50% and 10% cumulative volume, respectively.

4.2.4 Emulsion microstructure

An optical microscope, Axio Scope A1, from Carl Zeiss was used with a 40x objective to study the microstructure of all emulsions. The images were captured 24 hours after the preparation of the emulsion.

4.2.5 Rheology of emulsions

A controlled-stress rheometer AR 2000 (TA Instruments, Crawley, United Kingdom) with a rough plate-plate sensor (40 mm diameter) was used to carry out small amplitude oscillatory shear (SAOS) tests. Stress sweeps at three different frequencies (0.1, 1 and 3 Hz) were performed from 0.02 to 10 Pa in order to estimate the lineal viscoelastic range. Frequency sweep tests (from 30 to 0.01 rad/s) were performed selecting a stress well within the linear range. SAOS experiments were carried out after 1 and 75 days after preparation.

Flow curves were obtained by using a Mars rheometer from Haake Thermo Scientific (Germany). This is a controlled stress rheometer with a sandblasted Z20 coaxial cylinder sensor system (Ri=1cm, Re/Ri=1.085). Flow curves were carried out at 1, 30 and 75 days of emulsion storage.

All rheological measurements were performed at 20ºC ± 0.1ºC, using a C5P Phoenix circulator (Thermo-Scientific) for sample temperature control. Samples were taken at about 2 cm from the upper part of the container. Sampling from the top part of the container in contact with air was avoided. The results represent the mean of three measurements. Equilibration time prior to rheological tests was 180 s.

4.2.6 Viscosity of the continuous phase

The viscosity values for the continuous phase have been calculated using a Falling Ball Viscometer C (Haake). Viscosity is obtained from the following equation:

$$\eta = K(\rho_{ball} - \rho_l)t \quad (3)$$

where η is the viscosity of the continuous phase, ρ_{ball} is the density of the ball (2.2 g/cm^3), ρ_l is the density of the continuous phase (see Table 2), K is a constant that depends on the ball (0.007 mPa·s·cm^3·g^{-1}·s^{-1}) and t is the time

All the measurements were performed at 20ºC ± 0.1ºC and the result is the average of five measurements.

4.2.7 Stability

Multiple light scattering measurements with a Turbiscan Lab Expert were used in order to study the destabilization of the emulsions. Measurements were carried out during 75 days at 30ºC to determine the predominant mechanism of destabilization in each emulsion.

4.2.8 Interfacial tension measurements

A drop profile analysis tensiometer (CAM200, KSV, Finland) was used in this study. A droplet of the lightest phase is formed at the tip of a hooked capillary, which is immersed in the less dense phase and thermostatized at 20ºC. The surface pressure is defined as $\Pi = \gamma_0 - \gamma$, where γ is the interfacial tension of the rosin gum solution against limonene, and γ_0 = 44.0±0.5 mNm^{-1} is the interfacial tension of the limonene-water interface at 20ºC.

4.3 Results and Discussion

4.3.1 Influence of Rosin gum concentration on the stability and droplet size of the emulsions.

It has been shown that D-limonene emulsions are prone to break down due to creaming and/or Ostwald ripening. In a previous work an optimum formulation for Pluronic-covered D-limonene emulsions was found for ϕ = 50 wt% and 3 wt% Pluronic PE9400. Nevertheless, this emulsion suffers from Ostwald ripening growth driving, eventually, to a creaming destabilization. In order to improve the emulsion formulation a lipophilic biopolymer is added to the emulsions. Ostwald ripening destabilization was quantified by means of a normalized Ostwald ripening rate, k_{OR}. These values were determined from the linear part of the plot of r^3/r^3_0 vs. t, where r and r_0 are the droplet radius at a given time and the initial droplet radius respectively. Parameters r and r_0 were measured by laser diffraction measurements. As shown in Figure 1 addition of rosin gum diminished the normalized Ostwald ripening rate, k_{OR}, for emulsions containing 3 wt% PE9400 and with a disperse mass fraction of 50 wt%. For rosin gum concentrations above 10 wt% droplet growth is inhibited. Furthermore, Figure 1 shows on its right-hand y-axe the evolution of the initial droplet size as a function of rosin gum concentration. It is shown that emulsion droplet decreases with increasing rosin gum concentration, reaching a minimum value of approximately ca. 500 nm. The decrease in the emulsion droplet size is likely to be due to the adsorption of the rosin gum at the interface, which diminishes the interfacial tension, making it easier to create higher interfacial area by applying the same amount of energy during the emulsification process. In order to verify this assumption, the D-limonene-water interfacial tension was measured as a function of rosin gum concentration (Table 1). These experimental results

confirmed the adsorption of rosin gum at the D-limonene-water interface, leading to lower emulsion droplet sizes and hindering the migration of limonene across the interface.

Rosin gum (wt%)	Π (mNm^{-1})
1e-4	2
1e-3	7
1e-2	12
0.1	23
1	26
10	29
30	31

Table 1. Interfacial pressure of the D-limonene-water interface at different rosin gum concentrations at 20ºC.

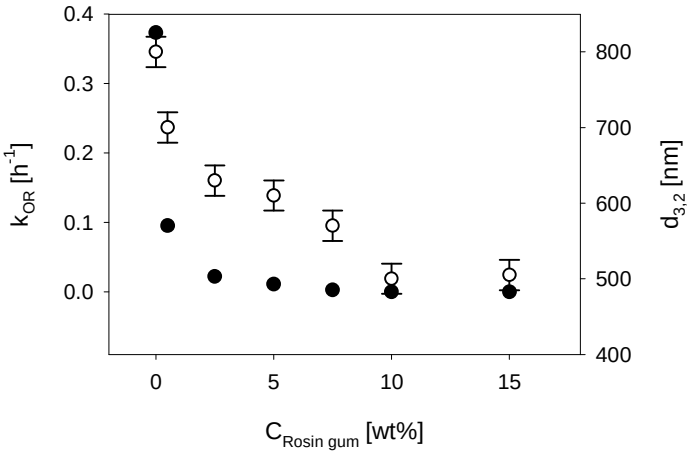

Figure 1. Ostwald ripening rate, kOR and sauter diameter, d3,2 as a function of rosin gum concentration.

4.3.2 Droplet size distributions and morphology of droplets

Figure 2A shows the droplet size distribution of the emulsions with different surfactant concentration aged for 24 hours. First, it should be stated that all emulsions showed monomodal distributions. Moreover, droplet size distributions shifted to lower

droplet diameters with increasing PE9400 bulk concentration and levelled off for surfactant concentrations above 5 wt%. Figure 2B shows the Sauter and volumetric mean diameters and span values of emulsions with different PE9400 concentration aged for 24 hours. For surfactant concentration above 1 wt%, submicron Sauter and volumetric mean diameters were achieved. The lowest mean diameter values were found for the 6 wt% emulsion. Despite this, it should be noted that span (droplet size polydispersity) dropped to a minimum around 4 wt%. It is stated that an increase in polydispersity highly influences the stability of the emulsion leading to an increase in the creaming rate due to higher values of the effective packing parameter (McClements, 2005).

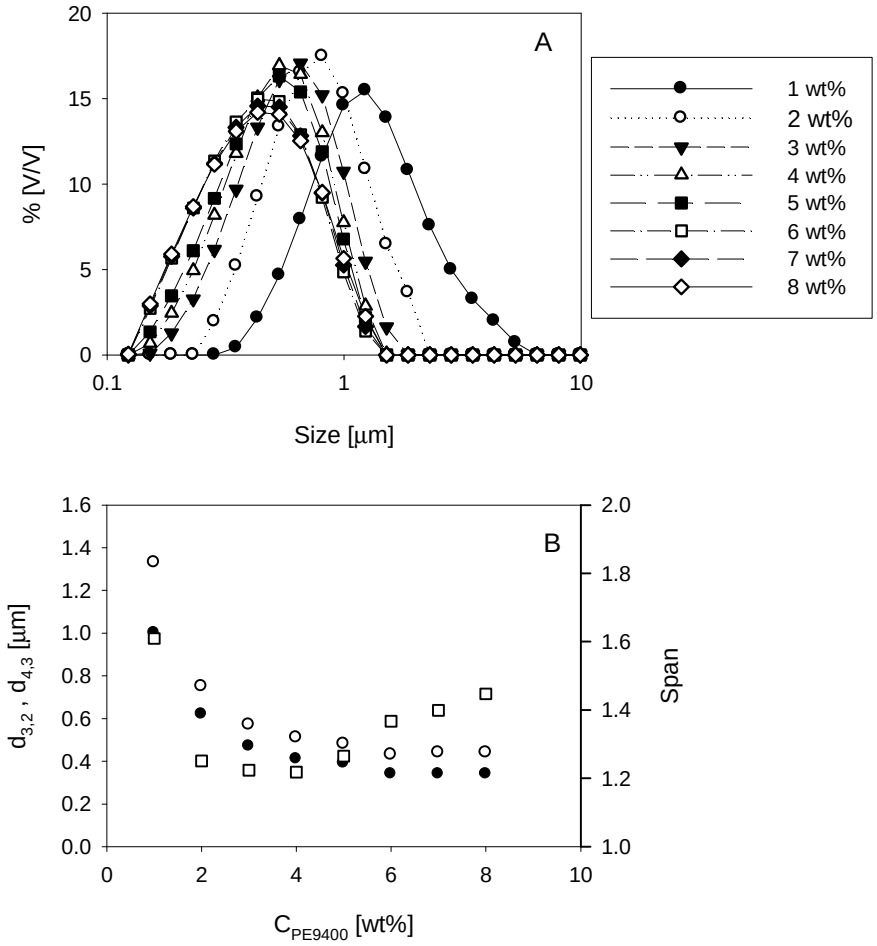

Figure 2. (A) Droplet size distribution and (B) Sauter mean diameter (d3,2), volumetric mean diameter (d4,3) and span as a function of Pluronic PE9400 concentration of emulsions aged for 24 hours.
Standard deviation of the mean (3 replicates) for d3,2, d4,3 and span < 5%

Figure 3 shows the time evolution for 75 days of the volume mean diameter for the eight emulsions. It is noteworthy that stable submicron emulsions were obtained at surfactant concentrations within 3-7 wt%. The increase in the $d_{4,3}$ values of the emulsions with less surfactant (1 and 2 wt%) can be ascribed to the occurrence of coalescence, enhanced by creaming of the bigger droplets in these emulsions. A slight increase in the $d_{4,3}$ value was observed for the most concentrated (8 wt%) emulsion after aging for 75 days. This increase is likely to be related to a depletion flocculation process

due to an excess of surfactant micelles in solution which cause the coalescence of emulsion droplets.

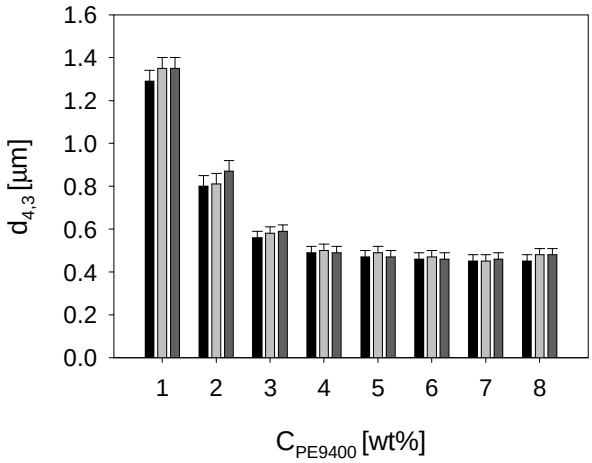

Figure 3. Volume mean diameter, d4,3 as a function of Pluronic PE9400 concentration. Emulsion samples were aged for 1 day (black bars), 30 days (light-grey bars) and 75 days (dark-grey bars).

Optical micrographs were acquired in order to confirm the laser diffraction results obtained so far. Emulsions were diluted (dilution ratio 1:20), so droplets were more easily observed. Figure 4 shows, by way of example, the micrographs obtained by optical microscopy with transmitted light (phase contrast mode) for the emulsions containing 4 wt% (Figure 4B) and 1 wt%, (Figure 4A) Pluronics PE9400. It is observed that 1 wt% emulsion is a more polydisperse emulsion with bigger droplets than 4 wt%, thus confirming the results shown in Figure 1.

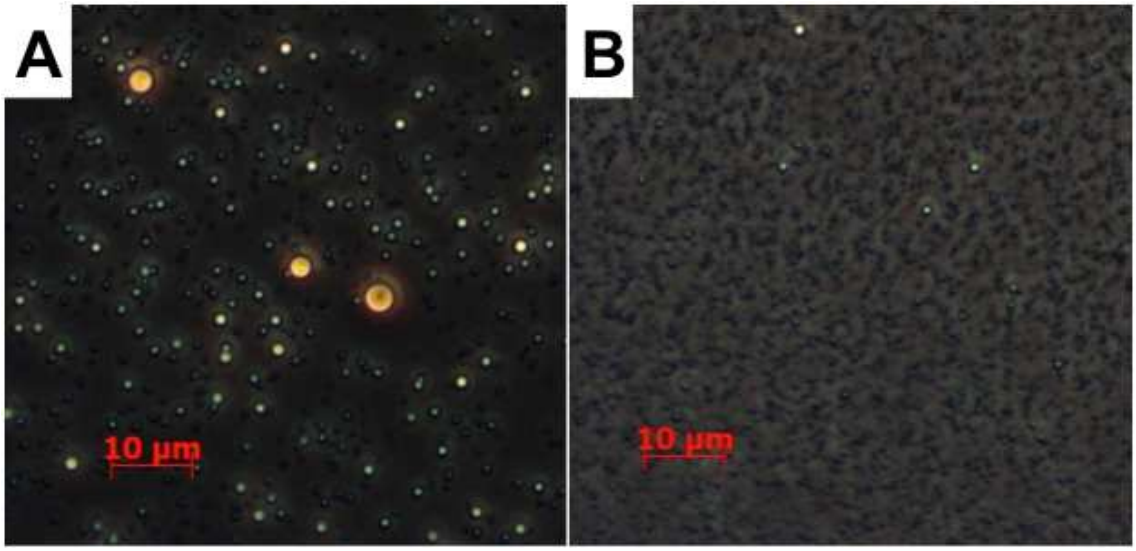

Figure 4. Micrographs using transmitted light in phase contrast mode (objective: 40x) for diluted emulsions (dilution ratio: 1/20) containing (a) 1 wt% Pluronics PE9400 and (b) 4 wt% Pluronics PE9400. Emulsion samples aged for 24 hours.

4.3.3 Rheology

Figure 5 shows the flow properties for the emulsions studied aged for 24 hours as a function of surfactant concentration. All the emulsions exhibited a trend to reach a Newtonian region at the lowest shear rate values, followed by a decrease in viscosity (shear-thinning behaviour) above a critical shear rate. This behaviour is likely to be produced due to shear-induced breaking of flocs (Chanamai, 2000). Greater tendency to flocculate has previously been associated to finer emulsions by Pal, 1996 and Barnes, 1994 (Pal, 1996; Barnes, 1994).

Viscosity curves were fitted to the Cross model:

$$\eta = \eta_{\infty} + \frac{\eta_0 - \eta_{\infty}}{1 + \left(\frac{\dot{\gamma}}{\dot{\gamma}_c}\right)^{1-n}} \qquad (4)$$

where η is the viscosity, η_{∞} is the limiting high shear rate viscosity, η_0 is the zero-shear viscosity, $\dot{\gamma}$ is the shear rate, $\dot{\gamma}_c$ is the critical shear rate and *n* is the power law index.

The inverse of the critical shear rate gives what is commonly known as the characteristic time for flow, $1/\dot{\gamma}_c$

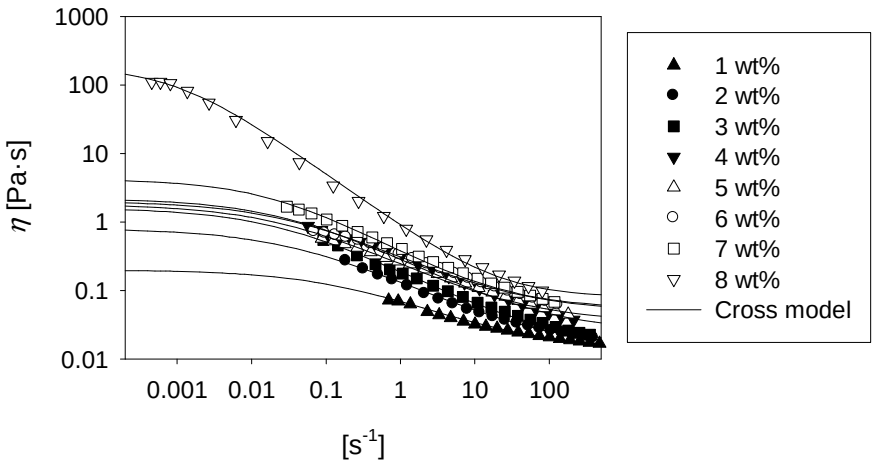

Figure 5. Flow curves for the studied emulsions as a function of Pluronic PE9400 concentration for 24 hours of aging time at 20ºC. Continuous lines illustrate data fitting to the Cross model.

Figure 5 also illustrates the fitting quality of the results obtained to the Cross model ($R^2 > 0.999$). The values of fitting parameters are shown in Table 2 as a function of surfactant concentration. An analysis of the fitting parameters allows the identification of three surfactant concentration regions (see figure 6).

I. Concentration region I (1-3) wt%: The zero-shear viscosity and characteristic time for flow increased, while the flow index decreased with Pluronic PE9400 concentration due to the fall in droplet diameter, which resulted in greater specific surface area available for friction. Most of the Pluronic surfactant was required to cover the increasing O/W interface. This fact is associated with a tendency for the apparent viscosity to increase when the Sauter diameter decreases (Barnes, 1994).

II. Concentration region II (3-6) wt%: The zero shear viscosity, the characteristic time for flow and the flow index levelled off. Excess amounts of Pluronic in the continuous phase are in dynamic equilibrium with surfactant on the interface and in addition micelle concentration start being significant.

III. Concentration region III (6-8) wt%: Mean droplet diameters levelled off, and polidispersity went clearly up leading to a striking increase in both zero-shear viscosity and characteristic time for flow. Furthermore, a marked drop in the flow index is shown, indicating the occurrence of more shear thinning emulsions. An excess of free micelles in the disperse phase is expected which is likely to lead to a depletion flocculation phenomenon influencing the rheological properties of the emulsion (Pal, 2011; Derkach, 2009). Therefore, the zero shear viscosity and the characteristic time for flow are expected to increase, whereas the flow index should decrease as shown in Table 1. This rheological change could be produced by either an enhanced viscosity of the continuous phase (due to the presence of lyotropic structures based on micelles), or the occurrence of a stronger oil network due to depletion flocculation (Palazolo, 2005; Manoj, 1998).

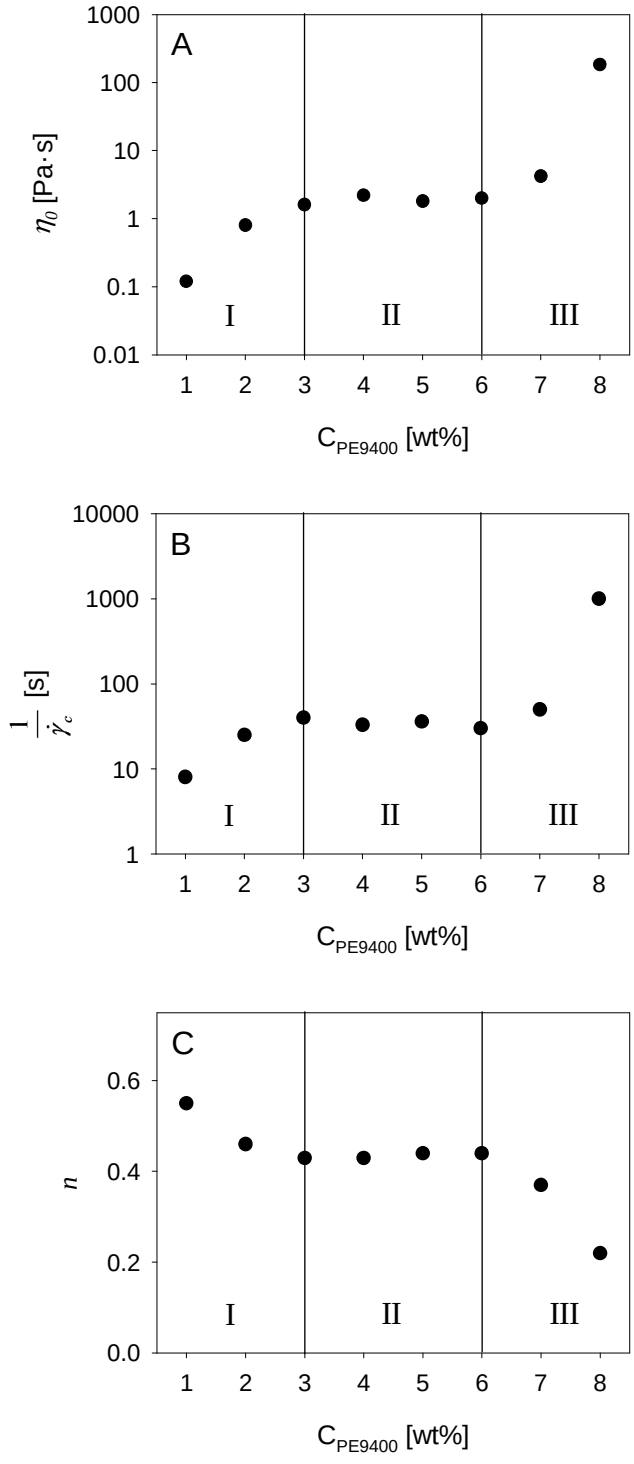

Figure 6. A) Zero shear viscosity, η_0; B) Characteristic time for flow, $1/\dot{\gamma}_c$; and C) flow index, n, as a function of Pluronic PE9400 concentration for emulsions aged for 24 hours.

Surfactant (wt%)	η_∞ (Pa·s)	η_0 (Pa·s)	$1/\dot{\gamma}_c$ (s)	n
1	0.014	0.2	8	0.55
2	0.015	0.8	25	0.46
3	0.015	1.6	40	0.43
4	0.025	2.2	33	0.44
5	0.028	1.8	36	0.44
6	0.045	2	30	0.44
7	0.055	4.2	50	0.37
8	0.080	184	1000	0.22

Table 2. Flow curves fitting parameters of the Cross model for the emulsions at 24 hours of aging time.

The viscosity of the continuous phase prior to emulsification was measured by means of the falling ball viscometer. It is seen that increasing surfactant concentration from 2 wt% to 16 wt% causes viscosity to increase from 1.1 to 4.6 mPa·s (Table 3). Nonetheless, the increase in the viscosity of emulsions from the lowest surfactant concentration to the highest one is about four orders of magnitude (from 100 to 100000 mPa·s). Hence, the marked increase in the viscosity of the emulsions is more likely to be related to a depletion flocculation phenomenon than to the viscosity of the continuous phase.

Surfactant (wt%)	ρ (g/ml)	η (mPa·s)
2	1.0012	1.08
4	1.0040	1.26
6	1.0065	1.51
8	1.0091	1.77
10	1.0122	2.67
12	1.0145	3.17
14	1.0170	3.72
16	1.0195	4.63

Table 3. Continuous phase density and viscosity values at 20ºC.

Figures 7 A, B, and C show the flow curves as a function of aging time for three emulsions which are representative of the three different regions explained above (1

wt%, 4 wt% and 7 wt%). Experimental data were fitted to the Cross model (equation 4) with the fitting parameters given in Table 4. Samples were taken from the upper part of the container to follow any rheological changes produced by creaming. The evolution of the rheological parameters for the emulsion containing 1wt% PE9400 pointed to the development of a more viscous and shear thinning structure at the top of the vial, which is likely to be due to the formation of a cream layer. The evolution of the flow curves for 7 wt% PE9400 emulsion showed a slower increase in the viscosity while maintaining the same flow index value. Hence, a slower formation of a serum layer is observed. Finally, the emulsion containing 4 wt% PE9400 was stable for all the aging time.

Surfactant (wt%)	Storage time (days)	η_∞ (Pa·s)	η_0 (Pa·s)	$1/\dot{\gamma}_c$ (s)	n
1	1	0.014	0.2	8	0.55
	30	0.017	0.7	77	0.48
	75	0.023	10	588	0.39
4	1	0.025	2.2	33	0.44
	30	0.022	2.3	33	0.45
	75	0.022	2.5	25	0.44
7	1	0.055	4.2	50	0.37
	30	0.056	4.6	42	0.39
	75	0.065	8.2	53	0.35

Table 4. Evolution over time of the flow curves fitting parameters of the Cross model

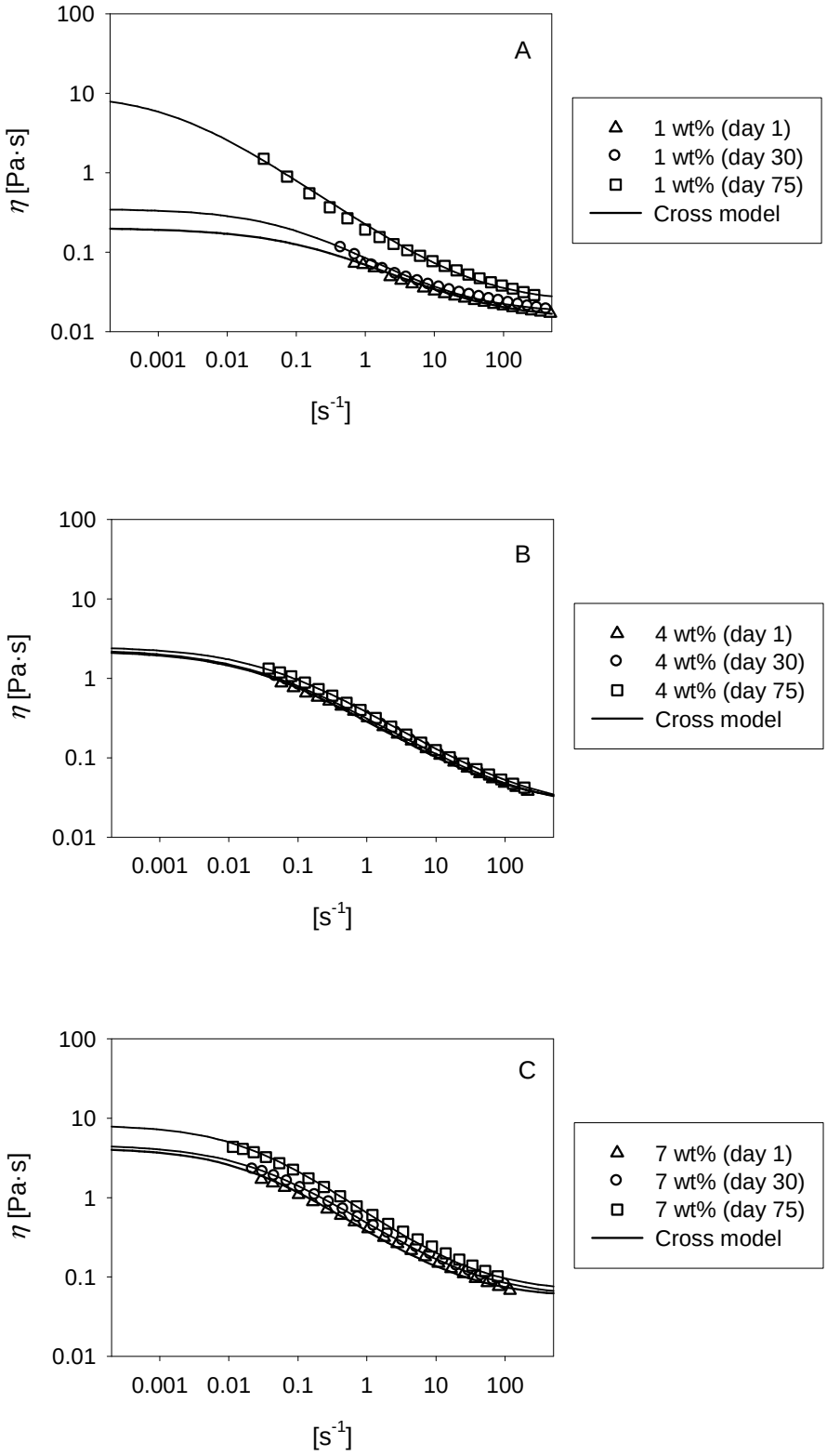

Figure 7. Flow curves as a function of aging time for emulsions with a surfactant concentration of A) 1 wt% B) 4 wt% and C) 7 wt%

A small amplitude oscillatory shear (SAOS) test is a technique widely used to determine the viscoelastic behavior of a system. And can provide useful information about the microstructure of the colloidal systems and their evolution over time. In order to ensure that the test does not provoke structural destruction in the sample, tests should be performed at a stress and strain within the linear viscoelastic range (LVR). Therefore, oscillatory torque sweep tests at three different frequencies were previously conducted in order to estimate the maximum amplitude value of the sinusoidal shear stress function that guarantees linear viscoelastic behavior. In a stress sweep, G’ and G’’ remain constant up to a critical stress and strain.

Figure 8 shows the frequency dependence of the linear viscoelasticity functions, G’ and G” for the aged emulsions that exhibited a measurable linear viscoelastic range as a function of time. The formulation with 7% surfactant after 24 hours presents fluid-like viscoelastic behaviour with higher values for G´´ than G´ throughout the measured frequency range. The difference between G´´ and G´ became larger with decreasing frequency. The transition between the terminal region and the relaxation plateau zone is not clear. The formulation with 7% surfactant exhibits a change in its viscoelastic properties after 75 days. In this sense, G" is lower than G' in the higher frequency regime and G" is greater than G' in the lower frequency regime as a consequence of a crossover point between G' and G". This crossover frequency (ω*) determines the onset of the terminal relaxation zone and moves to lower frequencies with aging time, which implies higher relaxation times (t_r). The terminal relaxation time was calculated as the inverse of the crossover angular frequency and change from a value below 0.05 s to 0.18 s. Shorter relaxation times indicate relatively fast rearrangements of the network and correlate well with the instability of emulsions against creaming. On the other hand, longer relaxation times pointed to a stronger droplet−droplet interaction, which can be

correlated with greater macroscopic stability against creaming in emulsions (Aven, 2012; Santos, 2013).

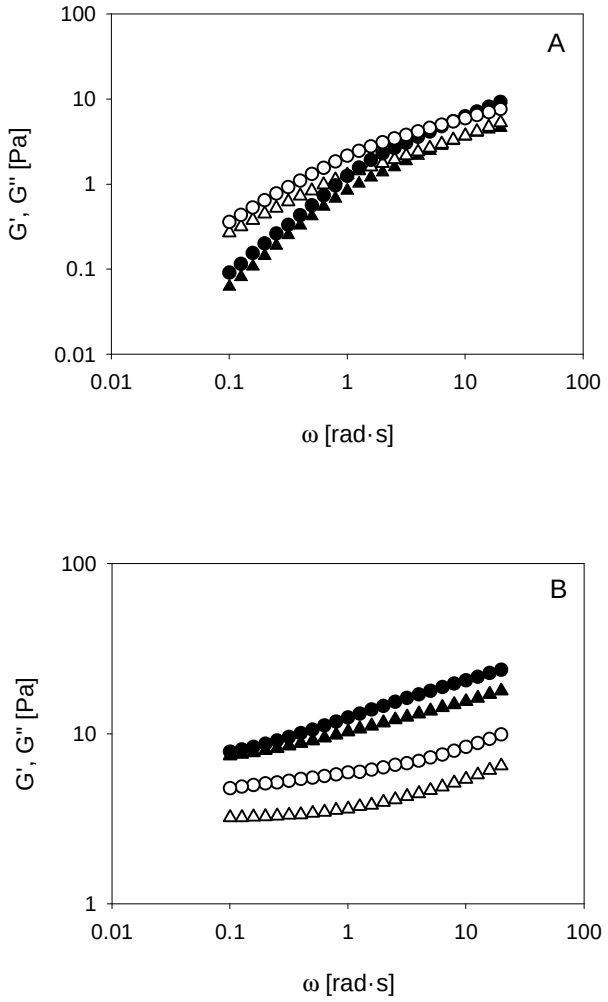

Figure 8. Influence of Pluronic PE9400 concentration and aging time on the mechanical spectra for the emulsions that exhibited measurable LVR. Shear stress amplitude: 0.05 Pa. A) 7 wt% of PE9400 and B) 8 wt% of PE9400. Filled and open symbols stand for storage and loss moduli, respectively. Triangles and circles are the mechanical spectra measured at 1 day and 75 days aging time, respectively.

On the other hand, the formulation with 8 wt% surfactant presents a dynamic behavior, which corresponds to a plateau zone in the mechanical spectrum, and it is non time-dependent. The G´ values are higher than the G´´ values and both show a slight

frequency-dependence. G´ and G´´ values experienced a minor increase with aging time which implies an increase in the viscoelastic properties of the emulsion. The results for this emulsion show a relaxation plateau zone that is typical for samples with weak-gel viscoelastic properties. This behavior has been seen in different systems like surfactants aqueous dispersions and/or polymers (Faers, 2005; Calero, 2010, Pérez-Mosqueda, 2013a), emulsions (Muñoz, 2012) and agrochemicals (Trujillo-Cayado, 2013).

This SAOS evolution is consistent with the development of structure. The increase in the G´ and G´´ values is associated with a depletion flocculation phenomenon which could help to favor an increase in the creaming rate if the compressive pressure on the droplet network due to gravity is greater than the maximum stress the gel can withstand (Buscall, 1987).

4.3.4 Physical stability

The physical stability of the emulsions was studied using the creaming index (CI) which is defined as (McClements, 2007):

$$CI = 100 \cdot \frac{H_S}{H_E} \tag{5}$$

where, H_E is the total height of the emulsion and H_S is the height of the serum layer.

The calculated creaming indexes for different emulsions aged for 75 days are represented in Figure 9 as a function of surfactant concentration. Similarly to the rheological characterization three regions are observed. First, a decrease in CI with increasing surfactant concentration from 1 wt% to 3 wt% was observed. Hence, emulsions became more stable against creaming due to the combination of the reduction of the droplet size and the increase in emulsion viscosity. In the second region from Pluronic PE9400 concentration ranging from 3 wt% to 6 wt% a CI value of around 1% was estimated, hence creaming is practically suppressed in this concentration interval.

Finally, from 6 wt% to 8 wt% the onset of creaming was detected from the increase in the CI values. This result is in agreement with the structural evolution of the emulsion suggested by the rheological measurements. Bearing in mind that droplet size remained the same over time, a destabilization process due to depletion flocculation phenomenon is inferred.

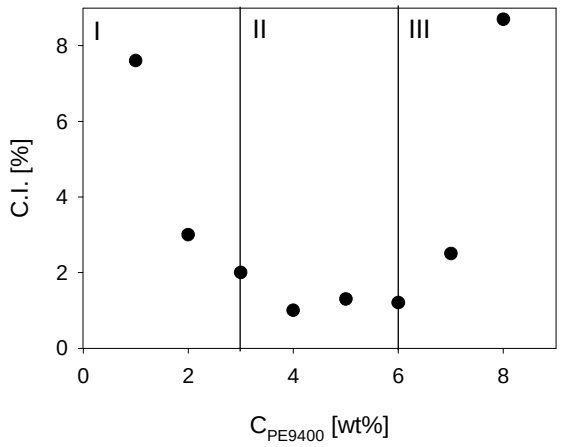

Figure 9. Creaming index as a function of Pluronic PE9400 concentration.

Figure 10 shows the visual aspect of three emulsions, which are representative of the three different regions, aged for 75 and 265 days. Furthermore, a tentative sketch of the emulsion droplet evolution in each region is also shown.

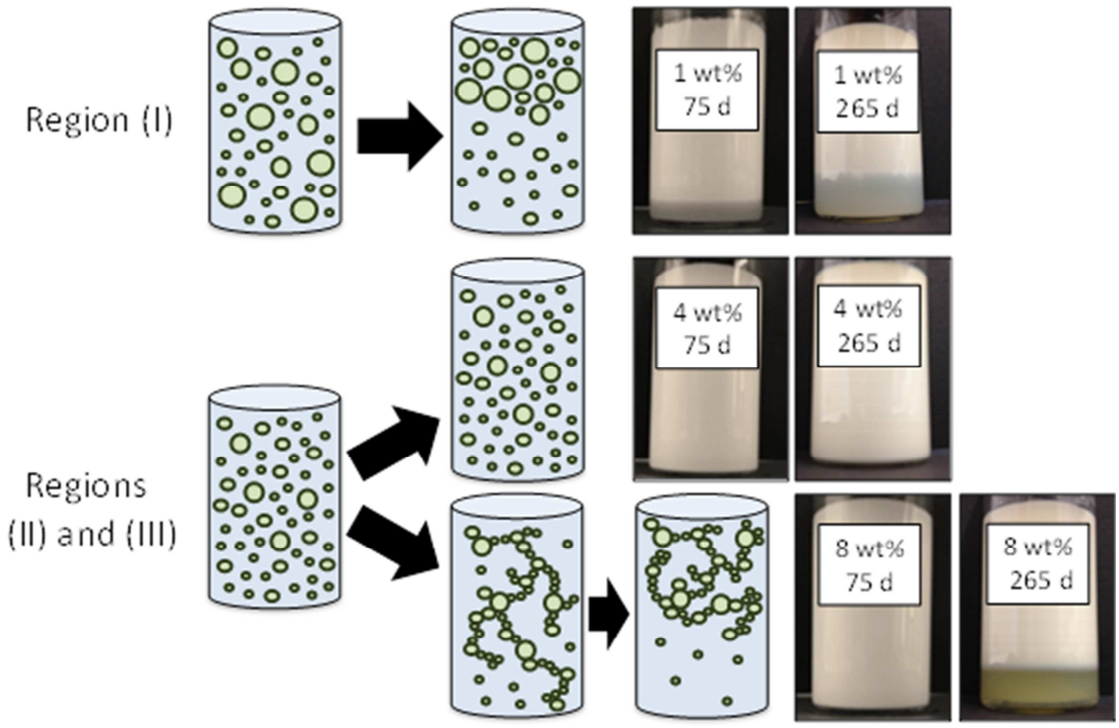

Figure 10. Visual aspect of the emulsions formulated with a Pluronic PE9400 concentration of 1 wt%, 4 wt% and 8 wt% aged for 75 days.

4. Conclusions

Slightly concentrated D-limonene-in-water submicron emulsions formulated with a non-ionic triblock copolymer as emulsifier and a lyophilic biopolymer as stabilizer can be readily prepared by using rotor/stator homogenizers.

Addition of a natural occurring lyophilic biopolymer, rosin gum, highly increased the stability of emulsions and reduced the droplet size. It was observed that rosin gum adsorbed at the interface, making it an interesting candidate for encapsulation purposes.

The influence of Pluronic PE9400 concentration on the stability, DSDs and rheological properties of the emulsions was studied. All emulsions exhibited Cross-type non-Newtonian flow properties. The zero shear viscosity, power-law flow index and

characteristic time for steady shear flow allowed the identification of three surfactant concentration regions. Furthermore, these emulsions only exhibited measurable linear viscoelastic (SAOS) properties from 7 wt% surfactant, when depletion flocculation started to be significant. Rheological measurements are demonstrated to be a powerful tool to assist in the prediction of destabilization processes in combination with laser diffraction and multiple light scattering techniques.

In short, below 3 wt% surfactant, emulsions are mainly destabilized by creaming, above 6 wt% surfactant, depletion flocculation phenomenon led to an increase in the creaming rate and in the range from 3 to 6 wt% surfactant, emulsions were highly stable.

This work opens up new possibilities for the development of environmentally-friendly emulsions in green chemistry. These emulsions may find applications as matrices for agrochemicals.

References

Aben, S., Holtze, C., Tadros, T., & Schurtenberger, P. (2012). Rheological Investigations on the Creaming of Depletion-Flocculated Emulsions. Langmuir, 28(21), 7967-7975.

Batrakova, E. V., & Kabanov, A. V. (2008). Pluronic block copolymers: evolution of drug delivery concept from inert nanocarriers to biological response modifiers. Journal of Controlled Release, 130(2), 98-106.

Barnes, H. A. (1994). Rheology of emulsions—a review. Colloids and Surfaces A: Physicochemical and Engineering Aspects, 91, 89-95.

Bibette, J. (1991). Depletion interactions and fractionated crystallization for polydisperse emulsion purification. Journal of Colloid and Interface Science, 147,474–478.

Brud, W. S. (2010) Industrial uses of essential oils. In Handbook of Essential Oils. Hüsnü Can Baser, K. and Buchbauer, G. (eds.). CRC Press.

Buscall, R., & White, L. R. (1987). The consolidation of concentrated suspensions. Part 1.—The theory of sedimentation. J. Chem. Soc., Faraday Trans. 1, 83(3), 873-891.

Caballero-Gallardo, K., Olivero-Verbel, J., & Stashenko, E. E. (2011). Repellent activity of essential oils and some of their individual constituents against Tribolium castaneum Herbst. Journal of agricultural and food chemistry, 59(5), 1690-1696.

Calero, N. et al., Rheological Behavior and Structure of a Commercial Esterquat Surfactant Aqueous System. Chemical Engineering and Technology. 33, 481-488 (2010).

Chanamai, R., Herrmann, N., McClements D.J. (2000). Probing Floc Structure by Ultrasonic Spectroscopy, Viscometry, and Creaming Measurements. Langmuir, 16, 5884-5891.

Chang-Moon Lee, Seung Lim, Gwang-Yun Kim, Dong-Woon Kim, Joon Haeng

Derkach, S.R.; Rheology of emulsions. Advances in Colloid and Interface Science. 151, (2009) 1–23

Dickinson, E., & Ritzoulis, C. (2000). Creaming and rheology of oil-in-water emulsions containing sodium dodecyl sulfate and sodium caseinate. Journal of Colloid and Interface Science, 224, 148–154.

Dimitrova, T. D., & Leal-Calderón, F. (1999). Forces between emulsion droplets stabilized with Tween 20 and proteins. Langmuir, 15, 8813–8821..

Fulzele, S.V., Satturwar, P.M., Kasliwal, R.H., Dorle, A.K.; Preparation and evaluation of microcapsules using polymerized rosin as a novel wall forming material, Journal of Microencapsulation 21 (1) , 83-89

Faers, M.A. et al., Syneresis and rheology of weak colloidal particle gels. Colloids and Surfaces A: Physicochem. Eng. Aspects., 288, 170-179 (2005)

Jafari, S.M., He, Y., Bhandari, B. (2007). Effectiveness of encapsulating biopolymers to produce sub-micron emulsions by high energy emulsification techniques. Food Research International, 40, 862-873

Jafari, S. M., Beheshti, P., & Assadpoor, E. (2012). Rheological behavior and stability of D-limonene emulsions made by a novel hydrocolloid (Angum gum) compared with Arabic gum. Journal of Food Engineering, 109(1), 1-8

A.B. Jódar-Reyes, A. Torcello-Gómez, M. Wulff-Pérez, M.J. Gálvez-Ruiz, A. Martín-Rodríguez, Different stability regimes of oil-in-water emulsions in the presence of bile salts, Food Research International 43 (2010) 1634–1641.

Jódar-Reyes, A. B., Martín-Rodríguez, A., & Ortega-Vinuesa, J. L. (2006). Effect of the ionic surfactant concentration on the stabilization/destabilization of polystyrene colloidal particles. Journal of Colloid and Interface Science, 298, 248–257.

Kabanov, A. V., Lemieux, P., Vinogradov, S., & Alakhov, V. (2002). Pluronic® block copolymers: novel functional molecules for gene therapy. Advanced drug delivery reviews, 54(2), 223-233.

Klein, M., Aserin, A., Svitov, I., & Garti, N. (2010). Enhanced stabilization of cloudy emulsions with gum Arabic and whey protein isolate. Colloids and Surfaces B: Biointerfaces, 77(1), 75-81

Kumar, S; Gupta, S. K.; Rosin: a naturally derived excipient in drug delivery systems. Polimery w medycynie 43 (1) , pp. 45-48, 2013

Leal-Calderon, F., Schmitt, V., & Bibette, J. (2007). Emulsion science: basic principles. Springer.

Lee, C.-M., Lim, S., Kim, G.-Y., Kim, D., Kim, D.-W., Lee, H.-C., Lee, K.-Y.; Rosin microparticles as drug carriers: Influence of various solvents on the formation of particles and sustained-release of indomethacin; Biotechnology and Bioprocess Engineering 9 (6) , pp. 476-481 (2004).

Lesaint, 2009. Dehydration efficiency of AC electrical fields on water-in-model-oil emulsions. ColSuA, 352, 63-69.

Lim,S.S., Baik,M.Y., Decker ,E.A., Henson, L., Popplewell ,L.M., McClements,D.J., Choi, S.J.; Stabilization of orange oil-in-water emulsions: A new role for ester gum as an Ostwald ripening inhibitor. Food Chemistry 128 (2011) 1023–1028

Manoj, P., Watson, A.D., Hibberd, D.J., Fillery-Travis, A.J., Robins, M.M.; Characterization of a depletion-flocculated polydisperse emulsion. II. Steady-state rheological investigations. Journal of Colloid and Interface Science 207 (2), (1998). 294-302

Maldonado-Valderrama, J., Fainerman, V. B., Gálvez-Ruiz, M. J., Martín-Rodriguez, A., Cabrerizo-Vílchez, M. A., & Miller, R. (2005). Dilatational rheology of β-casein

adsorbed layers at liquid-fluid interfaces. The Journal of Physical Chemistry B, 109(37), 17608-17616.

Maldonado-Valderrama, J., Miller, R., Fainerman, V. B., Wilde, P. J., & Morris, V. J. (2010). Effect of gastric conditions on β-lactoglobulin interfacial networks: Influence of the oil phase on protein structure. Langmuir, 26(20), 15901-15908.

Marcuzzo, E., Debeaufort, F., Sensidoni, A., Tat, L., Beney, L., Hambleton, A., & Voilley, A. (2012). Release Behavior and Stability of Encapsulated d-Limonene from Emulsion-Based Edible Films. Journal of agricultural and food chemistry, 60(49), 12177-12185.

McClements, D. J. (1994). Ultrasonic determination of depletion flocculation in oilin-water emulsions containing a non-ionic surfactant. Colloids and Surfaces A: Physicochemical and Engineering Aspects, 90, 25–35.

McClements, D.J., Food Emulsions: Principles, Practice, and Techniques, CRC Press, Boca Raton, 2005.

D.J. McClements, Critical review of techniques and methodologies for characterization of emulsion stability, Cri Rev Food Sci, 47 (2007) 611-649.

Muñoz, J. et al., Rheological behaviour of spray-dried egg yolk/xanthan gum aqueous dispersions. Rheological Acta 40, 162-175 (2012).

Murali, R., Karthikeyan, A., & Saravanan, R. (2012). Protective Effects of d‐Limonene on Lipid Peroxidation and Antioxidant Enzymes in Streptozotocin‐Induced Diabetic Rats. Basic & clinical pharmacology & toxicology

Pal, R.; Rheology of simple and multiple emulsion. Current Opinion in Colloid and Interface Science 16 (2011) 41-60

R. Pal, (1996). Effect of droplet size on the rheology of emulsions, AICHE J, 92 3181-3190.

G.G. Palazolo, D. A. Sorgentini, J.R. Wagner, Coalescence and flocculation in o/w emulsions of native and denatured whey soy proteins in comparison with soy protein isolates. Food Hydrocolloid, 19 (2005) 595-604.

Pan, L.G., Tomas, M.C., Anon, M.C. (2002) Effect of sunflower lecithins on the stability of water-in-oil and oil-in-water emulsions. Journal of surfactants and detergents, 5(2), 135-143.

Pérez-Mosqueda, L. M., Maldonado-Valderrama, J., Ramírez, P., Cabrerizo-Vílchez, M. A., Muñoz, J. (2013) Interfacial characterization of Pluronic PE9400 at biocompatible(air–water and limonene–water) interfaces. Colloids Surf. B, 111 171-178.

Pérez-Mosqueda, L.M.; Ramírez,P.; Alfaro,M.C.; Rincón,F.; Muñoz, J.; Surface properties and bulk rheology of Sterculia apetala gum exudate dispersions; Food Hydrocolloids. 32 (2013) 440-446

Radford, S. J., Dickinson, E.; (2004). Depletion flocculation of caseinate-stabilised emulsions: What is the optimum size of the non-adsorbed protein nano- particles. Colloids and Surfaces A: Physicochemical and Engineering Aspects, 238,71–81.

Rhee & Ki-Young Lee, Rosin nanoparticles as a drug delivery carrier for the controlled release of hydrocortisone, Biotechnology Letters (2005) 27: 1487–1490

Shields, M., Ellis, R., Saunders, B. R.; (2001). A creaming study of weakly flocculatedand depletion flocculated oil-in-water emulsions. Colloids and Surfaces A:Physicochemical and Engineering Aspects, 178, 265–276.

Santos, J., Trujillo-Cayado, L.A., Calero, N., Alfaro, M.C., Muñoz, J. (2013) Physical Characterization of a Commercial Suspoemulsion as a Reference for the Development of Suspoemulsions, Chemical Engineering & Technology, 36(11), 1883-1890.

Schmitt,V., Cattelet,C., Leal-Calderon, F.; Coarsening of Alkane-in-Water Emulsions Stabilized byNonionic Poly(oxyethylene) Surfactants: The Role ofMolecular Permeation and Coalescence. Langmuir 2004, 20, 46-52.

Tadros,T., Izquierdo,P., Esquena,J., Solans, C.; Formation and stability of nano-emulsions. Advances in Colloid and Interface Science 108 –109 (2004) 303–318

Tadros, T. (2009). Colloids in Agrochemicals. Wiley.

Torcello-Gómez, A., Santander-Ortega, M. J., Peula-García, J. M., Maldonado-Valderrama, J., Gálvez-Ruiz, M. J., Ortega-Vinuesa, J. L., & Martín-Rodríguez, A. (2011). Adsorption of antibody onto Pluronic F68-covered nanoparticles: link with surface properties. Soft Matter, 7(18), 8450-8461.

Torcello-Gómez, A., Maldonado-Valderrama, J., Martín-Rodríguez, A., & McClements, D. J. (2011). Physicochemical properties and digestibility of emulsified lipids in simulated intestinal fluids: influence of interfacial characteristics. Soft Matter, 7(13), 6167-6177.

Torcello-Gómez, A., Maldonado-Valderrama, J., Jódar-Reyes, A. B., & Foster, T. J. (2013). Interactions between Pluronics (F127 and F68) and Bile Salts (NaTDC) in the

Aqueous Phase and the Interface of Oil-in-Water Emulsions. Langmuir, 29(8), 2520-2529.

Torcello-Gómez, A., Maldonado-Valderrama, J., Jódar-Reyes, A. B., Cabrerizo-Vílchez, M. A., & Martín-rodríguez, A. (2014). Pluronic-covered oil-water interfaces under simulated duodenal conditions. Food Hydrocolloids, 34, 54-61.

Trujillo-Cayado, L.A., Santos, J., Calero, N., Alfaro, M.C., Muñoz, J. (2013) Rheological characterisation of a commercial suspoemulsion for agrochemical use. Afinidad, 70(561), 51-56.

Wisniekska, 2010, Influences of polyacrylic acid adsorption and temperature on the alumina suspension stability. Powder Technology, 198, 258-266

Wulff-Pérez, M.; de Vicente,J.; Martín-Rodríguez,A.; Gálvez-Ruiz, M.J.;Controlling lipolysis through steric surfactants: New insights on the controlled degradation of submicron emulsions after oral and intravenous administration. International Journal of Pharmaceutics 423 (2012) 161– 166

Wulff-Pérez, M., Torcello-Gómez, A., Gálvez-Ruiz, M. J., & Martín-Rodríguez, A. (2009). Stability of emulsions for parenteral feeding: Preparation and characterization of o/w nanoemulsions with natural oils and Pluronic f68 as surfactant. Food Hydrocolloids, 23, 1096–1102.

5

Conclusions

1. The interfacial behavior of pluronic PE 9400 has been studied by interfacial tension and interfacial dilatational rheology at the air/water and limonene/water interface. Two adsorption steps characterized by two different slopes in the *Π-c* plots, and two maxima which depend on the interfacial pressure have been observed in the *E- Π* plots. These experimental results fitted the thermodynamic protein model. This model is based on the occurrence of adsorbed layer compression and the likely formation of a bilayer at higher interfacial coverage at the limonene–water interface. Hence, a conformational transition from 2D flat conformation to 3D *brush/mushroom* conformation has been proposed to take place when increasing surface pressure at both interfaces.

2. The subphase exchange technique made it possible to study the desorption behavior of pluronic PE 9400 at the air/water and limonene/water interface. The results show that the polymer is irreversibly adsorbed at the interface regardless of the interface and the conformation of the polymer.

3. The combination of laser diffraction, rheology and multiple light scattering allow a comprehensive characterization of D-limonene emulsions stabilized by Pluronic PE9400 to be made. The influence of surfactant/oil ratio *(R)* and disperse mass fraction (ϕ) on the droplet size distribution and physical stability of the emulsions was studied using surface response methodology. From the optimum formulation monomodal submicron D-limonene-in-water emulsions were obtained by single-step rotor/stator homogenization.

4. Addition of a lyophilic biopolymer (rosin gum) to the disperse phase yields a marked increase in the physical stability of emulsions and a reduction of the emulsion droplet size. The enhanced physical stability is ascribed to three

reasons. The effect against creaming is due to the polymer performance as a weighting agent due to its high density. Rosin gum may play the role of a second disperse phase which promotes Ostwald ripening inhibition. Interfacial tension measurements show that rosin gum is a surface active chemical and this fact leads to smaller droplet size for the same energy input.

5. With regard to the influence of surfactant concentration on the emulsion stability and rheology of D-limonene emulsions containing PE9400 and rosin gum, three concentration regions have been defined. Below 3% wt surfactant, emulsions are mainly destabilized by creaming, above 6% wt surfactant, depletion flocculation triggers a rise in creaming rate and in the range from 3 to 6% wt surfactant, emulsions exhibit enhanced stability.

1. Se ha realizado la caracterización interfacial del pluronic PE 9400 en las interfases aire/agua y limoneno/agua mediante medidas de tensión interfacial y de reología dilatacional interfacial. La isoterma de adsorción muestra dos pendientes diferenciadas en ambas interfaces. También se ha apreciado en la representación *E-Π* la presencia de dos máximos siendo estos resultados experimentales ajustados correctamente con el modelo termodinámico de adsorción de proteínas. El modelo justifica una mayor compresibilidad de la capa de polímero adsorbida en la interfaz limoneno-agua y la probable formación de una bicapa a elevados recubrimientos interfaciales para la misma interfaz. Se propone un cambio conformacional desde una estructura bidimensional lineal a bajas presiones interfaciales a una conformación tridimensional en *champiñón/cepillo* a altas presiones interfaciales en ambas interfases.

2. El empleo de la técnica de intercambio de subfase nos ha permitido estudiar el comportamiento del pluronic PE 9400 frente a la desorción en las interfaces aire/agua y limoneno/agua. Los resultados experimentales muestran que el polímero se adsorbe de forma irreversible independientemente de la interfaz en la que se encuentre y de la conformación que presente.

3. La combinación de difracción láser, reología y dispersión múltiple de luz permite realizar una caracterización exhaustiva de emulsiones de D-limoneno estabilizadas con pluronic PE 9400. Se ha estudiado la influencia de la relación surfactante/aceite (R) y de la fracción de fase dispersa (ϕ) en la distribución del tamaño de gota mediante el uso de metodología de superficie de respuesta. La formulación óptima nos permite obtener una emulsión monomodal con tamaño

de partícula submicrónico de D-limoneno en agua mediante un proceso de homogenización en un paso empleando un sistema rotor/stator.

4. La adición de biopolímero lipofílico (goma rosin) a la fase dispersa produce un gran aumento en la estabilidad física de las emulsiones y una disminución del tamaño de gota. La mejora en la estabilidad física se asocia a tres razones. El efecto frente al cremado es asociado a que el biopolímero actúa como agente de peso debido a su alta densidad. La goma rosín puede actuar como segunda fase apolar dentro de la fase dispersa, lo que provoca la inhibición del Ostwald ripening. Medidas de tensión interfacial muestran que el biopolímero presenta actividad interfacial lo que permitiría obtener tamaños de partícula menores empleando la misma energía en el proceso de homogenización.

5. También se ha estudiado la influencia de la concentración de surfactante sobre la estabilidad física y sobre la reología de las emulsiones conteniendo la formulación D-limoneno, PE 9400 y goma rosín. Se han apreciado tres zonas en función de la concentración de suractante. Por debajo del 3% de tensioactivo las emulsiones se desestabilizan principalmente por cremado, por encima del 6% de surfactante se produce depletion flocculation que favorece la aparición de cremado, entre el 3% y el 6% de surfactante las formulaciones presentan una gran estabilidad física.